STAGNATION TEMPERATURE TEST METHODS FOR DETERMINING SOLAR COLLECTOR THERMAL PERFORMANCE DEGRADATION

by

Aaron Grayson Dawson, III

Dissertation submitted to the Faculty of the
Virginia Polytechnic Institute and State University
in partial fulfillment of the requirements for the degree of

DOCTOR OF PHILOSOPHY

in

Mechanical Engineering

APPROVED:

William C. Thomas, Chairman

Henry L. Wood

J. Robert Mahan

David Waksman

James R. Thomas

June, 1981

Blacksburg, Virginia

ACKNOWLEDGMENTS

The author would like to thank Dr. William C. Thomas for his advice and guidance in the preparation of this dissertation and throughout the author's graduate studies. Thanks are also extended to Dr. David Waksman, Dr. J. Robert Mahan, Dr. Henry L. Wood, and Dr. James R. Thomas for serving as committee members for this dissertation. The National Bureau of Standards (NBS) is gratefully acknowledged for the financial support of this investigation as part of the NBS Solar Collector Durability/Reliability Test Program.

Finally, a special thanks is extended to his parents for their support and encouragement throughout his education and to his wife, for her inspiration and patience during graduate school.

TABLE OF CONTENTS

LIST OF TABLES

LIST OF FIGURES

NOMENCLATURE

A_c	Collector aperture area (m^2)
C	Heat capacity (kJ/kg - C)
d	Air space thickness (m)
F( )	Functional relationship
g	Gravitation constant (m/s^2)
G	Total solar radiation (W/m^2)
Gr	Grashof number = $g\ \rho^2\beta\ (T_1 - T_2)\ d^3/\mu^2$
h	Heat transfer coefficient (W/m^2 - C)
J	Radiosity (W/m^2)
k	Thermal conductivity (W/m - C)
ℓ	One-half absorber width (m)
L	One-half absorber length (m)
L_c	Collector dimension in wind direction (m)
m	Mass per area of component (kg/m^2)
m^2	$= U_1/k_p\delta_p)$ (m^{-2})
$\hat{n}$	Solar index of refraction
Nu	Nusselt number = h d/k
P_{IN}	Power input to strip heaters (W)
Pr	Prandtl number = $C\mu/k$
q	Heat flow per unit area (W/m^2)
q_{12}	Heat flow by free convection; cover 1 to cover 2 (W/m^2)
q_{p1}	Heat flow by free convection; absorber to cover 1 (W/m^2)
q_w	Heat flow off outside cover as a result of wind (W/m^2)

r	Solar reflectance of a single interface
Ra	Rayleigh number = $Gr\ Pr$
Re_{L_c}	Reynolds number = $V_w L_c\ \rho/\mu$
S	Solar radiation absorbed on absorber plate (W/m^2)
t	Time (s)
T	Temperature (C or K)
T_1, T_2	Temperature of lower and upper plate, respectively (K)
u	Known parameters
U	Overall heat-transfer coefficient (W/m^2 - C)
U_L	Overall collector loss coefficient (W/m^2 - C)
U_{ex}	Edge loss coefficient; x direction (W/m^2 - C)
U_{ey}	Edge loss coefficient; y direction (W/m^2 - C)
V_w	Wind speed (m/s)
x	Unknown parameters, variable in the length direction of the absorber plate (m)
$\hat{x}$	Optimum set of parameters
y	Variable in the width direction of the absorber plate (m)
z	Variable in the direction normal to the absorber plate (m)

Greek Symbols

α	Absorptance
$(\hat{\alpha}_1), (\hat{\alpha}_2)$	Fraction of solar radiation absorbed in cover 1 or 2
β	Collector slope (deg), volumetric coefficient of expansion (K^{-1})
β_n	Characteristic value in x-direction
γ	Damping factor ($0 \leq \gamma \leq 1$)

γ_n	Characteristic value in y-direction
δ	Thickness (m)
δ_i	Finite difference used in numerical derivative
Δ	Change in a variable
ε	Emittance of a surface
η_d	Diffuse solar radiation fraction
θ	Incident angle of beam solar radiation with respect to the collector normal (deg), $T - T_a - S/U_L$, $T_p - T_a$ (C)
θ_o	Initial value of $(T_p - T_a)$ (C)
θ_2	Refracted angle of beam solar radiation (deg)
$\hat{\kappa}$	Solar extinction coefficient (m^{-1})
λ_n	Characteristic value in x-direction
$\lambda_{\Delta T}$	Maximum residual error
μ	Dynamic viscosity (kg/m · s)
$\mu_{\Delta T}$	Mean of residual errors
ξ_n	Characteristic value in y-direction
ρ	Reflectance, Density (kg/m^3)
σ	Stefan-Boltzmann constant ($W/m^2 - K^4$)
$\sigma_{\Delta T}$	Standard deviation of residual errors
τ	Transmittance, time constant (minute)
τ_a	Solar transmittance considering only absorptance
τ_d	Day length of solar radiation (h)
$(\hat{\tau\alpha})$	Transmittance-absorptance product
ϕ	Latitude (deg), sum of residuals squared
χ	$= (T_p - T_a)/G$
ψ_x, ψ_y	$= U_{ex}\ L/k_p$, $U_{ey}\ \ell/k_p$

ω	Experimental uncertainty

Subscripts

a	Ambient
b	Beam portion of solar radiation
B	Back-side
BC	Back cover
c	Cover, current value, cooling
d	Diffuse portion of solar radiation
h	Heating
i	Index counter
in	Insulation
j	Index counter
k	Index counter
ℓ	Number of known parameters
m	Number of measured values, parallel component
n	Number of unknown parameters, perpendicular component
p	Absorber plate, predicted value
r	Radiation
s	Sky
w	Wind

Superscripts

$\hat{}$	Solar radiation wavelength value

$\vec{}$	Vector value
$\tilde{}$	Measured value
$'$	Improved current value

1. INTRODUCTION

This investigation is concerned with test methods used to determine the degradation of solar collector thermal performance caused by material property changes resulting from long term environmental exposure. Material properties which effect thermal performance include absorber plate solar absorptance and infrared emittance, solar and infrared transmittance of the covers, and insulation thermal conductivity. The major environmental conditions which may cause changes in these properties are ultraviolet radiation, humidity, and elevated temperatures. The suitability of different test methods to identify property changes are explored, as are the means by which variable and nonrepeatable outdoor environments affect these methods.

The short-term objective of the research is to develop new techniques to measure collector property changes after environmental exposure. If these short-term objectives can be realized, then the long term objective of the research would be to improve solar collector reliability and long-term performance, determine mechanisms which cause property changes, and establish accelerated test procedures. The short-term objective is the main emphasis of this investigation.

1.1 Scope

The investigation reveals some of the limitations of the current test procedures used to determine the long-term performance of solar collectors. New test methods are proposed and evaluated. These new methods are based on measuring the "stagnation" temperature of solar collectors to determine solar collector thermal performance degradation. The stagnation temperature is defined as the equilibrium temperature obtained in a solar collector when there is no working fluid removing energy from the collector. This investigation is concerned with flat-plate nonconcentrating solar collectors of conventional design (i.e., no convection suppressing "honeycomb" grids or "accordian" folds, curved covers, or reflection devices). The method may apply to nonconventional designs, but this extension is not considered in the present investigation.

The investigation involves developing steady-state and transient stagnation temperature models. The analytical models are experimentally validated and used to determine the sensitivity of stagnation temperature to collector property changes and environmental conditions. In addition, indoor and outdoor experiments are designed to provide data to analyze test methods incorporating stagnation temperature. Although analyzing test methods is the main emphasis of this investigation, time constraints precluded obtaining elapsed time data of longer than three months to verify the new methods.

1.2 Background

The National Bureau of Standards (NBS) is currently sponsoring investigations of test methods for predicting the reliability of solar collectors. This study is a part of their Solar Collector Durability and Reliability Test Program [1-3]. The research in the present investigation is primarily an attempt to reconcile the test results that were obtained under the NBS test program. The test method used to obtain the initial and post stagnation exposure thermal performance tests was an energy output method [4]. The energy output thermal efficiency of a solar collector is defined as the amount of thermal energy transferred to the working fluid divided by the amount of solar radiation incident on the collector aperture. Previous investigations [3, 5, 6] have shown uncertainties in the measured efficiency of this energy output method to be $\pm$ 3 to 4 percentage units. The measured values which contribute to the uncertainty of the energy output method are mainly the mass flow rate, solar radiation, and the temperature difference between the exit and inlet temperatures of the working fluid. Figure 1.1 shows data from the NBS Durability and Reliability Program for the initial "baseline" thermal performance tests of collector B (the properties of this and other collectors are described later). These data were obtained at test sites 1 and 2 (test site numbers refer to test sites used in reference 1 and 2). The solid line in Fig. 1.1 is a linear least-squares fit to the data which is plotted in the manner prescribed by reference 4. The calculated experimental uncertainty associated with the test method is shown by the dotted lines. As expected, the experimental results

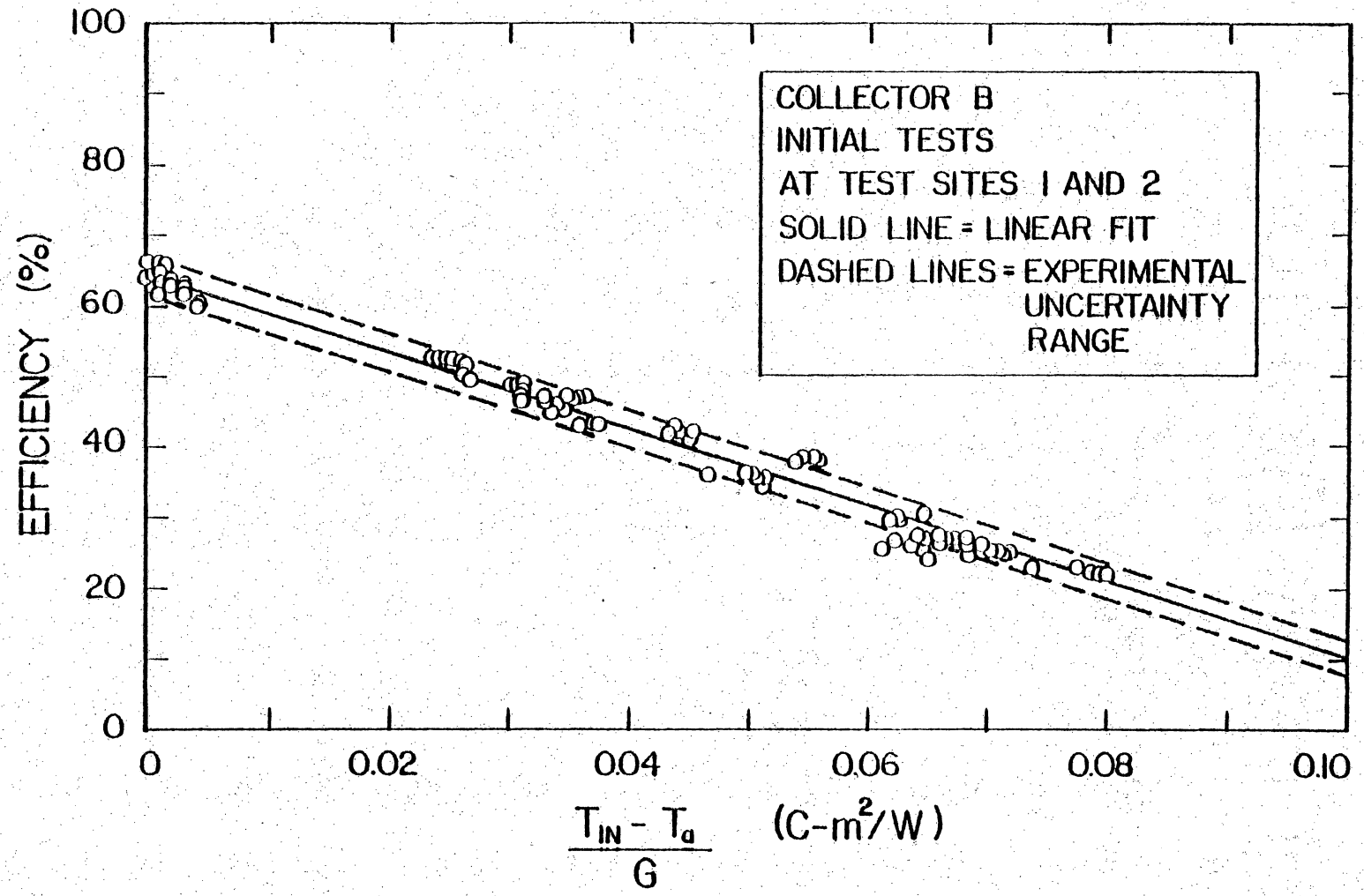

Fig. 1.1 Initial Thermal Performance Results of Collector B Measured at Test Sites 1 and 2 Using the Energy Output Test Method

generally lie within the measurement uncertainty range. Figure 1.2 shows the minimum amount of change in the solar absorptance of the absorber plate of collector B which results in a distinct separation of the uncertainty bands between the initial and degraded performance curves. This graph was constructed by using calculations from the well established Hottel-Whillier-Bliss analysis [7] and state-of-the-art extensions [8]. The theoretical curves in Fig. 1.2 were linearized in order to be consistent with the manner in which Fig. 1.1 was constructed. It appears unlikely that changes in absorber plate absorptance less than about 10 per cent can be statistically detected by using the energy output method.

Representative results show that the measurement uncertainty obscures determining possible changes with respect to time in terms of the two collector performance parameters. These two parameters are the ordinate intercept of the linearized efficiency curve (the so-called optical efficiency) and the slope of the efficiency curve which is proportional to the average heat loss coefficient for the collector. These two parameters are presented as a function of exposure time in Figs. 1.3 and 1.4. Both figures show results obtained at test site 1 using three collectors from the same manufacturer and production lot. Again, the measured results generally lie within the measurement uncertainty range for both parameters. Therefore, small collector property changes as a function of time would be difficult to differentiate from the experimental uncertainty in determining both parameters. A combination of low sensitivity to changes in collector

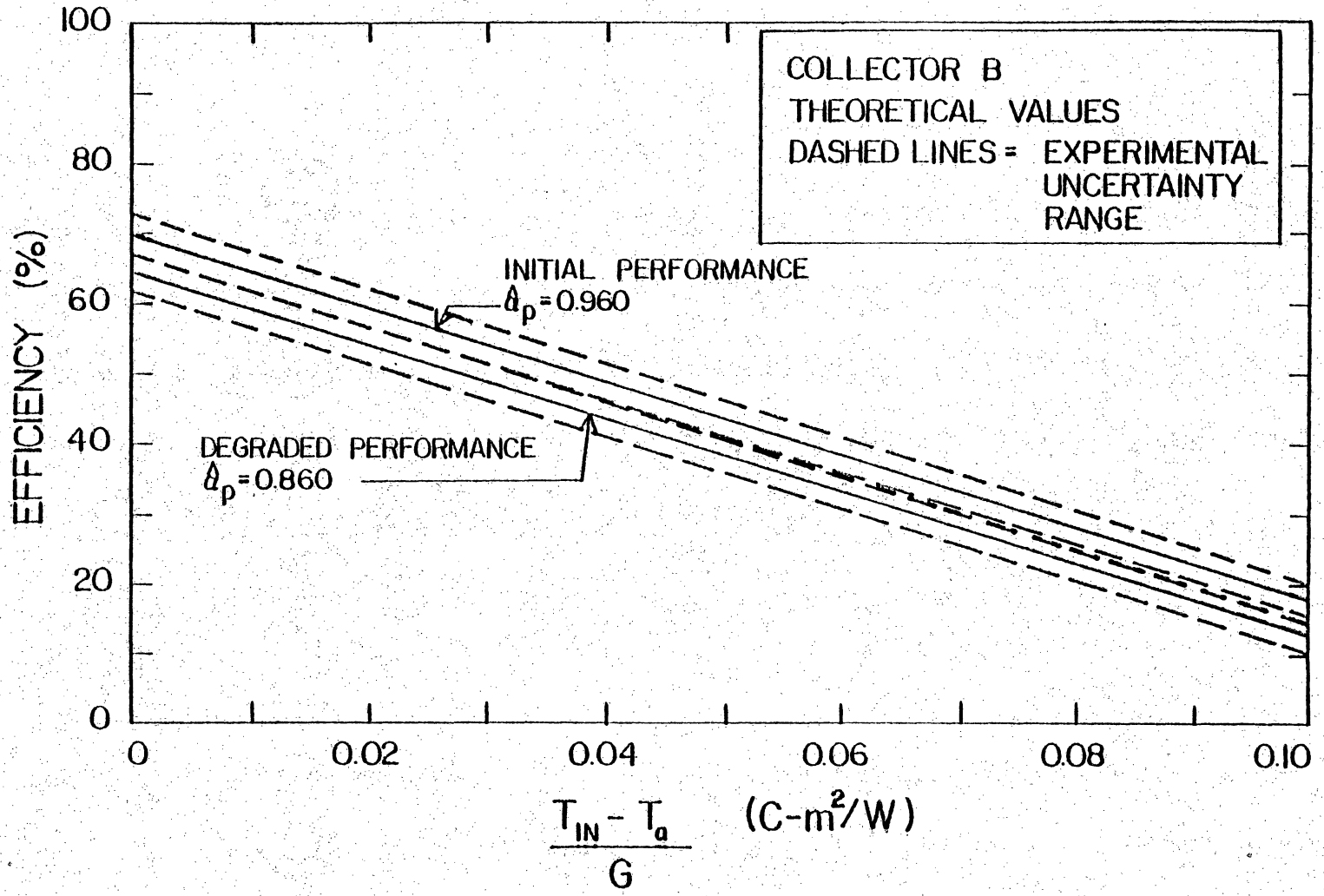

Fig. 1.2 Theoretical Effect of Reducing $\hat{\alpha}_p$ From 0.96 to 0.86 on the Thermal Performance of Collector B

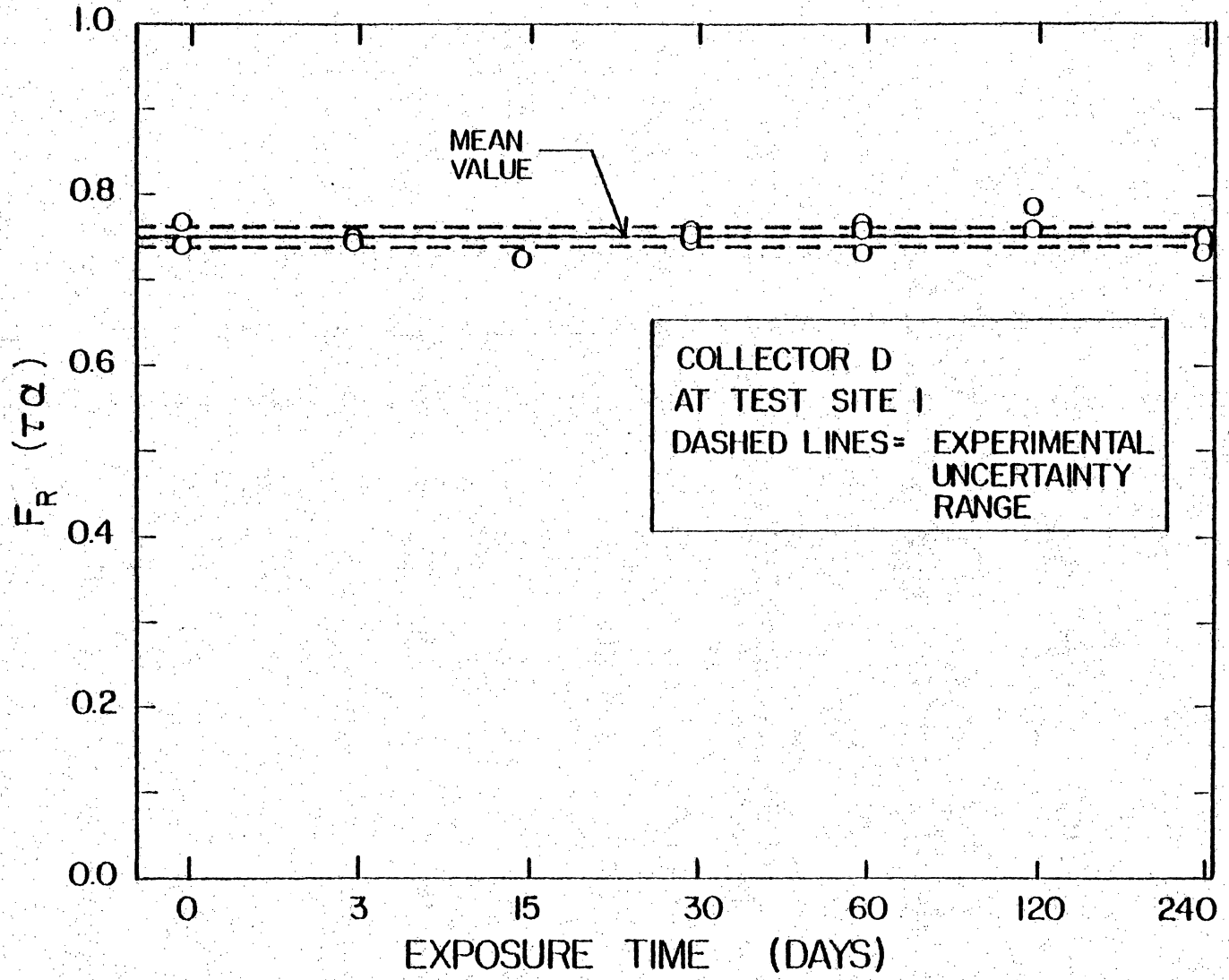

Fig. 1.3 Measured Values of F_R $(\tau\alpha)$ as a Function of Exposure Time for Collector D at Test Site 1

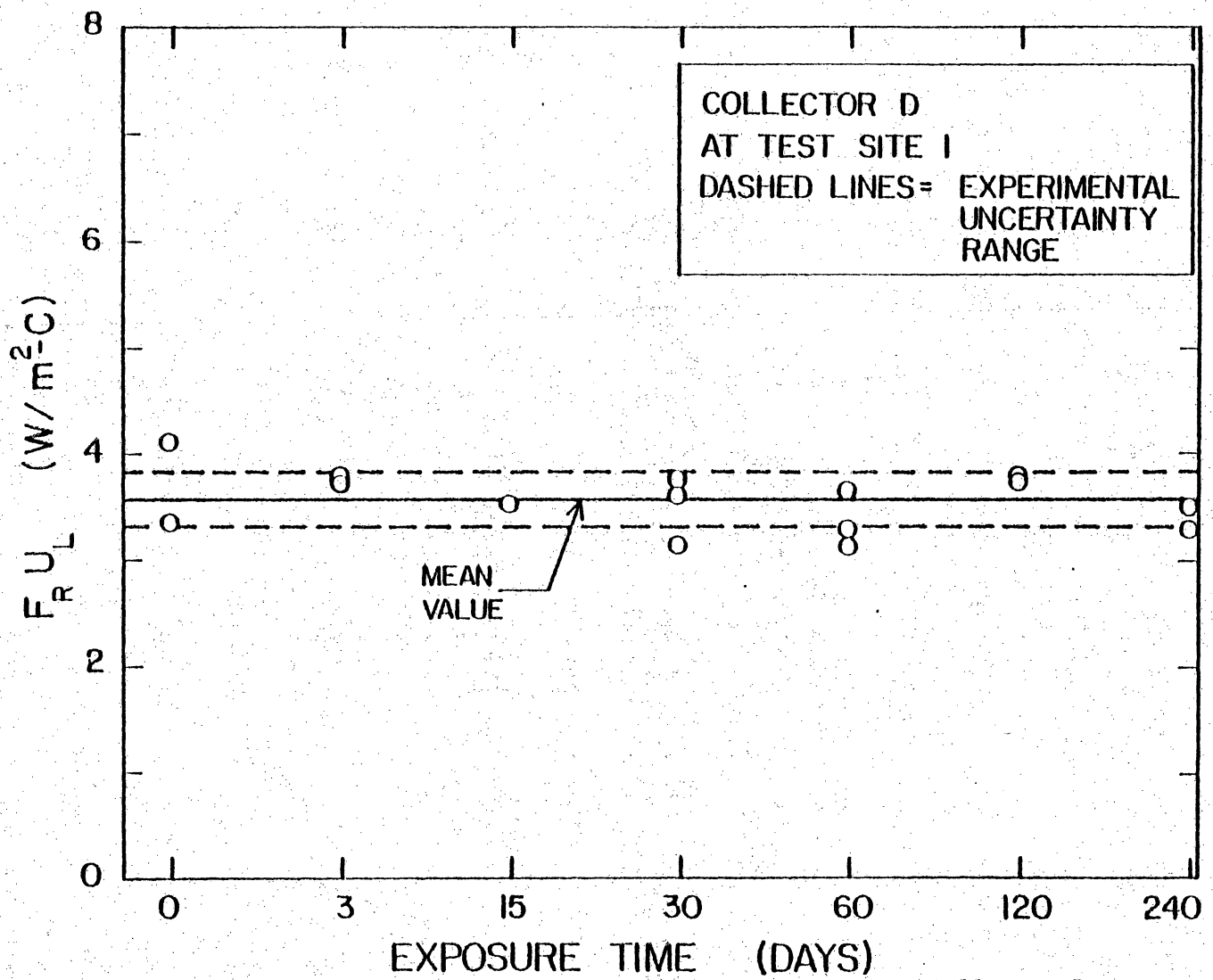

Fig. 1.4 Measured Values of $F_R U_L$ as a Function of Exposure Time for Collector D at Test Site 1

roperties and a relatively high measurement uncertainty limits the energy output method for detecting efficiency changes of less than approximately 10 per cent.

While Figs. 1.3 and 1.4 show the limitation of using the energy output efficiency as a means of revealing collector material property changes, a proposed test method based on measuring only the absorber plate temperature of a solar collector appears to have greater potential. The advantages include less measurement uncertainty and a relatively high sensitivity to collector property changes as compared to the energy output method. Since a working fluid is not used in the test, measurement uncertainties associated with measuring the flow-rate and determining the properties of the fluid are eliminated. Additionally, a 10 per cent reduction in the solar transmittance of a cover or the solar absorptance of the absorber plate causes approximately a 10 per cent reduction in the difference between the absorber and ambient temperature. This condition would produce a decrease in the absorber plate temperature from 10 C to 20 C which is readily measured using thermocouple temperature sensors. Also, changes in the infrared emittance from 0.20 to 0.30 result in approximately the same decrease in absorber plate temperature. An additional advantage in using the stagnation temperature to determine collector property changes is that the collector performance can be monitored continuously during the stagnation exposure. On the other hand, the energy output method requires periodic relocation of the collector from the exposure rack to a test stand and back. This relocation is inconvenient and as

much as a week or more of exposure time can be lost. In addition, testing by the energy output method is considerably more expensive.

However, a test method using stagnation temperature is not free from potential problem areas. These problem areas include relatively slow time response of collectors to changes in the solar irradiance, stronger effects of environmental conditions on measured temperatures, and the temperature distribution of the absorber plate. A typical time constant for the absorber plate temperature of a stagnating collector is one-half hour. This long time response can lead to errors in measuring steady-state temperatures long after a period of cloud cover. Environmental conditions, mainly wind speed, solar radiation, and ambient temperature, have a strong effect on the stagnation temperature of collector components as a result of the high temperature levels during stagnation. Heat losses around the perimeter of the collector combined with internal air stratification can cause the absorber plate temperature to be nonisothermal. This absorber plate temperature distribution results in difficulties in defining an "effective" absorber plate temperature. The significance and the methods of reconciling these potential problem areas are considered in the present investigation.

1.3 Literature Review

The body of literature dealing with stagnation temperature is divided into three main categories. The first of these categories deals with the degradation of materials during stagnation exposure. The second body of literature considers measuring the collector thermal performance by measuring the stagnation temperature of the absorber plate. Finally, there is the body of literature dealing with general collector performance models and specific heat transfer results which are of interest in formulating an analytical model to analyze different stagnation test methods. Each one of these categories is considered separately in the following sections.

Material Degradation Literature

Excessive temperatures within a solar collector during stagnation conditions can damage plastic covers, destroy the bond between the absorber plate and flow tubes, char backside insulation, and cause thermal expansion problems. Three days of stagnation exposure are required in the ASHRAE 93-77 test standard [4] before obtaining the thermal performance of a solar collector to detect short-term damage as a result of these high temperatures. Padillo [9] discusses problems dealing with solar collectors during stagnation and suggests possible ways to avoid stagnation. But as a result of installation, power failures, and long-term resident absences, the probability is high that a solar collector will stagnate sometime during its service life.

Several authors [10-13] have discussed exposing solar collectors in a stagnating mode as an accelerated exposure test. Although it is generally agreed by these authors that stagnating conditions accelerate the aging process in solar collectors, a time relationship between accelerated stagnation exposure and normal operation exposure has not been established. The National Bureau of Standards has developed several test standards [14-16] which require stagnation exposure as a means of accelerated testing to determine solar collector durability and reliability. The National Bureau of Standards Solar Collector Durability and Reliability Test Program [1-3] is currently evaluating different test standards used to determine long-term thermal performance of solar collectors and the time relationship between accelerated stagnation exposure and normal operation exposure.

Stagnation Temperature Methods

Currently, the thermal performance of solar collectors, before and after stagnation exposure, is measured using an energy output method as described in reference 4. Few articles are found in the literature which discuss using a change in stagnation temperature of the absorber plate as an indicator of a change in thermal performance after environmental exposure. Morehouse and Vachon [17] consider the use of stagnation temperature as a method for measuring solar collector thermal performance. Although Morehouse and Vachon do not directly address using stagnation temperature as an indicator of collector property

changes, their work could be applied to a method of this type. Problems dealing with transients, different environmental conditions, edge effects, and internal air stratification are not discussed in their paper. In addition, the amount of experimental data contained is limited. Goodman and Menke [18] have used the stagnation temperature of the absorber plate as an indicator of the additional benefits of using different cover plate treatments over untreated glass. Although the discussion of stagnation temperature is limited, a similar procedure could be used to detect decreases in cover transmittance, after environmental exposure. A temperature-dependent loss coefficient, U_L, obtained by stagnation temperature measurements, was described in an article by Gordon, et al. [19]. Different temperature levels of the absorber plate were obtained by partially shading the collector with nets of various mesh sizes. The measured results showed some scatter which was attributed to the variability in the wind speed during the test. The authors concluded that a test using this method requires a minimal degree of sophistication and equipment.

The methods using stagnation temperature in references 17-19 require steady-state conditions during the test. Steady-state conditions are approached only on very clear days near solar noon for a solar collector mounted in a fixed south-facing position. A dual axis, self tracking mount, which remains normal to direct solar radiation, can increase the length of the steady-state period, but only on very clear days. The other technique to obtain steady-state conditions is through the use of an indoor solar simulator. A solar

simulator generally uses either xenon arc or tungsten-halogen lamps to simulate the radiation from the sun. Although a solar simulator could solve the problems dealing with transients and non-repeating environmental conditions, the expense and short-term life of the simulator lamps remains an issue. Another limitation of solar simulators arises from the question of whether or not solar simulators truly duplicate the wavelength distribution of natural solar radiation.

A proposed method [20] has been discussed at various test standard meetings which eliminates the effects of outdoor transients on stagnation temperature measurements. This method integrates the solar radiation, ambient temperature, and absorber plate temperature over the period of one day. The integrated values for the solar radiation and the temperature difference between absorber plate and ambient temperature are compared before and after environmental exposure to determine collector property changes. The primary advantage of this all-day integration method is that both clear and partially cloudy days provide information on thermal performance degradation.

Heat Transfer Topics

References related to the development of the analytical models (Chapter 3) will be discussed in detail as the need arises. A summary of the heat transfer correlations and algorithms used in the analytical models are presented in this section. Studies dealing with free convection heat transfer inside the solar collector can be found in references 21-31. Correlations developed by Hollands, et al. [27, 28, 29, 31] are used to calculate the heat transfer by free convection in the analytical models. Investigations dealing with forced convection as a result of wind on the outside cover can be found in references 32-34. A relation developed by McAdams [32] is used to calculate the wind heat transfer coefficient. The amount of solar radiation absorbed in the covers and on the absorber plate in the analytical models comes from the analysis done by Ramsey, et al. [35]. Discussions on parameter estimation techniques used to determine input values to analytical models which are unknown or known with little certainty can be found in references 36-38.

Very little information is available in the literature dealing with determining the mechanisms which cause material property changes. The main problem holding up studies to determine these mechanisms is that currently recommended test methods, based on measuring efficiency as a function of exposed time, are inherently inaccurate with respect to the degree of changes. The proposed method of using the stagnation temperature as an indicator of material property changes is potentially beneficial in removing some of these inaccuracies. Although test

methods which use stagnation temperature have been considered in the literature, in-depth studies have not been established. Indoor and outdoor experiments are described along with the development of theoretical models in the following chapters to investigate stagnation temperature test methods.

2. EXPERIMENTAL APPARATUS

The main objectives of the experimental apparatus used in this investigation are to verify analytical models, investigate simplifying assumptions, analyze measurement techniques, compare indoor and outdoor measurements, and evaluate new test methods. In addition, experiments were needed to determine the absorber and cover plate temperature distribution caused by edge losses and internal air stratification which are difficult to model. To accomplish the above tasks, an indoor test facility was constructed and an existing outdoor test facility was used.

The indoor test facility was constructed mainly to determine steady and transient temperature distributions on the absorber and cover plates for predetermined solar radiation profiles. This indoor test facility consists of a highly instrumented commercial solar collector equipped with electrical strip heaters on the back-side of the absorber to simulate absorbed solar energy.

The outdoor test facility was used to obtain actual outdoor data with the environment as a variable and to confirm important results determined indoors. Two commercial collectors (one identical to the indoor collector) were mounted outdoors on a dual-mount, adjustable-tilt, test rack. The necessary instrumentation and sensors required to measure environmental conditions and temperatures of the absorber and cover plates of both collectors were used.

Additional experimental data were obtained from off-campus test facilities at test sites 4 and 5. Both of these test facilities

provided data taken on collectors different from the collectors used on campus. The test facility at test site 5 also supplied data obtained using a solar simulator.

2.1 Indoor Test Apparatus

An indoor test facility was needed to control environmental conditions, maintain steady-state conditions, and to avoid deterioration by weathering of instrumentation and sensors. Solar collector I, which is a single glass cover solar collector with a selective surface absorber plate, was chosen for the indoor tests. The dimensions and heat transfer properties of collector I are shown in Table 2.1. Solar radiation was simulated indoors by a uniform distribution of strip heaters manufactured by Electrofilm which were attached with epoxy underneath the absorber plate inside the solar collector. The power input to the strip heaters was controlled by a 110 V AC variable transformer. This arrangement enabled a constant input for steady-state measurements, a step input for transient responses, and an arbitrary input to simulate cloud spikes or other solar radiation profiles.

The specific models and identification of the instruments used in this and other experiments are given in Appendix A. There were fifteen 51 mm x 1.52 m strips, three 51 mm x 0.61 m strips, and three 51 mm x 0.23 m strips electrically connected in parallel to the variable transformer. Strip heaters of different lengths were used because the dimensions of the collector did not coincide with standard manufactured lengths. Measurements were made to verify that a uniform heat flux to

TABLE 2.1

Dimensions and Heat Transfer Properties for the Solar Collectors Used in This Investigation

Dimension or Property	Units	Collector A	B	D	E	H	I
Absorber							
Flow Configuration	-	parallel	parallel	parallel	parallel	serpentine	parallel
Effective Length	m	1.92	1.91	1.72	2.92	2.34	1.72
Effective Width	m	0.95	0.84	0.81	0.56	1.13	0.81
Flow Tubes: Number	-	8	6	10	5	8	10
O.D.	mm	22.2	10.4	8.1	16.1	15.9	8.1
Hydraulic Diameter	mm	15.8	9.6	4.9	12.7	12.7	4.9
Wetted Perimeter	mm	49.6	30.2	15.4	39.9	39.9	15.4
Thickness	mm	2.0	0.8	0.9	0.4	1.8	0.9
Thermal Conductivity	W/m-C	45.0	360.0	45.0	360.0	200.0	45.0
Emittance	-	0.21	0.89	0.22	0.87	0.88	0.22
Solar Absorptance	-	0.93	0.96	0.94	0.95	0.96	0.94
Cover Assembly							
Number of covers	-	1	2	2	1	2	1
Air Space: under cover 1/under cover 2	mm	32.0	25.4/6.4	37.0/25.0	60.0	25.4/12.7	65.0
Infrared Emittance: cover 1/cover 2	-	0.88	0.88/0.88	0.88/0.88	0.84	0.33/0.80	0.88
Infrared Transmittance: cover 1/cover 2	-	0.00	0.00/0.00	0.00/0.00	0.07	0.60/0.10	0.00
Index of Refraction: cover 1/cover 2	-	1.52	1.52/1.52	1.30/1.30	1.54	1.33/1.68	1.30
Extinction Coefficient: cover 1/cover 2	mm^{-1}	0.003	0.01/0.01	0.01/0.01	0.057	0.066/0.24	0.01
Thickness: cover 1/cover 2	mm	4.80	3.18/3.18	3.18/3.18	0.97	0.025/0.178	3.18
Insulation							
Thickness: Back	mm	76.2	76.2	89.0	25.4	25.4	89.0
Edge	mm	6.4	25.4	25.4	25.4	25.4	25.4
Conductivity: Back	W/m-C	0.035	0.04	0.040	0.02	0.02	0.040
Edge	W/m-C	0.035	0.04	0.040	0.02	0.02	0.040
Aperture Area	m^2	1.83	1.60	1.39	1.63	2.64	1.39
Gross Area	m^2	2.15	1.74	1.67	1.89	2.93	1.67

the absorber was achieved. With the collector in a horizontal position and a steady heat flux applied, absorber plate temperatures were symmetrical with respect to the center, to within $\pm$ 3 C when the center temperature was 190 C. Using the following relation, a power input of 1200 W into the strip heaters corresponds to a solar irradiance of 975 W/m^2.

$$G = \frac{P_{IN}}{A_c(\tau\alpha)} \tag{2.1}$$

where G = solar irradiance (W/m^2)

P_{IN} = input power (W)

A_c = aperture area (m^2)

$(\tau\alpha)$ = transmittance-absorptance product.

There were 20 locations on the absorber plate and six locations on the glass cover where the temperature was measured. The location of the absorber and cover thermocouples along with their identification numbers are shown in Fig. 2.1. All temperature measurements in this investigation were taken by copper-constantan (type T) thermocouples. The thermocouples on the absorber plate were attached by placing a thermocouple "bead" inside a small hole drilled into the absorber plate and peening the metal around the hole to secure the thermocouple. The glass cover thermocouples were attached by using a small amount of heat sink compound and securing them with clear plastic tape.

The collector was mounted on a test stand which allows adjustment of the tilt angle from the horizontal to the vertical position. The collector was located in a large room where the ambient temperature was

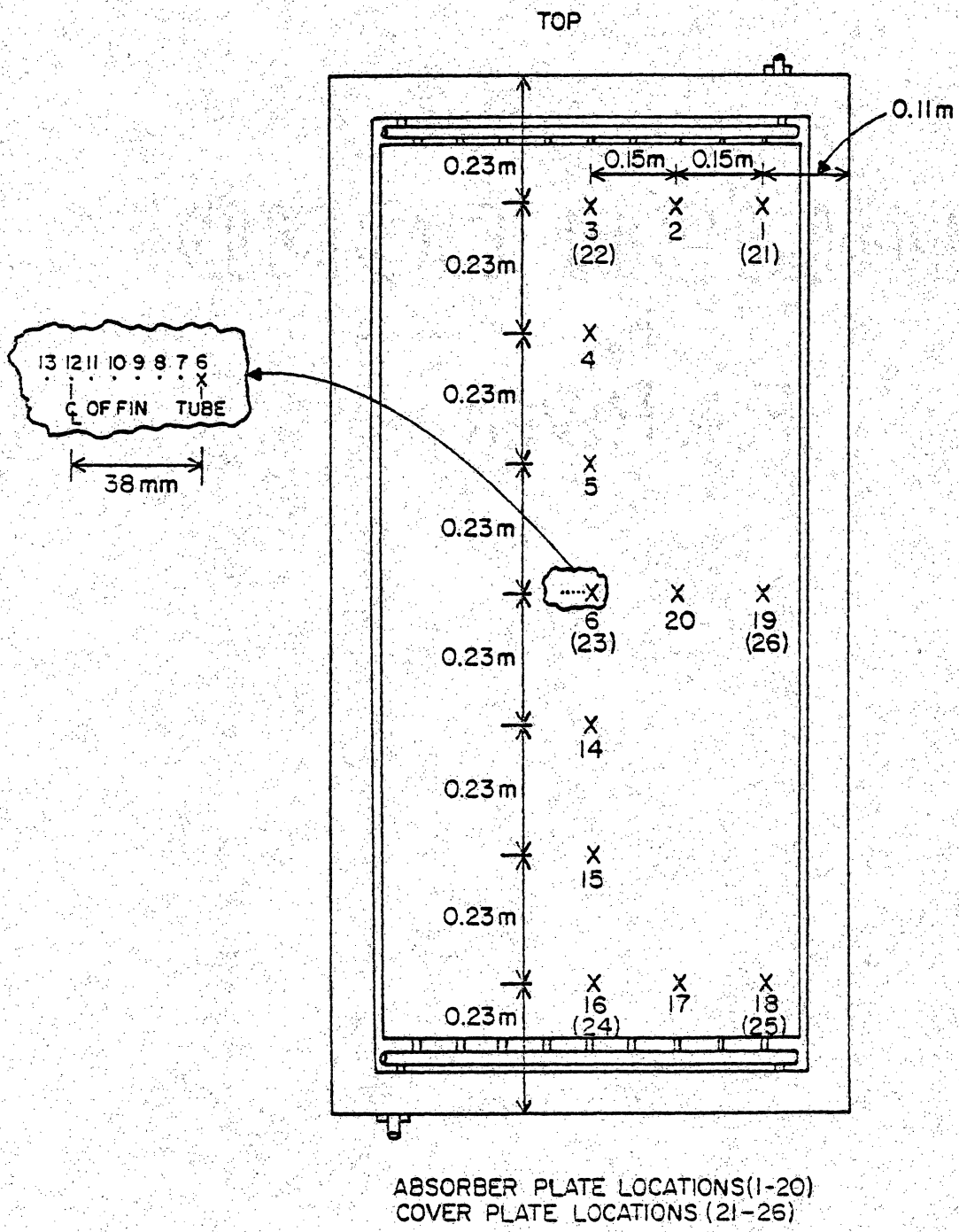

Fig. 2.1 Absorber and Cover Plate Thermocouple Locations for Collector I (Instrumented for Indoor Experiments)

held constant to within $\pm$ 0.5 C during tests. A rectangular sheet metal shield was supported 0.33 m above the glass cover in order to control and accurately measure the radiative environment temperature. The shield extended 0.50 m over each end of the collector and extended 0.35 m over each side to give a geometric configuration factor between the collector aperture and shield of 0.87. The effective radiative environment temperature was obtained by averaging the temperature measured at the lower, middle, and upper third sections of the shield. The shield temperature varied along its length when the slope of the collector was not horizontal. This variation was a result of a chimney effect caused by low temperature air entering the lower space between the glass cover and shield and rising in temperature before it left the top exit. The surface of the shield facing the collector was painted with a flat black paint with an infrared emittance of greater than 0.95. The ambient air temperature was measured with a shield thermocouple. The indoor wind speed for all tests was zero (i.e., free convection from the glass cover).

The power input to the strip heaters was measured both by a Weston AC power meter in combination with a 5-to-1 Weston current transformer and a Weston alternating current meter along with a Hewlett-Packard digital voltmeter. The last power measurement, used as a check, measured the correct power input, since the heaters were a purely resistive load. Also, the voltage for both power measurements was measured at the load, as a result of a significant voltage drop between the variable transformer and the load. The steady state thermocouple temperatures were

measured using a thermocouple switch and a Hewlett-Packard digital multimeter with a least count of one μV. Selected collector temperatures during transient tests were recorded at 30-second intervals on a Honeywell 24-channel multipoint recorder.

The amount of time required to reach steady-state conditions during steady-state tests was between two and four hours depending on the input power level and initial temperature. Conditions were considered to be steady-state when the center absorber plate temperature changed less than a rate of 2 C per hour. Power adjustment difficulties precluded using nominal values for power input. These difficulties were a result of the finite number of turns in the transformer coils. A repeatability test was performed with steady-state temperatures measured initially and again after 45 days using the same power input for both tests. The maximum change in $(T_p - T_a)$ between tests at any location was 3 C when the center absorber plate temperature was equal to 190 C.

2.2 Outdoor Test Apparatus

Solar collectors D and I from Table 2.1 were mounted on a dual-mount, adjustable-tilt, test rack. The test rack, at a latitude of 37.23° north, faced due sourth. The necessary instrumentation and data recording apparatus were located in a separate instrumentation room.

The total solar radiation, beam solar radiation, and infrared sky radiation were measured by an Eppley Model PSP pyranometer, an Eppley Model NIP pyrohelimeter, and an Eppley model PIR pyrgeometer, respectively. A three-cup Model W103B Weather Measure anemometer was

used to measure wind speed. The ambient temperature thermocouple was housed in a small white enclosure with louvers to insure adequate ventilation. Instantaneous values for the total solar radiation, beam solar radiation, and wind speed can change significantly in a matter of seconds. In order to keep the amount of recorded data reasonable, the instantaneous values for these three measurements were integrated over five-minute periods by electronic integrators, manufactured by AGM, Incorporated. The integrator output consists of a ramp voltage signal which was continuously recorded on strip chart recorders. The peak value of the ramp voltage, just before reset, corresponds to the five-minute average. The instantaneous output from the pyrgeometer was recorded directly on a strip chart recorder. The ambient temperature and the cover and absorber plate temperatures of both collectors were recorded at one-minute intervals on a 24-channel multi-point recorder.

The temperature of the collector covers was measured in the center of each glass. Significant errors in measuring cover plate temperatures may result from solar radiation being absorbed on the temperature sensors. This problem of measuring the temperature of a transparent medium in the presence of solar radiation was satisfactorily resolved by using a thermocouple of 0.0127 mm thick foil with a butt-bonded junction, 0.254 mm wide (Omega, C02-T). The foil thermocouple junction was attached to the glass by a thin film of clear silicone rubber adhesive. The reasoning behind using an unshielded thin foil thermocouple to measure cover temperature was that the small amount of solar radiation intercepted by the foil is easily dissipated into the glass with a

negligible temperature rise. Tests confirmed that the temperature difference between the same foil thermocouple, shaded and unshaded from normal solar radiation, was less than 1 C.

Variations in the absorber plate temperature occur as a result of internal air stratification and edge losses. As a result of this, the temperature of the absorber plate for both collectors was measured in the center of the lower, middle, and upper third sections. Since some collectors cannot be disassembled to install thermcouples on the backside of the absorber without damaging the collector, a spring loaded thermocouple probe was developed as shown in Fig. 2.2. The design of this probe is such that the same probe can be used for collectors with different thicknesses of back-side insulation. The thermocouple probe is mounted on the collector by drilling a 10 mm hole in the back-side cover and using a gasket cutter to remove a 10 mm diameter core of the glass fiber insulation. The probe, with heat transfer compound on the tip, is then inserted into the hole and fastened to the back-side sheet metal cover. The spring tension is adjusted to provide a nominal contact pressure of the probe's tip against the absorber. The probe's tip is constructed of a 25 mm long dowel of polyletrafluoroethylene to minimize heat conduction through the probe to ambient and thus sensing a lower than actual absorber plate temperature.

The environmental conditions and collector temperatures were recorded continuously all day. The tilt angle of the test rack was periodically adjusted so that the incident angle of beam solar radiation at solar noon was always less than 7.5 degrees.

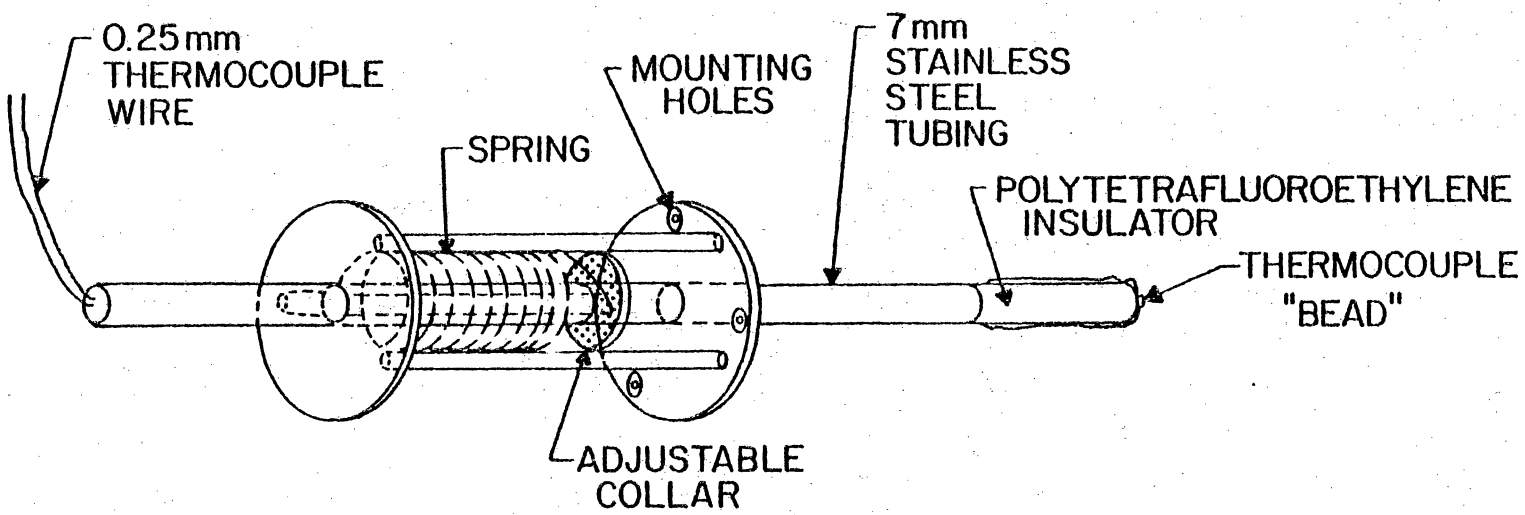

Fig. 2.2 Spring-Loaded Thermocouple Probe Used to Measure the Absorber Plate Temperature from the Backside

2.3 Off-Campus Testing

In addition to the data collected at VPI&SU, stagnation temperature data from an indoor solar simulator test facility at test site 5 and all-day outdoor data from the test facility at test site 4 were used in the investigation. Although the data from test sites 4 and 5 are not as detailed as that from the VPI&SU facilities, the additional data were important for validating the analytical model for other types of collectors and for tests conducted with a solar simulator. The dimensions and heat transfer properties of the four additional collectors (A, B, E, H) tested at test sites 4 and 5 are in Table 2.1. Cover plate temperatures were not measured at test site 4 or 5 and the absorber plate temperature was measured only at the center of the absorber plate. In addition, the diffuse fraction of solar irradiance and sky temperature were not measured at test site 4. The solar simulator used at test site 5 is composed of seven hexagonal modules containing 25 kW Xenon lamps, an aconic reflector, a spectral filter, and a collimator [40]. The irradiance produced by this simulator has a uniformity of $\pm$ 10 per cent and a beam divergence angle of $\pm$ 1.75 degrees. Data obtained from test site 5 were recorded at 5-minute intervals and the data from test site 4 were recorded continuously on strip charts.

The data from the experimental facilities were used mainly to validate analytical models used to predict stagnation temperatures. These models are developed in the next chapter.

3. ANALYSIS

This chapter develops analytical models for determining steady-state and transient stagnation temperatures in solar collectors. In addition, an approximate model for determining the two-dimensional temperature distribution on the absorber plate as a result of edge losses is developed. Finally, a parameter estimation method is developed for determining input parameters to the analytical models when these parameters are unknown or subject to much uncertainty.

This chapter deals specifically with modeling component temperatures of solar collectors in a stagnation mode as opposed to a normal operating mode. A solar collector in a stagnation mode has no energy removed from the collector by a working fluid. The stagnation temperature of the absorber plate, cover plate(s), back-side insulation, and back-side cover is modeled in this chapter. The first section deals with modeling steady-state component temperatures in solar collectors.

3.1 Solar Collector Steady-State Model

A steady-state model is needed to predict stagnation temperatures of collector components for sensitivity studies, material selection, and long-term durability studies. The following analysis is for flat-plate non-concentrating solar collectors of conventional design (i.e., no convection suppressing "honeycomb" grids or "accordian" folds, curved covers, or reflection devices).

Assumptions

The following assumptions are used:

1. One-dimensional heat transfer occurs through the covers and back-side insulation.
2. Steady-state conditions exist.
3. Cover surfaces obey ideal optic laws.
4. Solar radiation reflected off the absorber plate is diffuse.
5. All surfaces are diffuse-gray for infrared radiation.
6. Component surface and thermal properties are not temperature dependent.
7. Thermal conductive resistances of the absorber and covers are negligible.

Energy Balance

The stagnation temperatures of the primary collector components are obtained by performing energy balances on each of the N components. The result gives a system of N simultaneous non-linear algebraic equations which may be solved by an appropriate mathematical technique. The energy terms and the overall configuration of a two-cover collector are shown in Fig. 3.1. The following analysis is for a two-cover collector. The one-cover collector analysis is similar and is briefly described in Appendix B. Energy balances on the absorber plate, inside cover (No. 1), and outside cover (No. 2) give

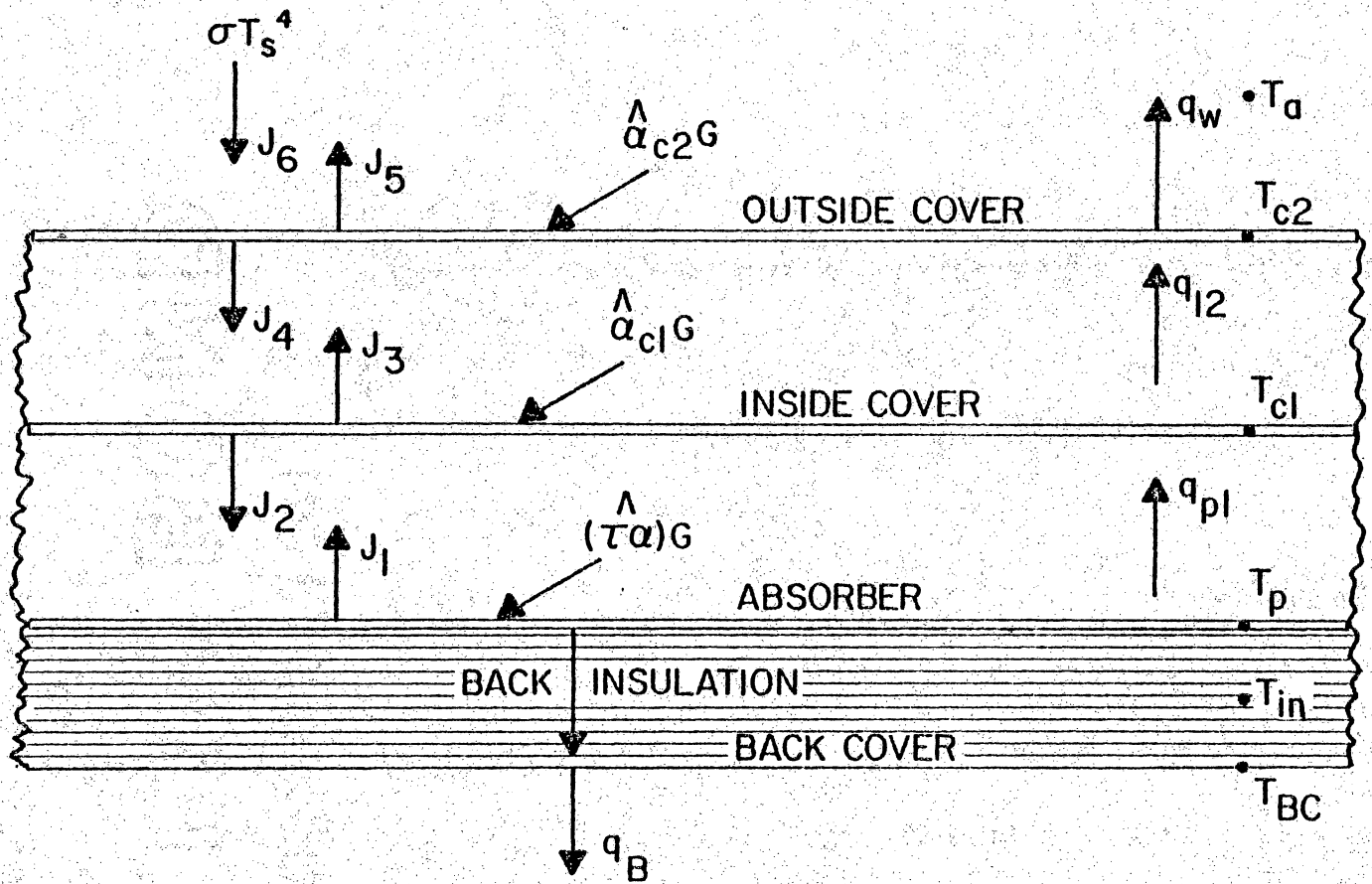

Fig. 3.1 Energy Balance Nomenclature for a Two-Cover Flat-Plate Solar Collector in a Stagnating Mode

$$(\hat{\tau\alpha})G + J_2 = q_{p1} + q_B + J_1 \tag{3.1}$$

$$(\hat{\alpha}_1)G + J_4 + J_1 + q_{p1} = J_3 + J_2 + q_{12} \tag{3.2}$$

$$(\hat{\alpha}_2)G + J_6 + J_3 + q_{12} = J_5 + J_4 + q_w \tag{3.3}$$

Introducing a convection heat transfer coefficient and a back-side loss coefficient, Eqs. 3.1-3.3 can be arranged as

$$(h_{p1} + U_B)\ T_p - h_{p1}\ T_{c1} = (\hat{\tau\alpha})G + J_2 - J_1 + U_B T_a \tag{3.4}$$

$$-h_{12}T_p + (h_{p1} + h_{12})\ T_{c1} - h_{12}T_{c2} = (\hat{\alpha}_1)G + J_1 + J_4 - J_2 - J_3 \tag{3.5}$$

$$-h_{12}T_{c1} + (h_{12} + h_w)T_{c2} = (\hat{\alpha}_2)G + J_3 + J_6 - J_4 - J_5 + h_w T_a \tag{3.6}$$

Equations 3.4-3.6 are highly non-linear because h_{p1} and h_{12}, U_B, and $J_1 - J_5$ are all functions of T_p, T_{c1}, and T_{c2}. The expressions for h_{p1}, h_{12}, h_w, U_B, $(\hat{\tau\alpha})$, $(\hat{\alpha}_1)$, $(\hat{\alpha}_2)$, and $J_1 - J_6$ are developed in the following sections.

Free Convection Coefficients

The free convection coefficients are needed in order to calculate the heat transfer between the absorber and inside cover and between the inside and outside cover. Many relevant studies dealing with free convection have been made and the results are found in references

21-31. The investigations by Hollands, et al. [27, 28, 29, 31] agree within 5 per cent of experimental data and are the most recently cited work in the literature. Therefore, the following correlation by Hollands is used in this investigation.

$$Nu = 1 + 1.44\left[1 - \frac{1708}{Ra\cos\beta}\right]^{\cdot}\left[1 - \frac{1708(\sin 1.8\beta)^{1.6}}{Ra\cos\beta}\right] + \left[\left(\frac{Ra\cos\beta}{5830}\right)^{1/3} - 1\right]^{\cdot} \tag{3.7}$$

where the dotted square brackets, $[\ ]^{\cdot}$, indicate that if the quantity inside the brackets is negative, the quantity is to be taken as zero, i.e., $[X]^{\cdot} = (X + |X|)/2$. The above dimensionless correlation equation has been experimentally verified [30] for inclined parallel planes, heated from below, at inclination angles of 0 to 60 degrees from horizontal. Also, the aspect ratio of the length or width of the collector divided by the air space thickness should be greater than 20 and Ra should be less than 10^5 for Eq. 3.7 to be valid. Equation 3.7 is expected to be valid for inclination angles up to 75° and $Ra > 10^5$, but experimental verification is lacking. In general, Holland's work applies directly to usual collector designs in terms of aspect ratios, Ra ranges, and inclination angles. Finally, the free convection coefficient, h, is obtained from the Nusselt number in Eq. 3.7.

$$h = Nu\ k/d \tag{3.8}$$

External Wind Coefficient

The external wind coefficient, h_w, accounts for both free and forced convection mechanisms. The importance of each mechanism depends on the wind speed, V_w. McAdams [32] suggests a correlation of the form

$$h_w = [a + b\ (V_w\ s/m)^n]\ \ W/m^2C \tag{3.9}$$

with a = 5.7, b = 3.8, and n = 1 for flow over smooth surfaces with $V_w \leq 5$ m/s. It has been pointed out in the recent literature [33, 34] that Eq. 3.9 is limited in determining h_w because this expression neglects the effects of wind direction, collector dimensions, and air temperature. In fact, Sparrow [34] recommends the following relation

$$h_w = 0.86\ k\ Re_{L_c}^{1/2}\ Pr^{1/3}/L_c \tag{3.10}$$

A difficulty with Eq. 3.10, however, is that free convection is neglected when the wind speed is zero. Since Eq. 3.9 is used extensively in the literature and accounts for free convection, at least approximately, it is used in this analysis.

Back Loss Coefficient

The back loss coefficient is obtained by considering one-dimensional heat conduction through the back-side insulation to the ambient air. The expression for U_B is

$$U_B = [\delta_{in}/k_{in} + 1/(h_w + h_r)]^{-1} \tag{3.11}$$

where $h_r = \varepsilon_{BC}\,\sigma\,(T_{BC}^2 + T_a^2)\,(T_{BC} + T_a)$ and the environmental temperature, in this case, is the ambient temperature.

By using U_B, the mid-point temperature of the back-side insulation and the temperature of the back-side cover are

$$T_{in} = T_p - 0.5\,U_B\delta_{in}(T_p - T_a)/k_{in} \tag{3.12}$$

$$T_{BC} = T_p - U_B\delta_{in}(T_p - T_a)/k_{in} \tag{3.13}$$

The mid-point temperature of the back-side insulation represents the average temperature of the insulation and is used as the temperature of the insulation node in the transient analysis.

Optical Properties and Solar Radiosity Analysis

Expressions for the transmittance-absorptance product, $(\hat{\tau\alpha})$, and the solar absorptance of the covers, $(\hat{\alpha}_1)$ and $(\hat{\alpha}_2)$, are essentially from Appendix A of Ramsey, et al. [35]. These authors used a generalized radiosity approach to determine the short wave properties of the absorber and cover system. The specular transmittance of a given cover is found by averaging the two components (perpendicular and parallel) of radiation,

$$\hat{\tau} = (\hat{\tau}_m + \hat{\tau}_n)/2 \tag{3.14}$$

where

$$\hat{\tau}_m = \tau_a\,(1 - r_m)^2/(1 - \tau_a^2\,r_m^2) \tag{3.15}$$

$$\hat{\tau}_n = \tau_a (1 - r_n)^2/(1 - \tau_a^2 r_m^2) \tag{3.16}$$

$$r_m = \sin^2 (\theta_2 - \theta)/\sin^2 (\theta_2 + \theta) \tag{3.17}$$

$$r_n = \tan^2 (\theta_2 - \theta)/\tan^2 (\theta_2 + \theta) \tag{3.18}$$

$$\theta_2 = \text{arc sin } [(\sin \theta)/\hat{n}] \tag{3.19}$$

$$\tau_a = \exp (-\hat{\kappa}\delta_c/\cos \theta_2) \tag{3.20}$$

Similarly, the specular reflectance of a given cover is

$$\hat{\rho} = (\hat{\rho}_m + \hat{\rho}_n)/2 \tag{3.21}$$

where

$$\hat{\rho}_m = r_m[1 + \tau_a^2(1 - r_m)^2/(1 - \tau_a^2 r_m^2)] \tag{3.22}$$

$$\hat{\rho}_n = r_n[1 + \tau_a^2 (1 - r_m)^2/(1 - \tau_a^2 r_m^2)] \tag{3.23}$$

The fraction of solar radiation absorbed in a given cover is

$$\hat{\alpha} = 1 - \hat{\tau} - \hat{\rho} \tag{3.24}$$

The short wave diffuse cover properties, $\hat{\tau}_d$, $\hat{\rho}_d$, and $\hat{\alpha}_d$ are obtained by numerically integrating Eqs. 3.14 and 3.21 by the following weighted integrals:

$$\hat{\tau}_d = \int_0^{\frac{\pi}{2}} \hat{\tau}(\theta) \sin (2\theta)\, d\theta \tag{3.25}$$

$$\hat{\rho}_d = \int_0^{\frac{\pi}{2}} \hat{\rho}(\theta) \sin(2\theta)\, d\theta \tag{3.26}$$

and the identity $\hat{\alpha}_d = 1 - \hat{\tau}_d - \hat{\rho}_d$.

For a two-cover and absorber system, the radiosity distribution is shown in Fig. 3.2. The left-hand side radiosities are for beam radiation and the right-hand side radiosities are for diffuse radiation. With the assumption that the absorber is a diffuse reflector, $\hat{J}_{b1}$ is zero. The following equations relate the short-wave beam and diffuse radiosities:

$$\hat{J}_{b1} = 0 \tag{3.27}$$

$$\hat{J}_{b2} = \hat{\tau}_1 \hat{J}_{b4} + \hat{\rho}_1 \hat{J}_{b1} \tag{3.28}$$

$$\hat{J}_{b3} = \hat{\tau}_1 \hat{J}_{b1} + \hat{\rho}_1 \hat{J}_{b4} \tag{3.29}$$

$$\hat{J}_{b4} = \hat{\tau}_2 (1 - \eta_d) + \hat{\rho}_2 \hat{J}_{b3} \tag{3.30}$$

$$\hat{J}_{b5} = \hat{\tau}_2 \hat{J}_{b3} + \hat{\rho}_2 (1 - \eta_d) \tag{3.31}$$

$$\hat{J}_{d1} = (1 - \hat{\alpha}_p) \hat{J}_{d2} + (1 - \hat{\alpha}_p) \hat{J}_{b2} \tag{3.32}$$

$$\hat{J}_{d2} = \hat{\tau}_{d1} \hat{J}_{d4} + \hat{\rho}_{d1} \hat{J}_{d1} \tag{3.33}$$

$$\hat{J}_{d3} = \hat{\tau}_{d1} \hat{J}_{d1} + \hat{\rho}_{d1} \hat{J}_{d4} \tag{3.34}$$

$$\hat{J}_{d4} = \hat{\tau}_{d2} \eta_d + \hat{\rho}_{d2} \hat{J}_{d3} \tag{3.35}$$

$$\hat{J}_{d5} = \hat{\tau}_{d2} \hat{J}_{d3} + \hat{\rho}_{d2} \eta_d \tag{3.36}$$

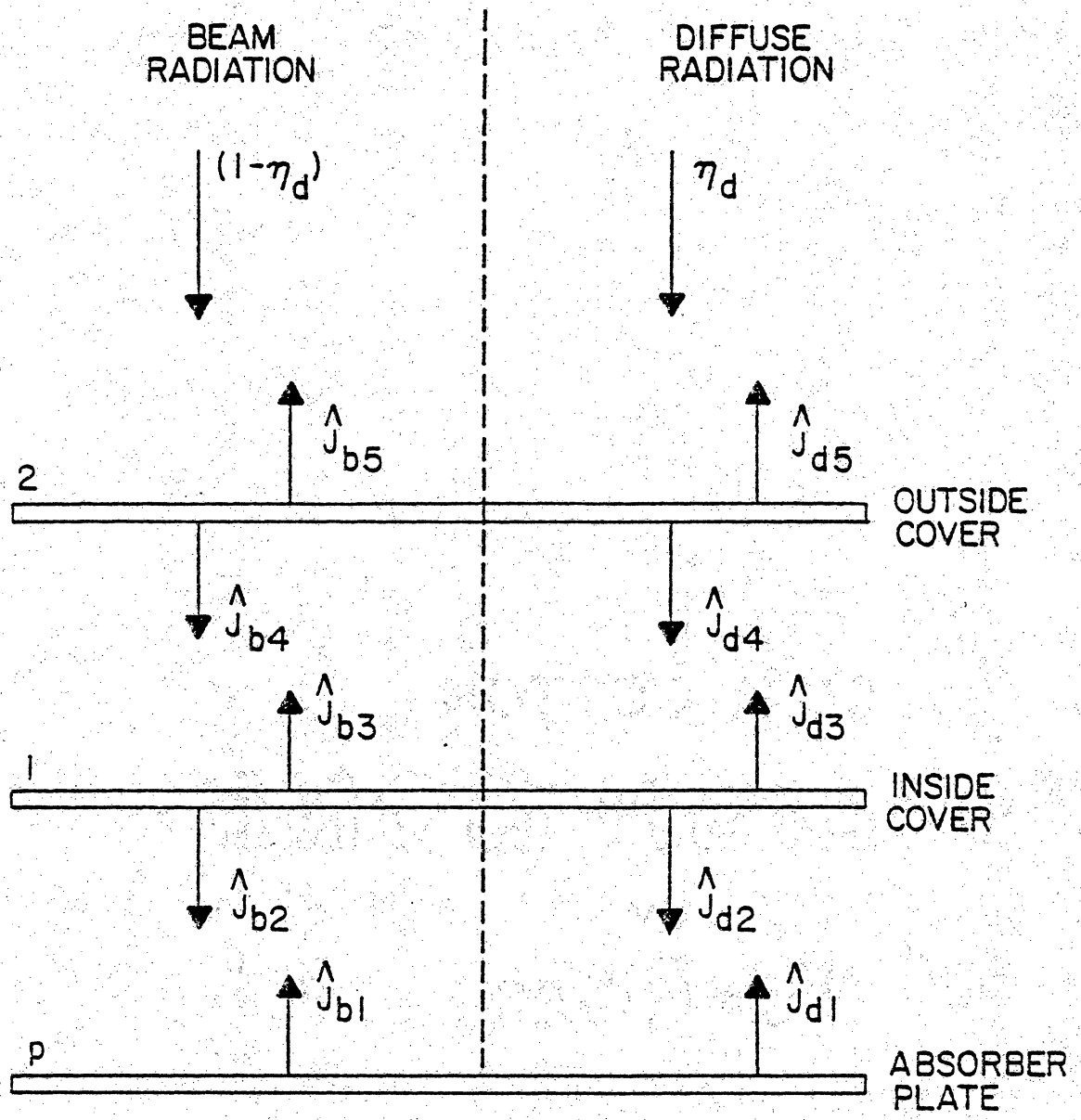

Fig. 3.2 Solar Wavelength Radiosity Distributions in a Two-Cover Collector

Equations 3.27-3.31 are solved simultaneously and the value for $\hat{J}_{b2}$ is inserted into Eq. 3.32, thus permitting Eqs. 3.32-3.36 to be solved simultaneously. The values for the short-wave radiosities are then used to calculate $(\hat{\tau\alpha})$, $(\hat{\alpha}_1)$, and $(\hat{\alpha}_2)$ as follows:

$$(\hat{\tau\alpha}) = \hat{J}_{b2} + \hat{J}_{d2} - \hat{J}_{d1} \tag{3.37}$$

$$(\hat{\alpha}_1) = \hat{J}_{b4} - \hat{J}_{b2} - \hat{J}_{b3} + \hat{J}_{d1} + \hat{J}_{d4} - \hat{J}_{d2} - \hat{J}_{d3} \tag{3.38}$$

$$(\hat{\alpha}_2) = 1 + \hat{J}_{b3} - \hat{J}_{b4} - \hat{J}_{b5} + \hat{J}_{d3} - \hat{J}_{d4} - \hat{J}_{d5} \tag{3.39}$$

Infrared Radiosity Analysis

A radiosity method, rather than the network analogy, must be used to calculate the radiation heat transfer when a surface is partially transparent to infrared radiation. Figure 3.3 shows the radiosities to be determined. The following equations relate the infrared radiosities:

$$J_1 = \varepsilon_p \sigma T_p^4 + (1 - \varepsilon_p) J_2 \tag{3.40}$$

$$J_2 = \varepsilon_{c1} \sigma T_{c1}^4 + \rho_{c1} J_1 + \tau_{c1} J_4 \tag{3.41}$$

$$J_3 = \varepsilon_{c1} \sigma T_{c1}^4 + \rho_{c1} J_4 + \tau_{c1} J_1 \tag{3.42}$$

$$J_4 = \varepsilon_{c2} \sigma T_{c2}^4 + \rho_{c2} J_3 + \tau_{c2} J_6 \tag{3.43}$$

$$J_5 = \varepsilon_{c2} \sigma T_{c2}^4 + \rho_{c2} J_6 + \tau_{c2} J_3 \tag{3.44}$$

$$J_6 = \sigma T_S^4 \tag{3.45}$$

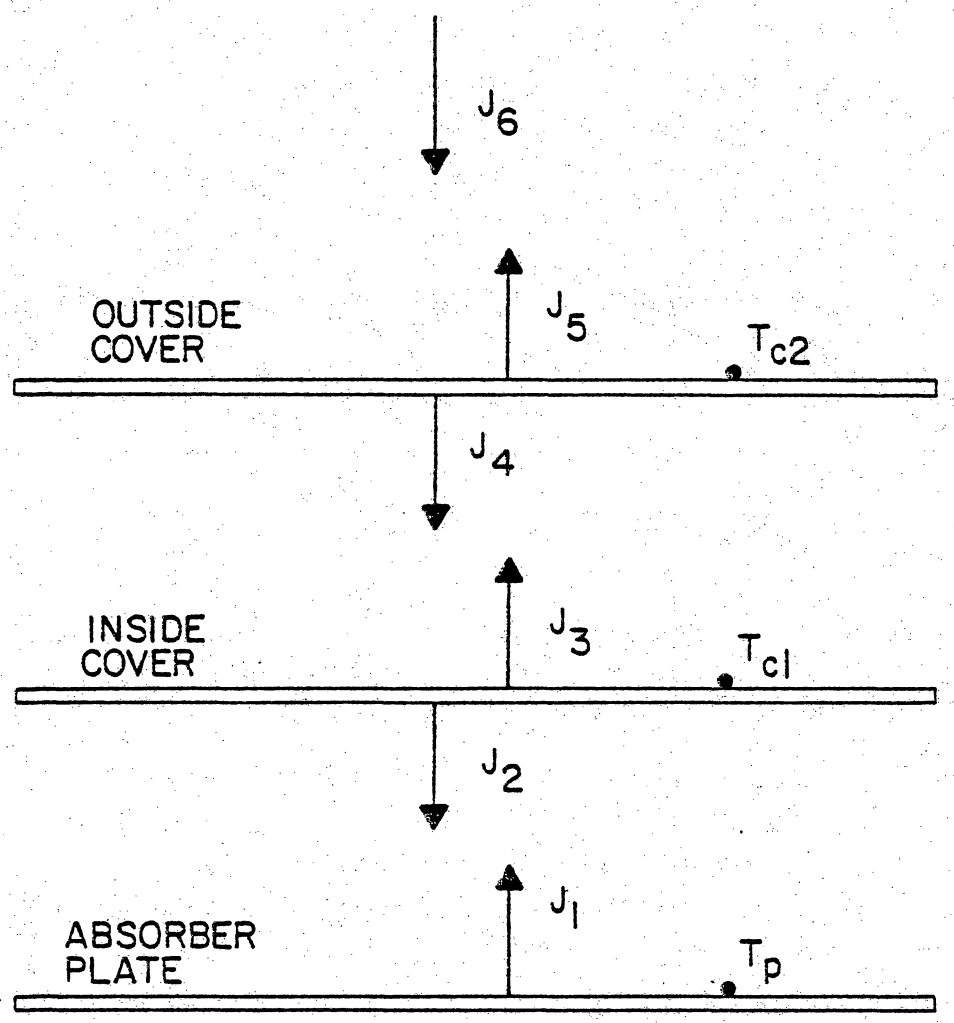

Fig. 3.3 Infrared Radiosity Distributions in a Two-Cover Collector

For specified temperatures T_p, T_{c1}, T_{c2}, and T_s Eqs. 3.40-3.45 can be solved simultaneously to determine the infrared radiation distribution. The resulting values are then used in the preceding energy balances.

Solution Technique

To solve Eqs. 3.4-3.6 for T_p, T_{c1}, and T_{c2}, a successive substitution iterative approach is employed because of the nonlinearity in these equations. The solar optical properties $(\hat{\tau\alpha})$, $(\hat{\alpha}_1)$, and $(\hat{\alpha}_2)$ are obtained first because these values are not functions of temperature and will not change during the iterative process. Next, an initial estimate for the temperature of each component is assumed. Using the initial temperature estimates, the infrared radiosities, free convection coefficients, and the back loss coefficient can be calulated. Equations 3.4-3.6 can be considered linear using these temperature estimates and a standard Gauss elimination technique is then used to solve these equations for improved estimates of the component temperatures.

The current component temperatures are then compared with the previous estimates. If the difference is greater than the specified accuracy, then a combination of the old estimate and the updated temperature is applied in the following manner to obtain a new estimate.

$$T_{new} = (1 - \gamma)\, T_{update} + \gamma T_{old} \tag{3.46}$$

where γ is a damping factor ($0 \leq \gamma \leq 1$). A damping factor is necessary to avoid potential stability problems resulting from inappropriate initial estimates. The calculation procedure is repeated until changes in component temperature are within a prescribed convergence requirement (0.05 K is typically used). These new estimates are used to recalculate values for $J_1 - J_6$, h_{p1}, h_{12}, and U_B and Eqs. 3.4-3.6 are solved again. The process is repeated until convergence occurs.

The next section deals with the transient behavior of a solar collector in a stagnating mode. The transient equations are similar to the steady-state equations except the heat capacities of the components are taken into account and a time-marching solution technique is used.

3.2 Solar Collector Transient Model

Clear-day solar radiation incident on a fixed-mount collector is inherently an unsteady phenomenon and variations in cloud cover result in strong transients. Therefore, a transient model is needed to predict all-day collector stagnation temperatures.

Assumptions

The same assumptions used in the steady-state collector analysis are included in the transient collector analysis. It is also assumed in the transient analysis that the component heat capacities do not vary with temperature and a lumped-heat-capacity model for each component is valid.

Energy Balance

An energy balance, similar to the steady-state energy balance, is performed on a two-cover collector with an energy storage term included for each component. These energy balances on the absorber plate, two covers, back-side insulation, and back-side cover lead to the following differential equations:

$$(\hat{\tau\alpha})G + J_2 - J_1 - h_{p1}\,(T_p - T_{c1}) - 2k_{in}\,(T_p - T_{in})/\delta_{in} = m_p\,C_p\,dT_p/dt \qquad (3.47)$$

$$(\hat{\alpha}_1)G + J_1 + J_4 + h_{p1}\,(T_p - T_{c1}) - J_2 - J_3 - h_{12}\,(T_{c1} - T_{c2}) = m_{c1}\,C_{c1}\,dT_{c1}/dt \tag{3.48}$$

$$(\hat{\alpha}_2)G + J_3 + J_6 + h_{12}\,(T_{c1} - T_{c2}) - J_4 - J_5 - h_w\,(T_{c2} - T_a) = m_{c2}\,C_{c2}\,dT_{c2}/dt \tag{3.49}$$

$$2k_{in}(T_p - T_{in})/\delta_{in} - 2k_{in}\,(T_{in} - T_{BC})/\delta_{in} = m_{in}\,C_{in}\,dT_{in}/dt \tag{3.50}$$

$$2k_{in}\,(T_{in} - T_{BC})/\delta_{in} - (h_w + h_r)(T_{BC} - T_a) = m_{BC}C_{BC}\,dT_{BC}/dt \tag{3.51}$$

Equations 3.47-3.51 are solved by a well-known time marching technique. The numerical integration technique used is a second-order Runge-Kutta method called Heun's method [39]. The simultaneous first-order non-linear ordinary differential equations to be solved are of the general form

$$d\vec{T}/dt = \vec{F}(\vec{T},t) \tag{3.52}$$

where $\vec{T}$ is a vector of collector component temperatures. In the Huen method, the temperatures are computed at $t + \Delta t$ in the following manner.

$$\vec{T}_{i+1} = \vec{T}_i + 0.5\,\Delta t[\vec{F}(\vec{T}_i,t) + \vec{F}(\vec{T}_i + \Delta t\vec{F}(\vec{T}_i,t),\ t + \Delta t)] \tag{3.53}$$

where $\vec{T}_i$ is the temperature vector at time, t, and $\vec{T}_{i+1}$ is the temperature vector at time, $t + \Delta t$. Caution must be exercised in the selection of a time step, Δt, in order to avoid cumulative integration errors and solution instability. The determination of a time step, Δt,

can be obtained in practice by choosing a reasonable time step for a given application and reducing the time step by increments of one-half until the temperature solution changes less than a specified amount. Difficulties arise when modeling a solar collector having components with relatively small heat capacities. Examples of these problems include thin plastic films for covers and thin metal foil for the back-side cover. These problems can be solved, at the expense of excessive computer time, by making the time step very small or by neglecting the thermal capacity of that component and solving directly for the temperature of the component at each time step.

The required component material properties and dimensions along with the environmental conditions during the simulation are needed as inputs to the model. A linear interpolation routine is used to estimate environmental conditions when the integration time step does not coincide with the environmental data input interval. A typical input interval for environmental data is five or more minutes while the integration time step in the model is typically one minute or less.

3.3 Absorber Plate Temperature Distribution

One of the assumptions used in the steady-state and transient stagnation temperature models is that the edge losses can be uniformly distributed over the absorber plate. In practice, one effect of edge losses is to significantly lower the temperatures in the perimeter area of the absorber. This temperature variation can lead to difficulties in experimentally determining the mean absorber plate temperature by using only a few temperature sensors. The following analysis takes into account edge losses in determining the steady-state absorber plate temperature distribution for a stagnating collector. With this temperature distribution known, a value for the mean absorber plate temperature can be calculated. Figure 3.4 defines the coordinate system, differential element, and nomenclature for the following analysis.

Assumptions

1. Edge losses are concentrated along the edge of the absorber plate.
2. Temperature variation in the z direction is neglected.
3. Symmetry exists about both centerlines of the absorber plate.
4. Heat losses from the top and back-side of the collector can be combined into an overall loss coefficient, U_L, which is temperature independent. (The value of U_L would be based on the center absorber plate temperature.)

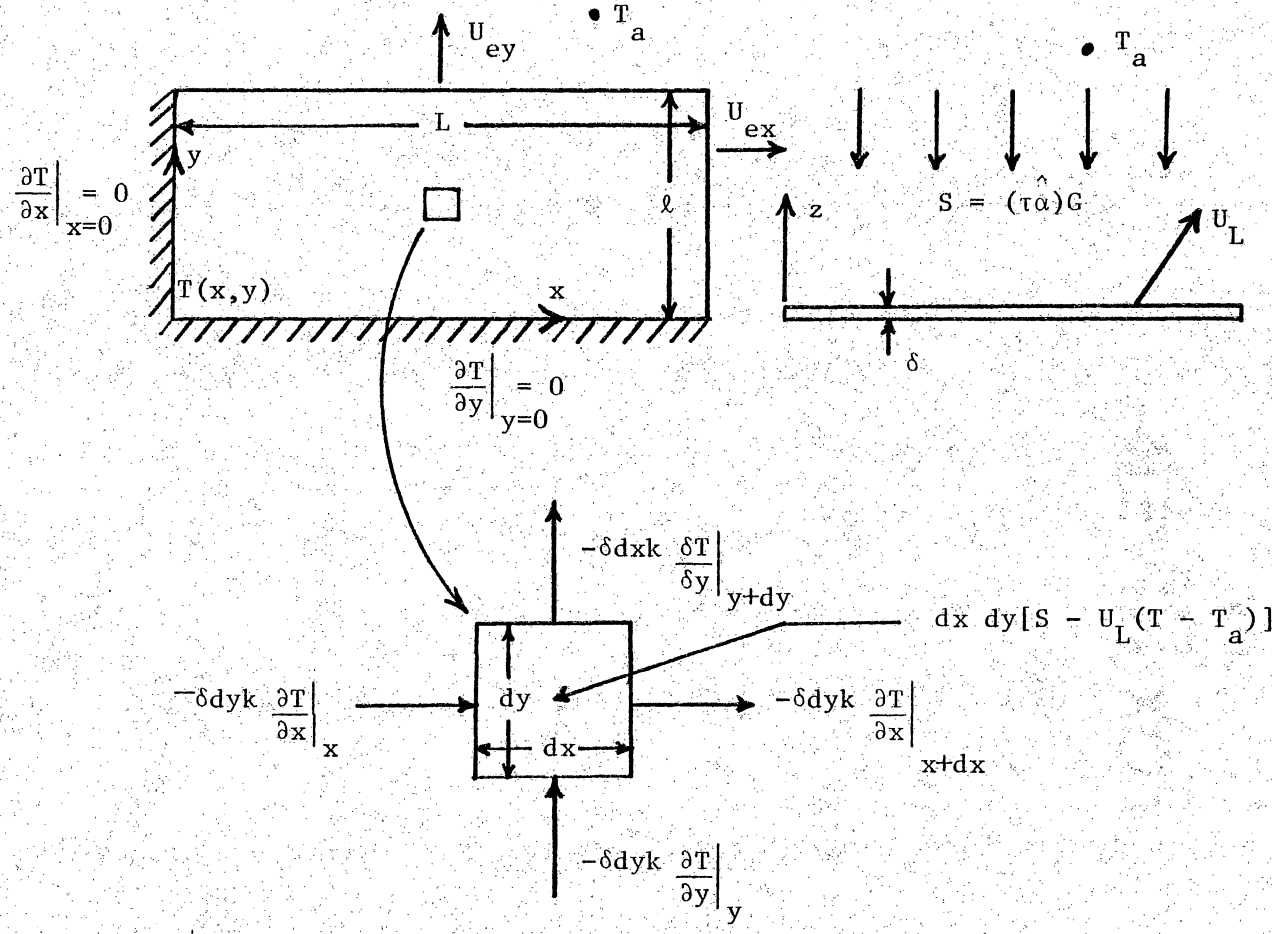

Fig. 3.4 Nomenclature and Differential Element Energy Balance for Determining the Two-Dimensional Absorber Plate Stagnation Temperature Distribution

Energy Balance

An energy balance on the differential element in Fig. 3.4 results in the following partial differential equation

$$\frac{\partial^2 T}{\partial x^2} + \frac{\partial^2 T}{\partial y^2} - m^2 T = - m^2 S/U_L - m^2 T_a \tag{3.54}$$

where

$$m^2 = U_L/(k_p \delta_p).$$

The associated boundary conditions for Eq. 3.54 are

$$\frac{\partial T}{\partial x}(0,y) = 0 \tag{3.55}$$

$$\frac{\partial T}{\partial y}(x,0) = 0 \tag{3.56}$$

$$\frac{\partial T}{\partial x}(L,y) + (U_{ex}/k_p)\, T\,(L,y) = (U_{ex}/k_p)T_a \tag{3.57}$$

$$\frac{\partial T}{\partial y}(x,\ell) + (U_{ey}/k_p)\, T\,(x,\ell) = (U_{ey}/k_p)T_a \tag{3.58}$$

To make Eq. 3.54 homogeneous, the following substitution is made

$$\theta = T - T_a - S/U_L \tag{3.59}$$

Equations 3.54-3.58 then become

$$\frac{\partial^2 \theta}{\partial x^2} + \frac{\partial^2 \theta}{\partial y^2} - m^2\, \theta = 0 \tag{3.60}$$

$$\frac{\partial \theta}{\partial x}(0,y) = 0 \tag{3.61}$$

$$\frac{\partial \theta}{\partial y}(x,0) = 0 \tag{3.62}$$

$$\frac{\partial \theta}{\partial x}(L,y) + (U_{ex}/k_p)\,\theta\,(L,y) = -\,U_{ex}\,S/(U_L k_p) \tag{3.63}$$

$$\frac{\partial \theta}{\partial y}(x,\ell) + (U_{ey}/k_p)\,\Theta\,(x,\ell) = -\,U_{ey}\,S/(U_L k_p) \tag{3.64}$$

To reduce the number of non-homogeneous boundary conditions to one and thus permit a solution by separation-of-variables, the method of superposition is employed. Let

$$\Theta(x,y) = \theta_1(x,y) + \theta_2(x,y) \tag{3.65}$$

The boundary conditions on θ_1 and θ_2 can be selected so that the resulting two problems in θ_1 and θ_2 have a single non-homogeneous boundary condition each. The governing equations and boundary conditions for θ_1 and θ_2 are

$$\frac{\partial^2 \theta_1}{\partial x^2} + \frac{\partial^2 \theta_1}{\partial y^2} - m^2\,\theta_1 = 0 \tag{3.66}$$

$$\frac{\partial \theta_1}{\partial x}(0,y) = 0 \tag{3.67}$$

$$\frac{\partial \theta_1}{\partial y}(x,0) = 0 \tag{3.68}$$

$$\frac{\partial \theta_1}{\partial x}(L,y) + (U_{ex}/k_p)\,\theta_1\,(L,y) = 0 \tag{3.69}$$

$$\frac{\partial \theta_1}{\partial y}(x,\ell) + (U_{ey}/k_p)\,\theta_1\,(x,\ell) = \psi_y\,S/(U_L \ell) \tag{3.70}$$

and

$$\frac{\partial^2\theta_2}{\partial x^2} + \frac{\partial^2\theta_2}{\partial y^2} - m^2\,\theta_2 = 0 \tag{3.71}$$

$$\frac{\partial\theta_2}{\partial x}(0,y) = 0 \tag{3.72}$$

$$\frac{\partial\theta_2}{\partial y}(x,0) = 0 \tag{3.73}$$

$$\frac{\partial\theta_2}{\partial x}(L,y) + (U_{ex}/k_p)\,\theta_2\,(L,y) = \psi_x\, S/(U_L L) \tag{3.74}$$

$$\frac{\partial\theta_2}{\partial y}(x,\ell) + (U_{ey}/k_p)\,\theta_2\,(x,\ell) = 0 \tag{3.75}$$

where

$$\psi_x = U_{ex}\, L/k_p \tag{3.76}$$

$$\psi_y = U_{ey}\, \ell/k_p \tag{3.77}$$

Omitting the details in the separation-of-variables procedure, the following solutions are obtained:

$$\theta_1(x,y) = -4 \sum_{n=1}^{\infty} \frac{\psi_y (S/U_L)\,\sin(\lambda_n L)\cos(\lambda_n x)\cosh(\beta_n y)}{(\lambda_n L)[(\beta_n \ell)\sinh(\beta_n \ell)+\psi_y \cosh(\beta_n \ell)]\dfrac{[2+\sin 2(\lambda_n L)]}{(\lambda_n L)}} \tag{3.78}$$

$$\theta_2(x,y) = -4 \sum_{n=1}^{\infty} \frac{\psi_x (S/U_L)\,\sin(\xi_n \ell)\cos(\xi_n y)\cosh(\gamma_n x)}{(\xi_n \ell)[(\gamma_n L)\sinh(\gamma_n L)+\psi_x \cosh(\gamma_n L)]\dfrac{[2+\sin 2(\xi_n \ell)]}{(\xi_n \ell)}} \tag{3.79}$$

where λ_n and ξ_n are the solutions to the following equations

$$(\lambda_n L) \tan (\lambda_n L) = \psi_x \quad n = 1, 2, 3, \ldots \tag{3.80}$$

$$(\xi_n \ell) \tan (\varepsilon_n \ell) = \psi_y \quad n = 1, 2, 3, \ldots \tag{3.81}$$

$$\beta_n^2 = m^2 + \lambda_n^2 \tag{3.82}$$

$$\gamma_n^2 = m^2 + \xi_n^2 \tag{3.83}$$

Finally, the temperature distribution is

$$T(x,y) = T_a + S/U_L + \theta_1 (x,y) + \theta_2(x,y) \tag{3.84}$$

The mean absorber plate temperature is

$$T_{pm} = (\ell L)^{-1} \int_0^L \int_0^\ell T(x,y)\, dydx \tag{3.85}$$

It is interesting to note that the absorber temperature distribution and the mean plate temperature at a given solar radiation and overall loss coefficient are only a function of the two parameters ψ_x and ψ_y. A difficulty exists in obtaining values for ψ_x and ψ_y because effective values of U_{ex} and U_{ey} are difficult to determine from collector design information. If experimental data are available on the temperature distribution of the absorber plate, a parameter estimation method can obtain estimates for ψ_x and ψ_y. Only a few temperature measurements would be needed to characterize the collector and obtain values for these parameters since the parameters do not change with temperature. The next section deals with the development of a

parameter estimation algorithm to estimate these and other important collector parameters.

3.4 Parameter Estimation

Parameter estimation theory is a useful method for determining input parameters for analytical models when these parameters are unknown or subject to much uncertainty. There are several methods currently employed for parameter estimation including the gradient method, second-order (Gauss-Newton) algorithm, and the Gaussian least-square-differential-correction (LSDC) algorithm. References 36 and 37 recommend the Gaussian LSDC algorithm over the other methods because it converges better. The LSDC algorithm is, therefore, chosen for this analysis.

Gaussian Least-Square-Differential-Correction

The Gaussian LSDC method was developed by Gauss [38] in 1809 and employed to determine planetary orbits. This nonlinear method is a generalization of Newton's method for finding roots of equations in the form

$$\vec{y} - \vec{F}(\vec{x}) = \vec{0} \tag{3.86}$$

The following formulation of the LSDC method is based on using measured stagnation temperature to estimate effective collector parameters such as heat capacity, edge loss coefficient, etc. Assume that the stagnation temperature can be modeled as

$$T_j = F_j(x_1, x_2, \ldots, x_n, u_1, u_2, \ldots, u_\ell); \; j = 1, 2, 3, \ldots m; \quad m > n \tag{3.87}$$

where T_j are m calculated temperatures of collector components and F_j are m arbitrary independent functions of the unknown parameters, x_i, and known parameters, u_i. For example, F_j would be the analytical models of Sections 3.1, 3.2, and 3.3 with x_i possibly being α_p and k_{in}. In addition, F_j and all the partial derivatives with respect to x_i of F_j must be single-valued and continuous. Suppose that a set of measured temperatures

$$(\tilde{T}_1, \tilde{T}_2, \ldots, \tilde{T}_m) \tag{3.88}$$

are available corresponding to calculated temperatures T_j. Then the objective is to find a particular set of x-values

$$(\hat{x}_1, \hat{x}_2, \ldots, \hat{x}_n) \tag{3.89}$$

which minimizes the sum of squares of the residuals

$$\phi = \sum_{j=1}^{m} [\Delta T_j]^2 \tag{3.90}$$

where

$$\Delta T_j = \tilde{T}_j - F_j(x_1, x_2, \ldots, x_n, u_1, u_2, \ldots, u_\ell); \; j=1,2,3,\ldots m \tag{3.91}$$

Direct minimization of Eq. 3.90 by means of calculus to obtain an explicit closed form solution is not possible because of the complicated functions F_j. Therefore, a linearized successive approximation procedure designed to converge to accurate least-square estimates,

given approximate starting values, is used. Let the current estimates be

$$(x_{1c}, x_{2c}, \ldots, x_{nc}) \tag{3.92}$$

Let

$$\hat{x}_i = x_{ic} + \Delta x_i \quad ; \; i = 1, 2, \ldots n \tag{3.93}$$

where Δx_i is an unknown set of sufficiently small corrections which when added to the current estimates yield estimates which minimize the sum of squares of the residuals, ϕ.

The current residuals corresponding to the current estimates, x_{ic}, are

$$\Delta T_{jc} = \tilde{T}_j - F_j (x_{1c}, x_{2c}, \ldots, x_{nc}, u_1, u_2, \ldots, u_\ell); \quad j = 1, 2, \ldots, m \tag{3.94}$$

The linearly predicted residuals, ΔT_{jp}, after the correction, Δx_i, using a Taylor series expansion of Eq. 3.94 about x_{ic}, are

$$\Delta T_{jp} = \Delta T_{jc} - \sum_{i=1}^{n} \left(\frac{\partial F_j}{\partial x_i} \bigg|_c \right) \Delta x_i \quad ; \; j = 1, 2, \ldots, m \tag{3.95}$$

The objective is to now find the Δx_i's which minimize Eq. 3.90. Substitution of Eq. 3.95 into Eq. 3.90 yields

$$\phi_p = \sum_{j=1}^{m} \left[\Delta T_{jc} - \sum_{i=1}^{n} \left(\frac{\partial F_j}{\partial x_i} \bigg|_c \right) \Delta x_i \right]^2 \tag{3.96}$$

In order that the corrections Δx_i yield a minimum, the necessary conditions are

$$2 \sum_{j=1}^{m} [\Delta T_{jc} - \sum_{i=1}^{n} \left(\frac{\partial F_j}{\partial x_i} \right|_c \Delta x_i][- \left. \frac{\partial F_j}{\partial x_k} \right|_c] = 0; \; k=1,2,\ldots n \quad (3.97)$$

Rearranging

$$[\sum_{j=1}^{m} \left(\frac{\partial F_j}{\partial x_1} \right) \left(\frac{\partial F_j}{\partial x_k} \right)] \Delta x_1 + [\sum_{j=1}^{m} \left(\frac{\partial F_j}{\partial x_2} \right) \left(\frac{\partial F_j}{\partial x_k} \right)] \Delta x_2 + \ldots$$

$$+ [\sum_{j=1}^{m} \left(\frac{\partial F_j}{\partial x_n} \right) \left(\frac{\partial F_j}{\partial x_k} \right)] \Delta x_n = \sum_{j=1}^{m} \frac{\partial F_j}{\partial x_k} \Delta T_{jc} \; ; \; k = 1, 2, \ldots, n \quad (3.98)$$

The corrections Δx_1, Δx_2, ..., Δx_n are computed by a standard Gauss elimination process for a linear set of n equations and n unknowns. The parameter estimates are then improved, i.e.,

$$x'_{ic} = x_{ic} + \Delta x_i \; ; \; i = 1, 2, \ldots, n \quad (3.99)$$

where x'_{ic} is the improved current estimate.

Tests for convergence are usually based on achieving a negligible change in ϕ after updating or a negligibly small set of Δx_i's. The process is summarized in block diagram form in Fig. 3.5.

Practical Considerations

The LSDC method is not free from convergence difficulties. The initial parameter estimates may need to be relatively close to the

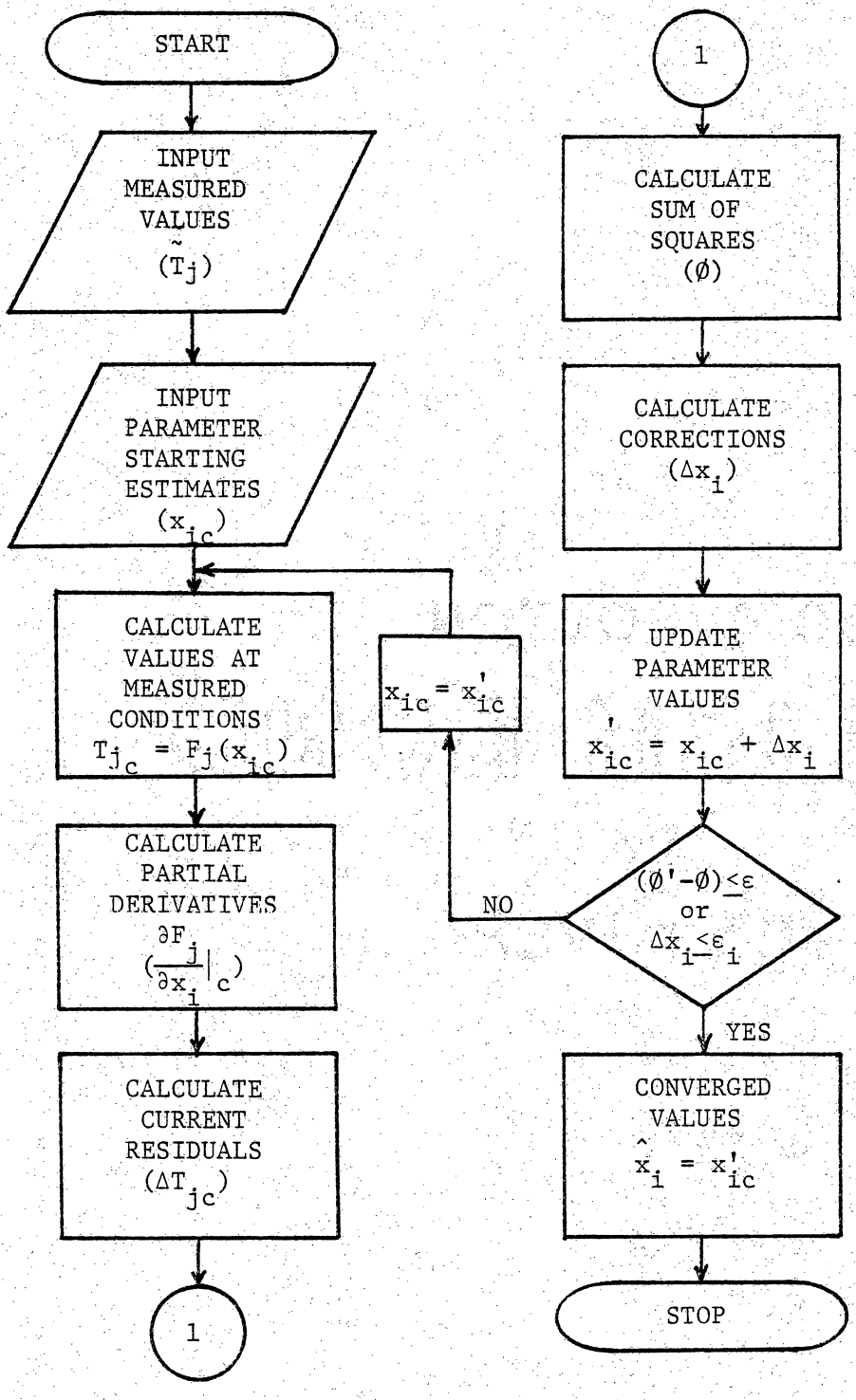

Fig. 3.5 Block Diagram for Gaussian LSDC Algorithm

final estimates if the functions, F_j, are highly nonlinear. Damping of the corrections is usually required for highly nonlinear cases, i.e.

$$x'_{ic} = x_{ic} + (1 - \gamma)\,\Delta x_i \quad ; \; i = 1, 2, \ldots, n \tag{3.100}$$

where γ is a damping factor ($0 \leq \gamma \leq 1$). Physical limitations, in the form of maximums and minimums, should be placed on the parameters to aid in convergence and to avoid physically unrealistic results (i.e., $0 \leq \hat{\alpha}_p \leq 1$). Three statistical values that aid in interpreting the results are the mean of residual errors, $\mu_{\Delta T}$, the standard deviation of residual errors, $\sigma_{\Delta T}$, and the maximum residual error, $\lambda_{\Delta T}$. These statistical values in equation form are

$$\mu_{\Delta T} = m^{-1} \sum_{j=1}^{m} \Delta T_j \tag{3.101}$$

$$\sigma_{\Delta T} = \left[m^{-1} \sum_{j=1}^{m} \Delta T_j^2\right]^{1/2} \tag{3.102}$$

$$\lambda_{\Delta T} = \max(\Delta T_j;\; j = 1, 2, \ldots, m) \tag{3.103}$$

In general, good agreement between the analytical model and the experimental measurements will give a near zero $\mu_{\Delta T}$ and a $\sigma_{\Delta T}$ approximately equal to the uncertainty of the measured values. Outlying and questionable data points will be identified by $\lambda_{\Delta T}$.

The complexity of most analytical models precludes obtaining $\frac{\partial F_j}{\partial x_i}$ analytically. Therefore, numerical derivatives are taken in the form

$$\frac{\partial F_j}{\partial x_i} = [F_j(x_i + \delta_i) - F_j\ (x_i)]/\delta_i \qquad (3.104)$$

Forward difference derivatives are generally used rather than central difference derivatives because of the savings in computer time by already having $F_j\ (x_i)$ calculated in previous steps. Values for δ_i depend on the convergence criteria in the function $F_j\ (x_i)$ and the degree of nonlinearity in the function $F_j\ (x_i)$. Since the derivatives $\frac{\partial F_j}{\partial x_i}$ are used to "steer" in the convergence process, δ_i equal to 5 per cent of x_i are usually sufficient.

In the following discussion of results chapter, the LSDC method, in conjunction with the stagnation temperature theory developed in this chapter, is used to obtain collector parameters from experimental temperature measurements.

4. RESULTS AND DISCUSSION

Test methods are analyzed which use stagnation temperature as a means for determining collector thermal property changes after environmental exposure. The chapter begins with a discussion of steady-state data obtained using the indoor instrumented collector. These data are analyzed and compared to temperatures predicted by the analytical model. Next a discussion of different techniques for measuring the absorber plate temperature is presented. Following this section, transient data, measured both outdoors and indoors, are analyzed and compared with calculated values. After the analytical models have been experimentally verified, sensitivity studies are presented which deal with changes in absorber plate stagnation temperature as a result of collector thermal properties changes and changes in environmental conditions. Following the sensitivity studies, instantaneous methods of measuring stagnation temperature are analyzed and associated problems are discussed. Finally, a test method which uses all-day integrated values is investigated using experimental data and analytical models.

4.1 Experimental Verification of Analytical Models

This section analyzes experimental data obtained from indoor and outdoor temperature measurements and compares these data with predicted values. In addition, four different techniques used to measure an effective absorber stagnation temperature are discussed. The section begins with the steady-state indoor results and measurement techniques followed by transient results from indoor and outdoor tests.

Steady-State Results

Steady-state measurements were obtained using the highly instrumented indoor solar collector previously discussed. Tests using this collector were performed at inclination angles of 0, 45, and 90 degrees. At each of these inclination angles, the power input to the strip heaters mounted on the absorber was nominally set at 200, 400, 600, 800, 1000, and 1200 W which correspond to solar radiation levels of 162, 325, 487, 650, 812, and 975 W/m^2, respectively. Conditions were deemed steady-state for all tests when the component temperatures changed less than a rate of 2 C per hour. During each test the ambient temperature remained constant to within $\pm$ 0.5 C. In addition, the sky shield was used for each test to control and measure the effective radiative temperature of the surroundings.

Figures 4.1-4.3 show representative results of these tests for the three inclination angles at nominal power inputs to the strip heaters of 400, 800, and 1200 W. Data taken at the other power levels are similar

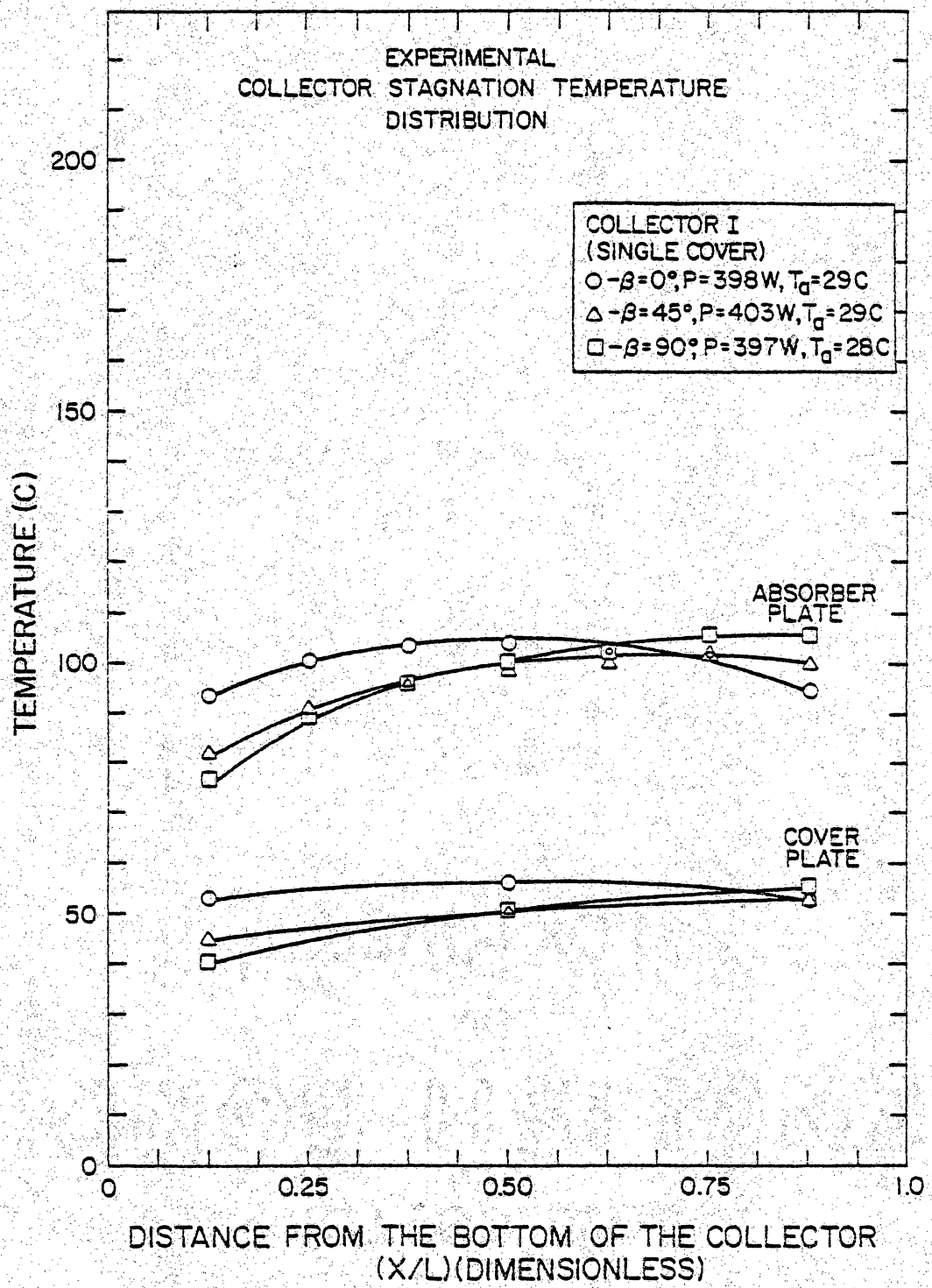

Fig. 4.1 Indoor Measurements of Absorber and Cover Plate Temperature Distribution for Collector I with a Power Input of Approximately 400 W

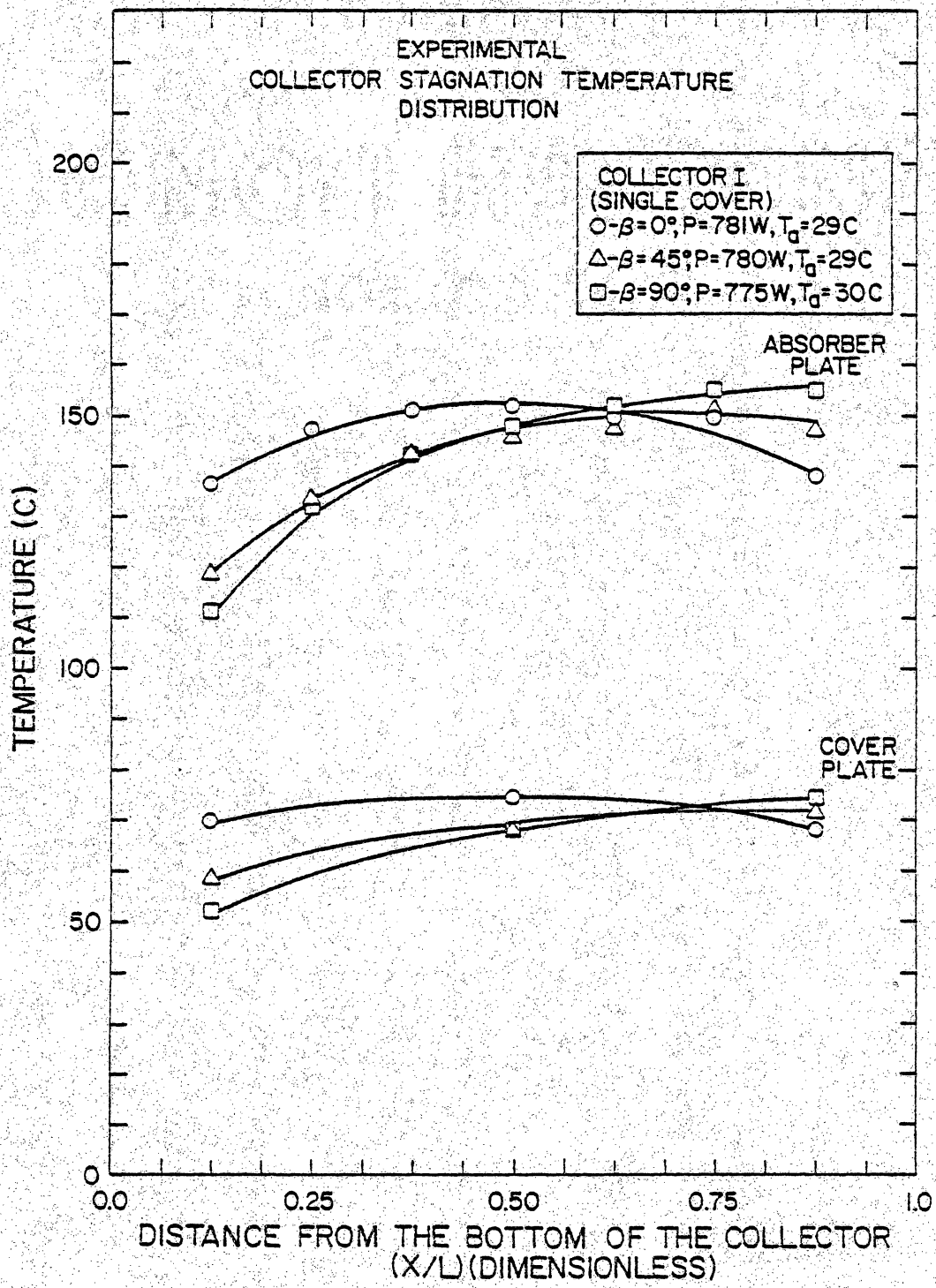

Fig. 4.2 Indoor Measurements of Absorber and Cover Plate Temperature Distribution for Collector I with a Power Input of Approximately 800 W

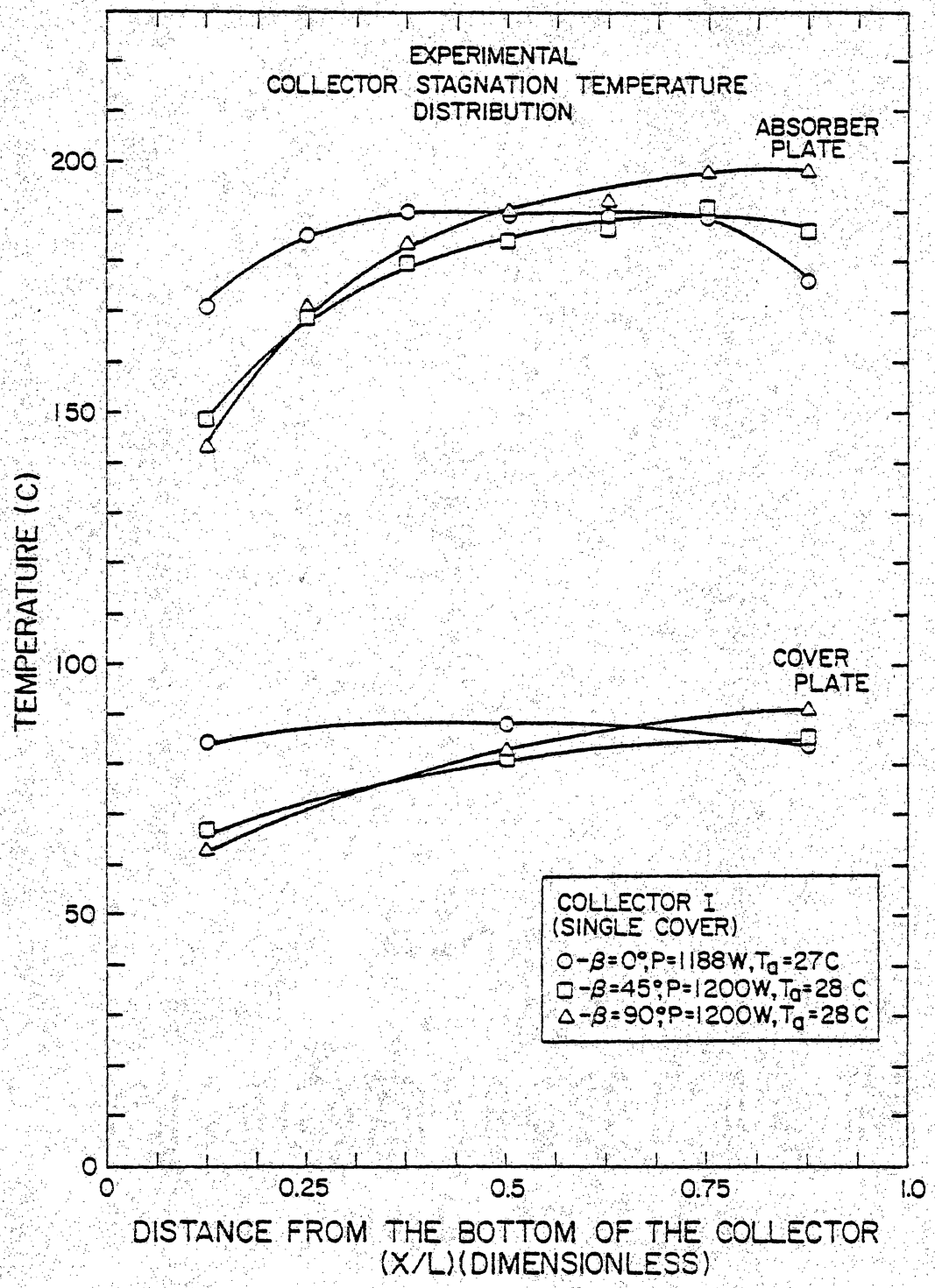

Fig. 4.3 Indoor Measurements of Absorber and Cover Plate Temperature Distribution for Collector I with a Power Input of Approximately 1200 W

to Figs. 4.1-4.3 and, therefore, are not shown. The temperature distribution of the absorber plate and cover plate is along the lengthwise centerline, starting at the lower end and ending at the top.

There are two major observations resulting from Figs. 4.1-4.3. The first observation is that edge losses cause the absorber plate and cover plate temperature distribution to be highly nonisothermal as illustrated by the $\beta = 0^{o}$ cases. The second observation is that increasing the inclination angle of the collector from the horizontal to the vertical position causes the temperature of the absorber and cover plates to decrease towards the lower end and increase towards the upper end. This effect is caused by internal thermal stratification of the air between the absorber and cover plate. The effect of both of these observations is to make the absorber and cover temperature a function of location and inclination angle. However, the temperature at the center of the absorber plate varies a maximum of only 6 C between the horizontal and vertical positions at the highest power level. The temperature distribution along the width direction centerline and other locations, not shown but measured, results in similar observations.

Figure 4.4 compares steady-state measured and calculated stagnation temperatures for the absorber and cover plates. The solid line in Fig. 4.4 represents the locus of points where the measured and calculated values are equal. Since the steady-state model does not take into account air stratification between the absorber and cover plates, only the data with the collector oriented horizontally are shown. Likewise, the measured temperatures are from the center of the absorber and cover

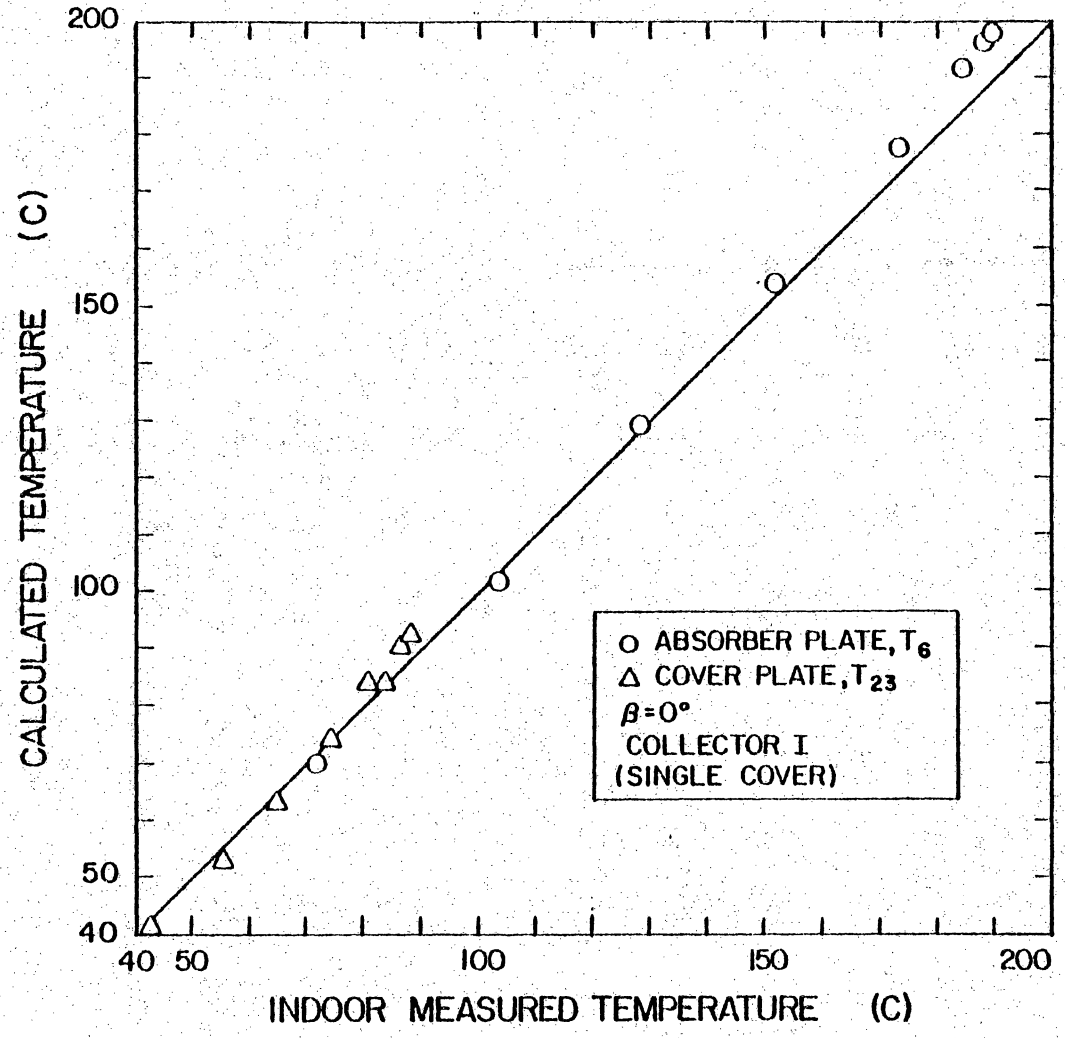

Fig. 4.4 Comparison of Steady-State Measured and Calculated Collector Stagnation Temperatures for Collector I Indoors

plates because edge losses also are not taken into account in the model. These temperatures were used because the center 0.3 m diameter portion of both the absorber and cover plates is nearly isothermal and the effect of edge heat losses is negligible. The calculated values in Fig. 4.4 were computed using the power input, ambient temperature, and sky temperature measured during each test. The collector dimensions and properties used in these calculations are those of collector I in Table 2.1 with the exception of the extinction coefficient. Since the indoor collector simulates solar radiation absorbed only on the absorber plate and not in the cover plate, the extinction coefficient was set equal to zero to correspond to the experimental apparatus. The maximum difference between measured and predicted temperatures in Fig. 4.4 is 8 C for the absorber plate and 4 C for the cover plate. Also, there is a trend in the data contained in Fig. 4.4 which suggests that some of the collector properties may be temperature dependent. The trend is to gradually over-predict the temperature of the absorber and cover as both temperatures increase. This trend is probably a result of properties, such as the infrared emittance of the absorber plate or thermal conductivity of the insulation, increasing as the temperature increases. Considering the assumptions of no edge losses and constant properties, the agreement between measured and predicted temperatures in Fig. 4.4 is excellent.

An important characteristic of a solar collector is how the overall heat loss coefficient, U_L, varies as a function of absorber plate temperature. Since all the energy absorbed on the absorber plate of a stagnated collector is transferred to the environment as heat loss,

values of U_L as a function of temperature can be calculated as follows

$$U_L = \frac{P_{IN}}{A_c(T_p - T_a)} \tag{4.1}$$

Figure 4.5 was constructed using Eq. 4.1 and the steady-state temperature data taken with the collector in a horizontal position at input power levels from 200 to 1200 W. The solid line in Fig. 4.5 is a linear least squares fit to the data. The relation between U_L and $(T_p - T_a)$ is closely approximated by a linear function. The relation between U_L and $(T_p - T_a)$ for the indoor instrumented collector is

$$U_L = [2.67 + 0.016\ (T_p - T_a)]\ W/m^2\ C \tag{4.2}$$

Equation 4.2 will be used in later sections to calculate U_L as a function of temperature in the absorber temperature distribution model and in the transient analysis.

Table 4.1 statistically compares the measured absorber plate temperature distribution with the calculated absorber plate temperature distribution using the two-dimensional model discussed in Section 3.3. Only the data taken with the collector oriented horizontally were used in order to eliminate temperature gradients caused by internal air stratification. The parameter estimation algorithm from Section 3.4 was used to determine the parameters, ψ_x and ψ_y, used in the two-dimensional model. These parameters were analytically determined from experimental data because of the large uncertainty in calculating U_{ex} and U_{ey}. Measured and calculated temperatures were compared at locations 1-6 and 14-20 in Fig. 2.1. Values for U_L in Table 4.1 were calculated using Eq. 4.2.

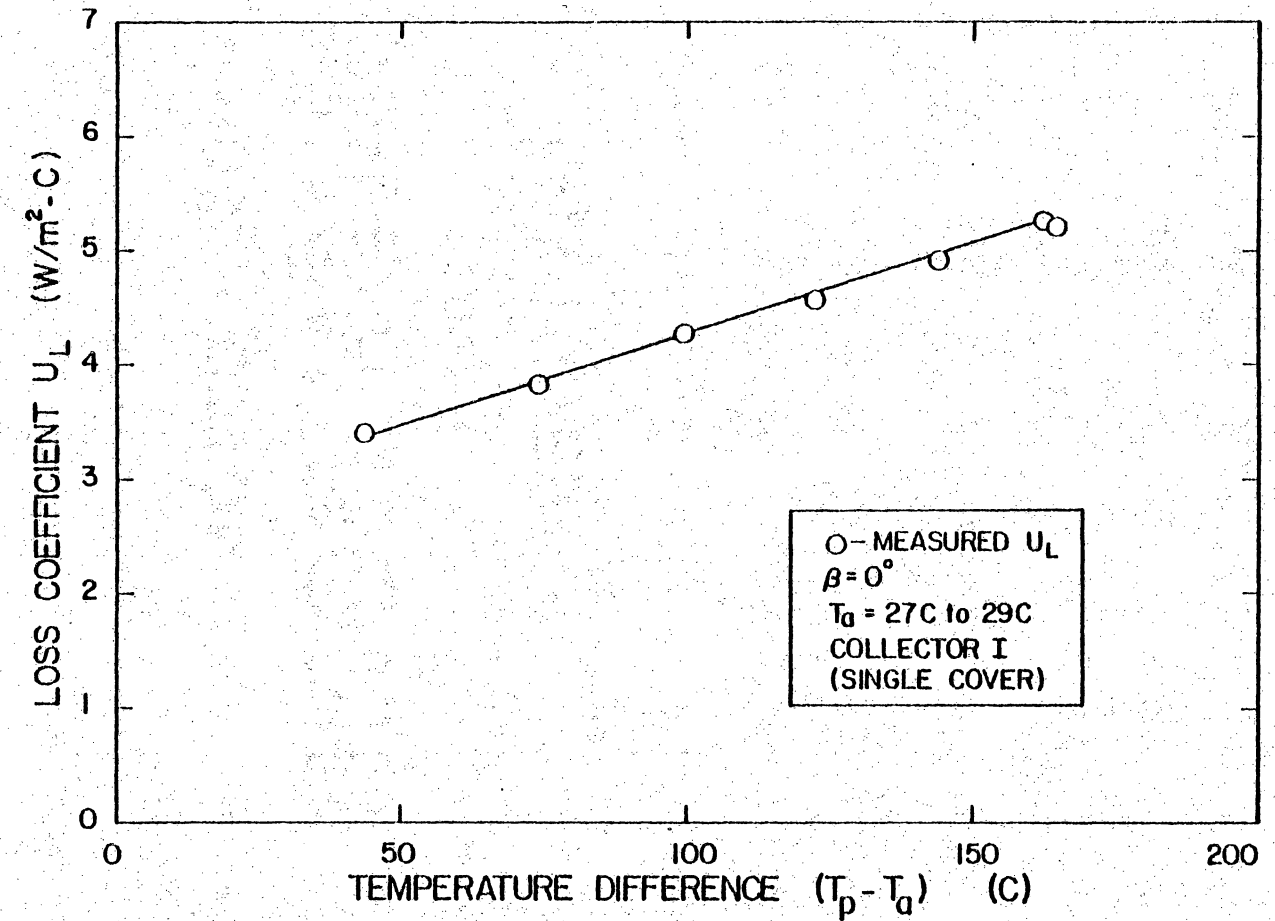

Fig. 4.5 Overall Loss Coefficient as a Function of Temperature Measured Indoors for Collector I

Table 4.1 Statistical Comparison of Measured and Calculated Absorber Temperature Distributions for Collector I Indoors

P_{IN} (W)	$*(T_p-T_a)$ (C)	U_L (W/m^2C)	ψ_x	ψ_y	$\mu_{\Delta T}$ (C)	$\sigma_{\Delta T}$ (C)	$\lambda_{\Delta T}$ (C)
200	44.2	3.4	13.9	4.04	-0.01	$\pm$0.31	0.53
400	74.6	3.9	20.7	4.42	-0.27	$\pm$0.71	-1.68
600	100.3	4.3	26.1	4.84	-0.36	$\pm$0.89	-2.05
800	123.0	4.6	25.7	4.87	-0.32	$\pm$1.11	-3.32
1000	144.6	5.0	26.9	5.07	-0.29	$\pm$0.98	-2.04
1200	165.5	5.3	29.6	4.95	0.00	$\pm$1.54	3.39

*Temperature difference using the center absorber plate temperature

There are three main observations resulting from Table 4.1. The first observation is that the standard deviation of residual errors, $\sigma_{\Delta T}$, between measured and calculated temperatures is approximately $\pm$ 1 C. This result indicates that the assumptions used in the two-dimensional model are probably valid. In addition, the near zero values of $\mu_{\Delta T}$ and the low values of $\lambda_{\Delta T}$ indicate good agreement between measured and calculated temperatures. The second observation deals with the temprature dependence of ψ_x and ψ_y. With the exception of the 200 and 400 W cases, these parameters are essentially independent of temperature as discussed in Section 3.3. Therefore, once the values for ψ_x and ψ_y have been determined, the mean temperature and temperature distribution of the absorber can be obtained for any temperature level. The low values of ψ_x and ψ_y determined from the 200 and 400 W tests would not pertain to testing at normal levels of solar radiation. The last observation is that values of ψ_x are about five times as large as the values for ψ_y. This difference is most likely a result of higher conduction heat losses from the inlet and exit piping and the fact that the length dimension, L, is about twice as large as the width dimension, ℓ.

Stagnation Temperature Measurement Techniques

Four measurement techniques and investigated for use in determining an appropriate stagnation temperature to determine property changes. The four methods were: measuring the absorber temperature through the back-side cover with a spring loaded probe; measuring the temperature of

stagnant air inside the flow tube header; measuring the center cover temperature; and measuring the temperature of air flowing through the absorber plate flow tubes when the inlet air temperature was maintained at the outlet temperature.

Using the stagnant air temperature inside the flow tube header was unsuccessful for several reasons. The stagnant air temperature of the header contained inside the indoor instrumented collector was 124 C, as compared with a center absorber plate temperature of the same collector of 185 C. The temperature of the header is probably lower as a result of the header being near the edge of the collector. Since a property change causes $(T_p - T_a)$ to change by a certain fraction, sensitivity to property changes would be less using the header temperature as compared to the center absorber temperature. In addition, since the temperature sensor is inserted "blindly" into the header through the inlet or outlet pipe opening, the repeatability of this type of measurement may be poor.

Using the center cover plate temperature was also unsuccessful. The advantage of this method is the ease of measuring the exposed outer cover temperature with either a shielded thermocouple or a hand held infrared pyrometer. One of the problems associated with this method is the lower sensitivity to collector property changes since the cover temperature is much less than the absorber temperature. Furthermore, large errors can be introduced into the measurements as a result of the strong effect of wind on the outside cover temperature. There are also problems in measuring cover temperatures accurately. Errors can be introduced into the thermocouple measurement by absorbed solar radiation

on the sensor and into the pyrometer measurement when the cover is highly transparent to infrared radiation.

Measuring the temperature of air flowing through the collector when the inlet and exit air temperatures are equal has several advantages. The collector would be in a stagnating mode during this test because no energy is removed from the collector since the inlet and exit air temperatures are equal. The flow loop apparatus would consist only of a hot air gun, a thermopile between the inlet and exit manifolds, and a thermocouple in the inlet or exit manifold. The temperature of the inlet air would be adjusted by the hot air gun until the thermopile output voltage vanishes. A temperature measurement of this type would eliminate temperature sensors mounted in the collector and possibly average out the effects of edge losses and internal air stratification.

The air flow method, however, did not produce satisfactory results. Figure 4.6 compares the temperature distribution along the center and edge flow tubes, with and without air flow, for the indoor instrumented collector. The inlet and exit air flow temperatures were 131 C. This temperature is 57 C less than the center absorber plate temperature for the no-air-flow case. The low inlet and exit air temperatures are most likely a result of the relatively low temperature inlet and exit headers. Once again, the sensitivity to property changes in using this method would be less than a method using the center absorber plate temperature as a result of the lower temperature levels. Furthermore, the temperature of the flowing air was determined to be a weak function of the air flow rate through the collector. Flow rates of relative

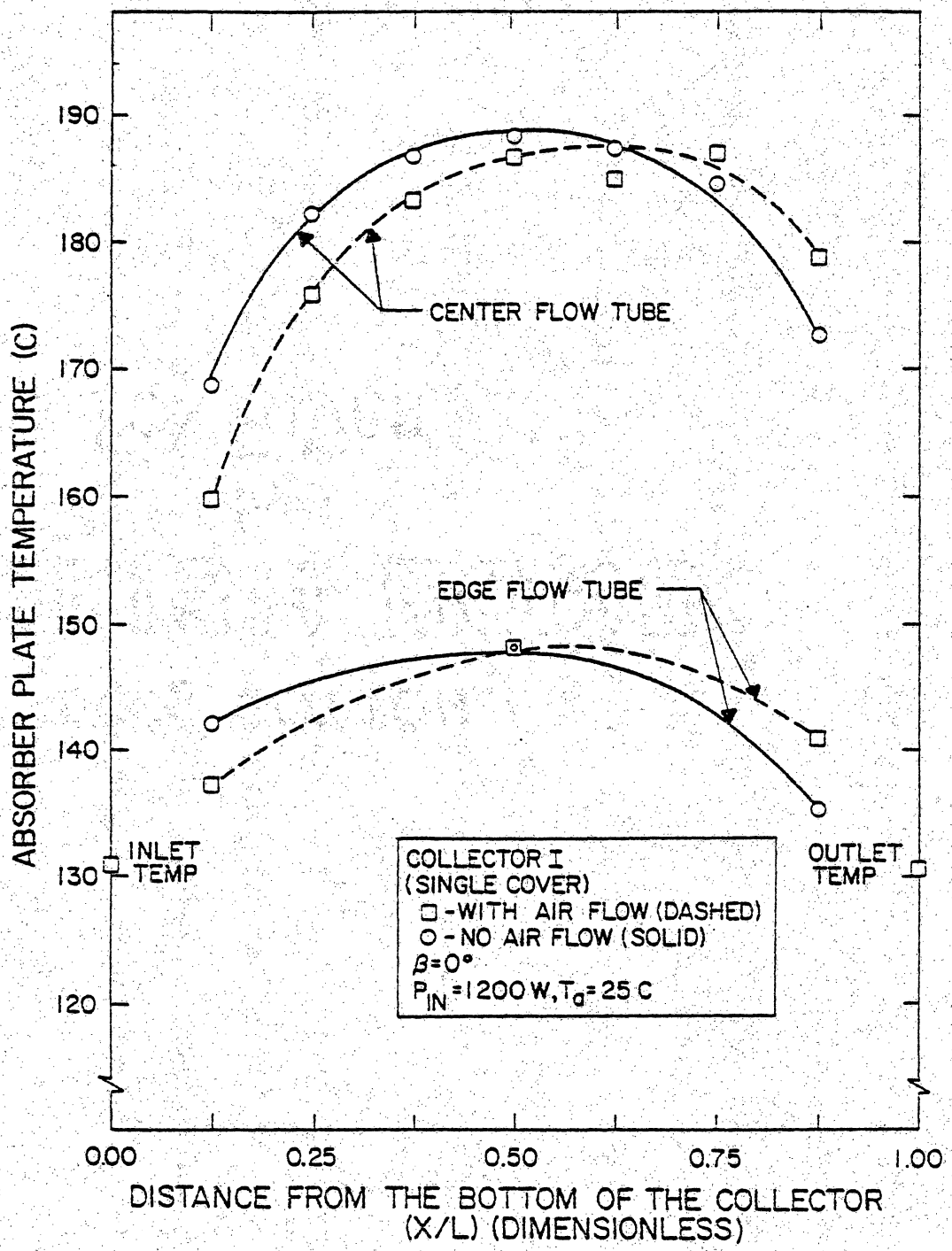

Fig. 4.6 Comparison of Absorber Plate Temperature Distribution with and without Air Flowing Through the Flow Tubes Measured Indoors for Collector I

magnitudes of approximately one-half, one, and two caused the air temperature to vary by 7 C, with the air temperature increasing as the flow rate increased. As a result of these problems, the air flow rate method was abandoned.

Measuring the absorber plate temperature with a spring loaded thermocouple probe proved to be the best of the four methods considered. This probe is described in detail in Section 2.2. The probe is relatively easy to mount on the back-side of a collector without having to disassemble the collector. In addition, the adjustable length of the probe makes it versatile for collectors having different insulation thicknesses. Since the absorber plate temperature is higher than the temperature obtained using the other three methods, the sensitivity to collector properties changes would be the highest using this method. As a result of these reasons, the technique of using a spring loaded probe to measure absorber plate stagnation temperature is recommended.

Transient Results

Transient temperature measurements were made using the indoor and outdoor test apparatus. Measurements made at test sites 4 and 5 are also considered. The indoor transient measurements consisted of measuring the stagnation temperature response of the indoor instrumented collector to step changes in power supplied to the strip heaters. The outdoor transient measurements consisted of measuring all-day stagnation temperatures of two collectors at VPI&SU and four collectors at test sites 4 and 5.

There were two indoor transient tests which measured the response of the indoor instrumented collector to a step increase in input power from 0 to 1200 W and a step decrease in input power from 1200 to 0 W. Initial conditions for both of these tests were steady-state temperatures before the step change in input power. Figure 4.7 is a comparison of the measured and calculated temperatures of the absorber and cover plate to a step change in input power from 0 to 1200 W. The solid lines represent the calculated results while the squares and circles represent the measured absorber and cover temperatures, respectively. Temperature data was taken at 30-second intervals for both indoor tests. The temperature was measured at the center of the absorber and cover plate during the test. The parameter estimation algorithm developed in Section 3.4 was used in conjunction with the transient model developed in Section 3.2 to produce the analytical results. The two parameters optimized in the analysis were the heat capacity of the absorber plate, $(m_p C_p)$, and the thermal conductivity of the insulation, k_{in}. Both of the values obtained for these parameters are in close agreement with handbook values. The agreement between measured and calculated values is within 6 C and the standard deviation of residual errors is 3.0 C. Figure 4.8 is a similar comparison except the transient temperature response is to a step decrease in input power from 1200 to 0 W. The same values for $(m_p C_p)$ and k_{in} as used in Fig. 4.7 are used in Fig. 4.8. The reason these parameters were not changed is that the actual collector properties would not have changed between tests. The maximum temperature difference between measured and calculated values in Fig.

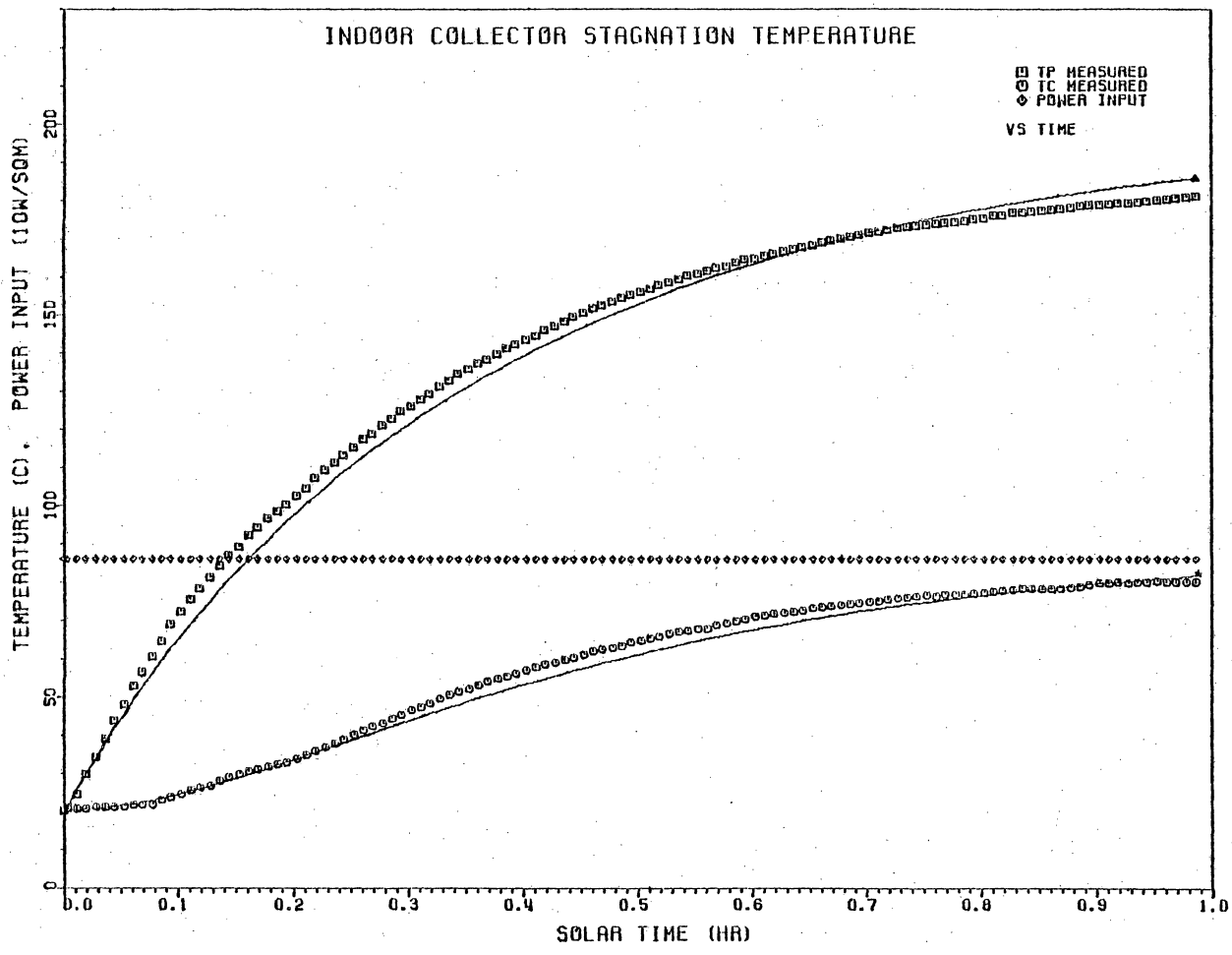

FIG. 4.7 COMPARISON OF MEASURED AND CALCULATED INDOOR STAGNATION TEMPERATURES OF COLLECTOR I AT VPI&SU TO A STEP INCREASE IN INPUT POWER

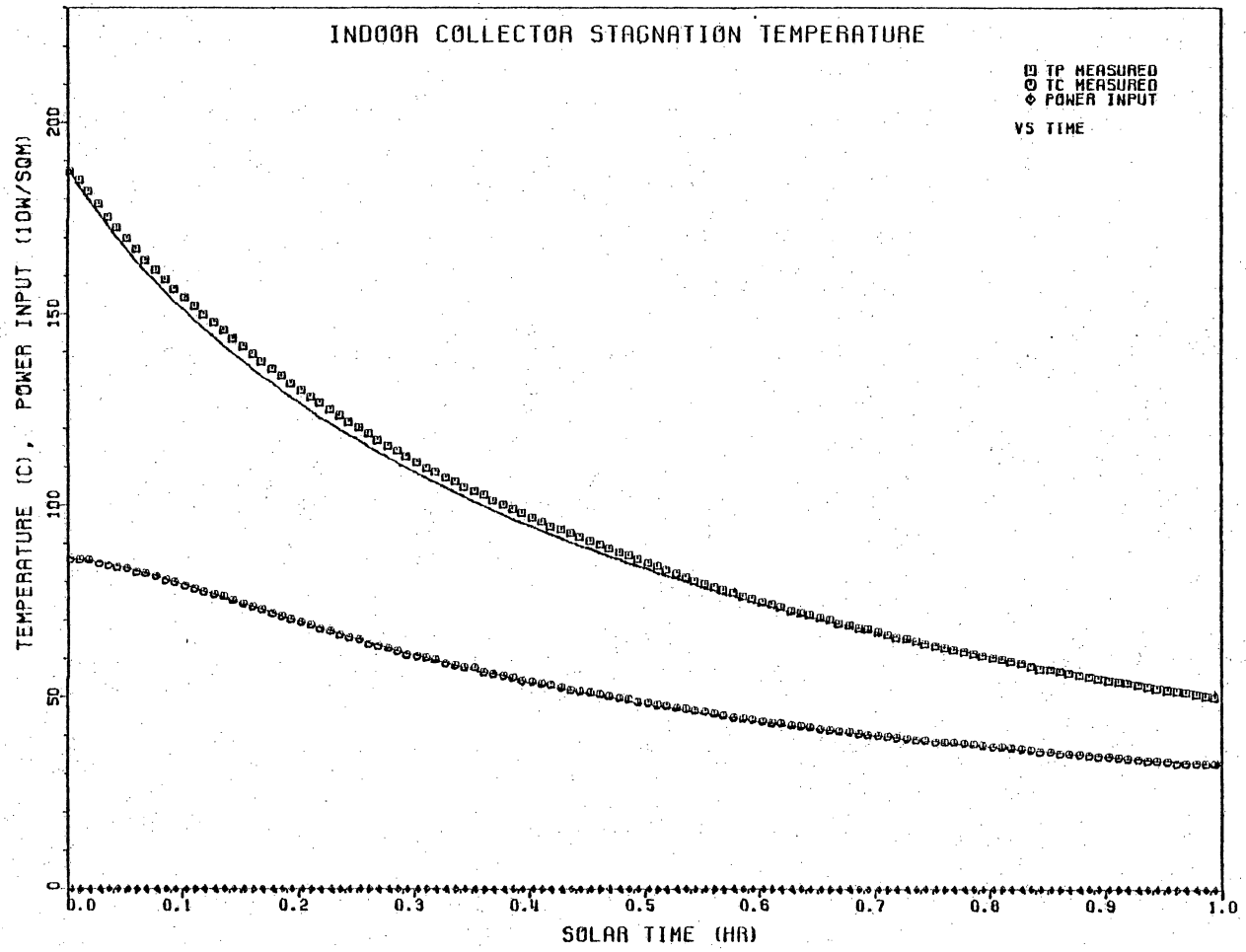

FIG. 4.8 COMPARISON OF MEASURED AND CALCULATED INDOOR STAGNATION TEMPERATURES OF COLLECTOR I AT VPI&SU TO A STEP DECREASE IN INPUT POWER

4.8 is 4 C and the standard deviation of residual errors is 1.6 C. The agreement between measured and calculated values in Fig. 4.8 is slightly better than the agreement in Fig. 4.7. The reason for this better agreement may be a result of controlling the power input to exactly 0 W in Fig. 4.8 while the power input in Fig. 4.7 was controlled to within $\pm$ 1 per cent of 1200 W. Overall, the agreement between measured and calculated temperatures in Figs. 4.7 and 4.8 is good. Table 4.2 summarizes the statistical comparison between measured and calculated temperatures in Figs. 4.7 and 4.8.

All-day outdoor data taken at VPI&SU were recorded at 5-minute intervals. Figures 4.9-4.11 show measured and calculated stagnation temperatures for collectors D and I described in Table 2.1. Figure 4.9 was constructed from data measured using collector I on 12/17/80 at an inclination angle of 60 degrees. Figures 4.10 and 4.11 were constructed from data measured using collectors D and I on 2/13/81 at an inclination angle of 45 degrees. Since the tests were performed at inclination angles other than horizontal, the stagnation temperature of the lower, middle, and upper third portions of the absorber plate were averaged to obtain the absorber plate temperature data in Figs. 4.9-4.11. With an inclination angle of 45 degrees on 2/13/81, the outdoor measured temperature difference between the upper and lower third sections of collectors D and E at solar noon was 32 C and 24 C, respectively. The parameters $(m_p C_p)$ and k_{in} were optimized using all the outdoor data from Figs. 4.9-4.11. The value for $(m_p C_p)$ obtained from the indoor measurements was not used for the outdoor data because the outdoor collectors

Table 4.2 Statistical Comparison of Measured and Calculated Collector Stagnation Temperatures for Figs. 4.7-4.15

Figure Number	$(m_p C_p)$ $(W \cdot h/m^2\text{-}C)$	k_{in} (W/m-C)	$\mu_{\Delta T}$ (C)	$\sigma_{\Delta T}$ (C)	$\lambda_{\Delta T}$ (C)
4.7	1.67	0.055	1.6	$\pm$3.0	6.6
4.8	1.67	0.055	0.9	$\pm$1.6	4.1
4.9	1.13	0.085	-3.8	$\pm$4.6	-8.4
4.10	1.13	0.085	-2.0	$\pm$4.6	-9.6
4.11	1.13	0.085	-3.0	$\pm$3.9	-8.2
4.12	2.90	0.070	0.7	$\pm$2.6	-7.0
4.13	0.29	0.083	0.8	$\pm$2.9	-8.8
4.14	0.84	0.019	0.0	$\pm$1.1	-1.9
4.15	1.76	0.033	-0.1	$\pm$0.9	-4.2

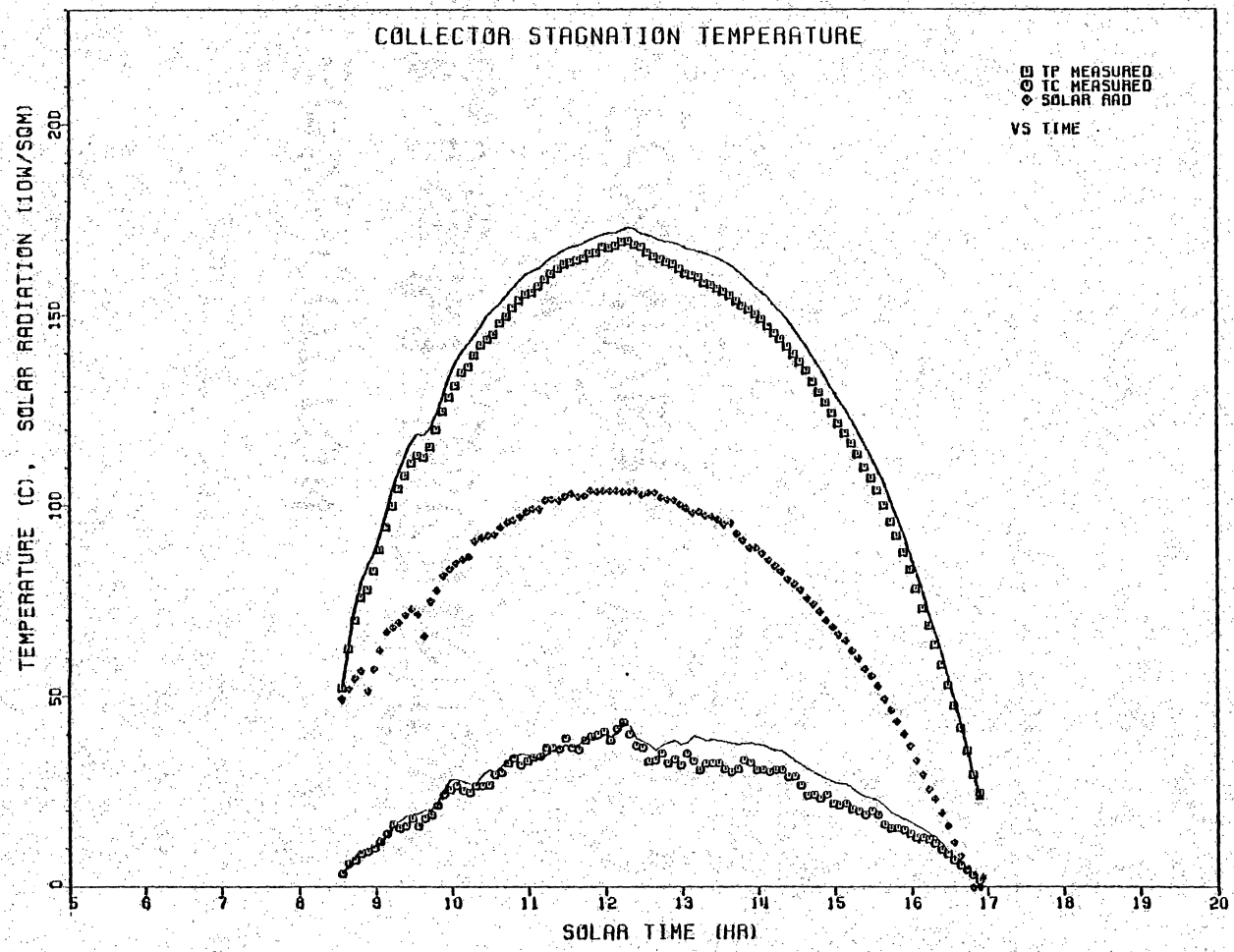

FIG. 4.9 COMPARISON OF MEASURED AND CALCULATED STAGNATION TEMPERATURES OF COLLECTOR I AT VPI&SU ON 12/17/80

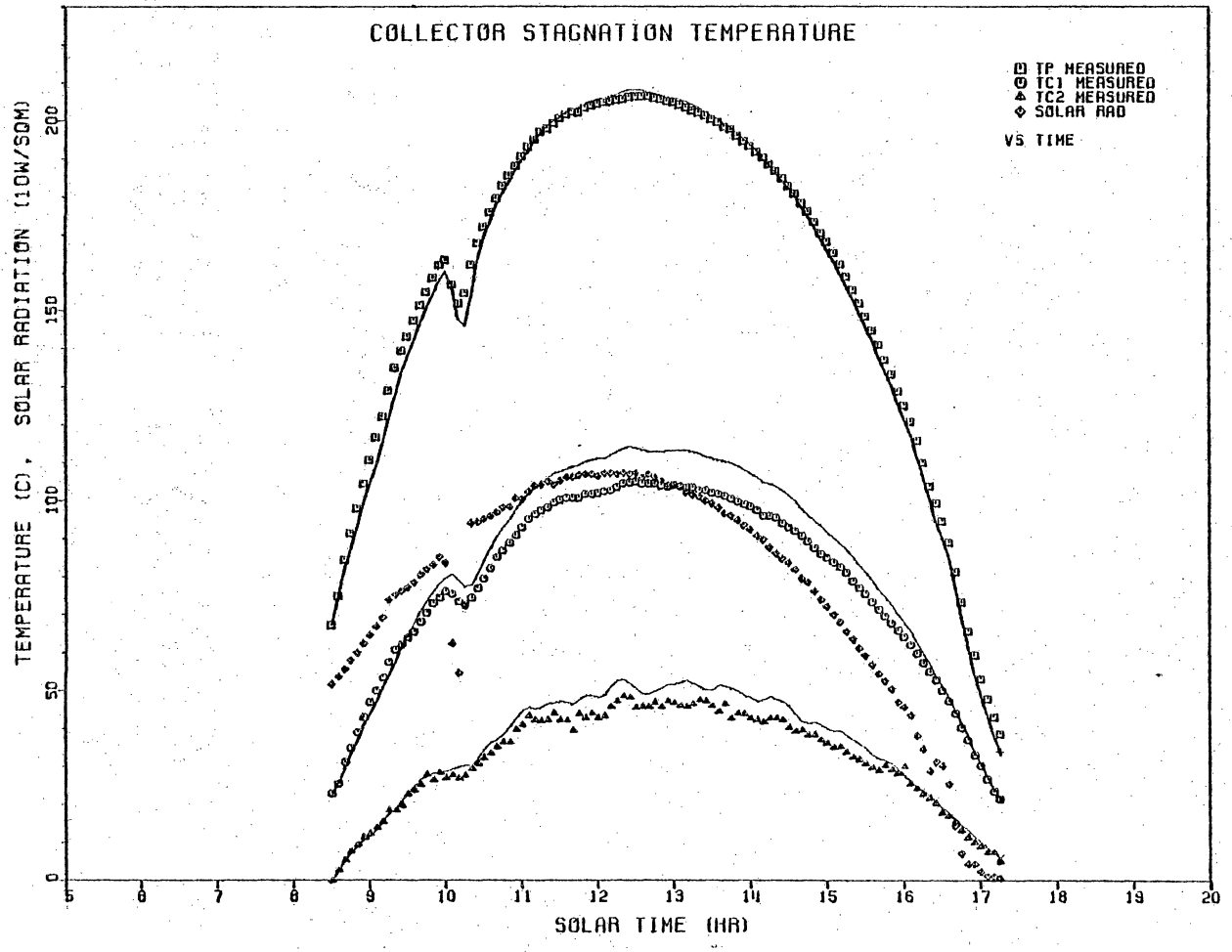

FIG. 4.10 COMPARISON OF MEASURED AND CALCULATED STAGNATION TEMPERATURES OF COLLECTOR D AT VPI&SU ON 2/13/81

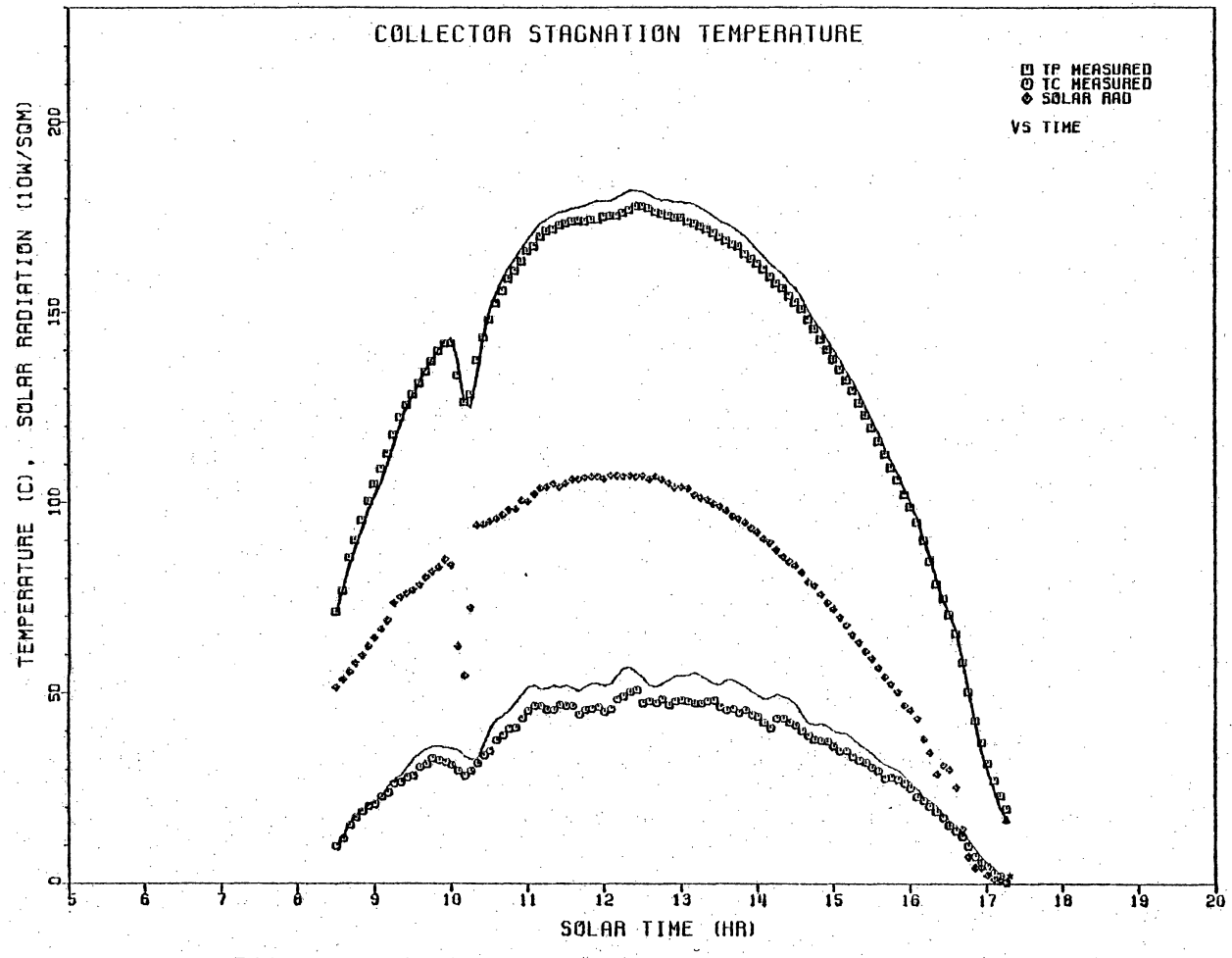

FIG. 4.11 COMPARISON OF MEASURED AND CALCULATED STAGNATION TEMPERATURES OF COLLECTOR I AT VPI&SU ON 2/13/81

do not have the extra heat capacity associated with the strip heaters. Also, k_{in} derived from the indoor data was not used because the outdoor insulation may have different amounts of contained moisture. The statistical values comparing the measured and calculated results in Figs. 4.9-4.11 and the values for $(m_p C_p)$ and k_{in} are shown in Table 4.2. On the average, the calculated collector temperatures in Figs. 4.9-4.11 are higher than measured. This discrepancy is most likely a result of the collector properties being a function of temperature while the analytical model assumes they are constant. Properties such as ε_p and k_{in} generally increase with temperature. This increase in ε_p and k_{in} as the temperature increased would explain the higher calculated temperatures in Figs. 4.9-4.11. The calculated temperatures do, however, follow the trends of the measured temperatures very well.

In addition to the data obtained at VPI&SU, Figs. 4.12 and 4.13 contain outdoor data taken at test site 4 for collectors A and B. Figures 4.14 and 4.15 contain indoor solar simulator data taken at test site 5 for collectors E and H. The measured data in Figs. 4.12 and 4.13 were taken from a continuously recorded strip chart at 15-minute intervals. The cover plate temperatures were not measured at test site 4. In addition, the inclination angle for collectors A and B was 40 degrees during the test. The solar radiation profile for the tests using the solar simulator is an initial step increase from 0 to 1000 W/m^2, a linear increase from 1000 to 1100 W/m^2 over the next 2.5 hours, a linear decrease from 1100 to 1000 W/m^2over the remaining 2.5 hours, and finally a step decrease from 1000 to 0 W/m^2. The temperature data in Figs. 4.14

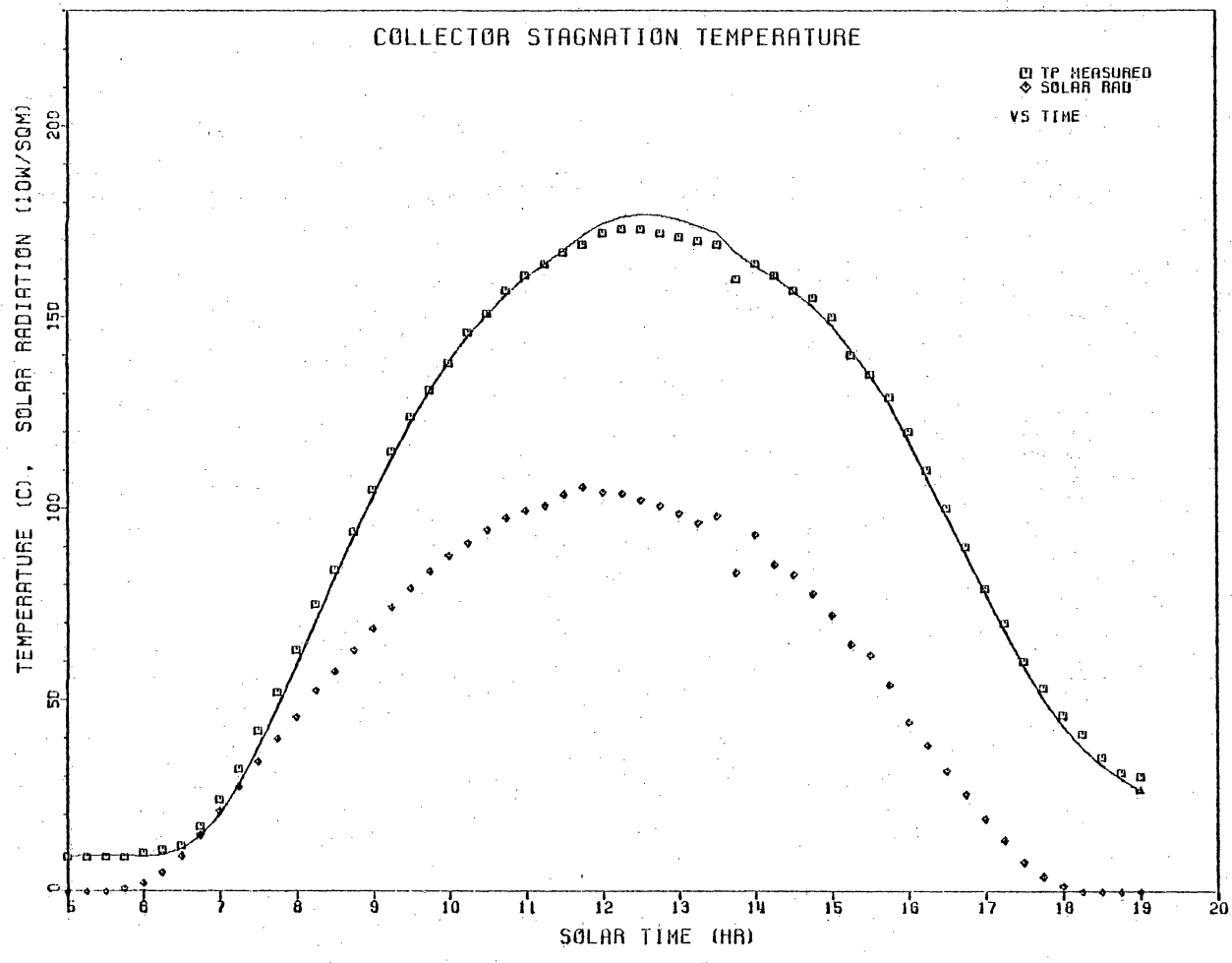

FIG. 4.12 COMPARISON OF MEASURED AND CALCULATED ABSORBER TEMPERATURES OF COLLECTOR A AT TEST SITE 4 ON 9/9/79

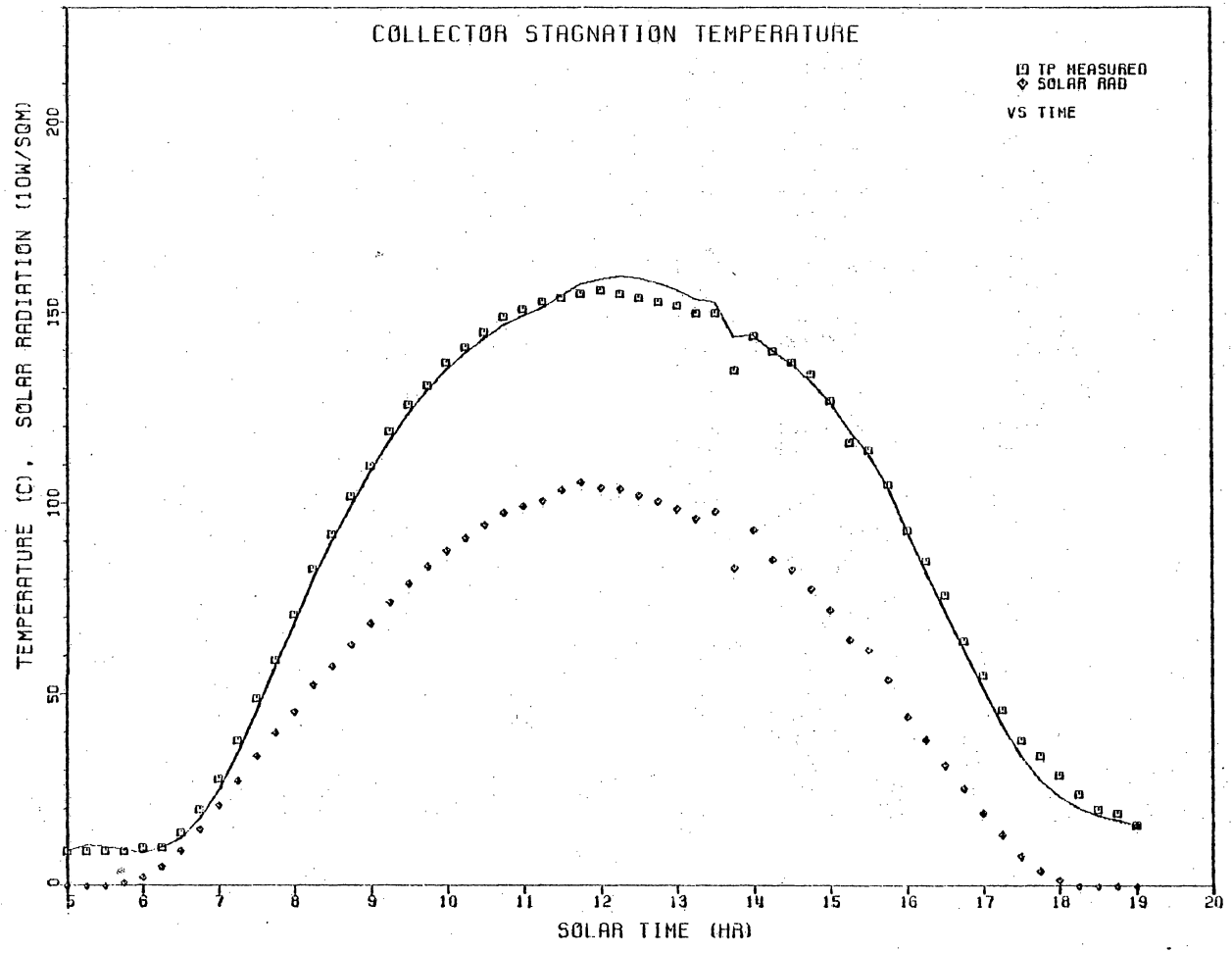

FIG. 4.13 COMPARISON OF MEASURED AND CALCULATED ABSORBER TEMPERATURES OF COLLECTOR B AT TEST SITE 4 ON 9/9/79

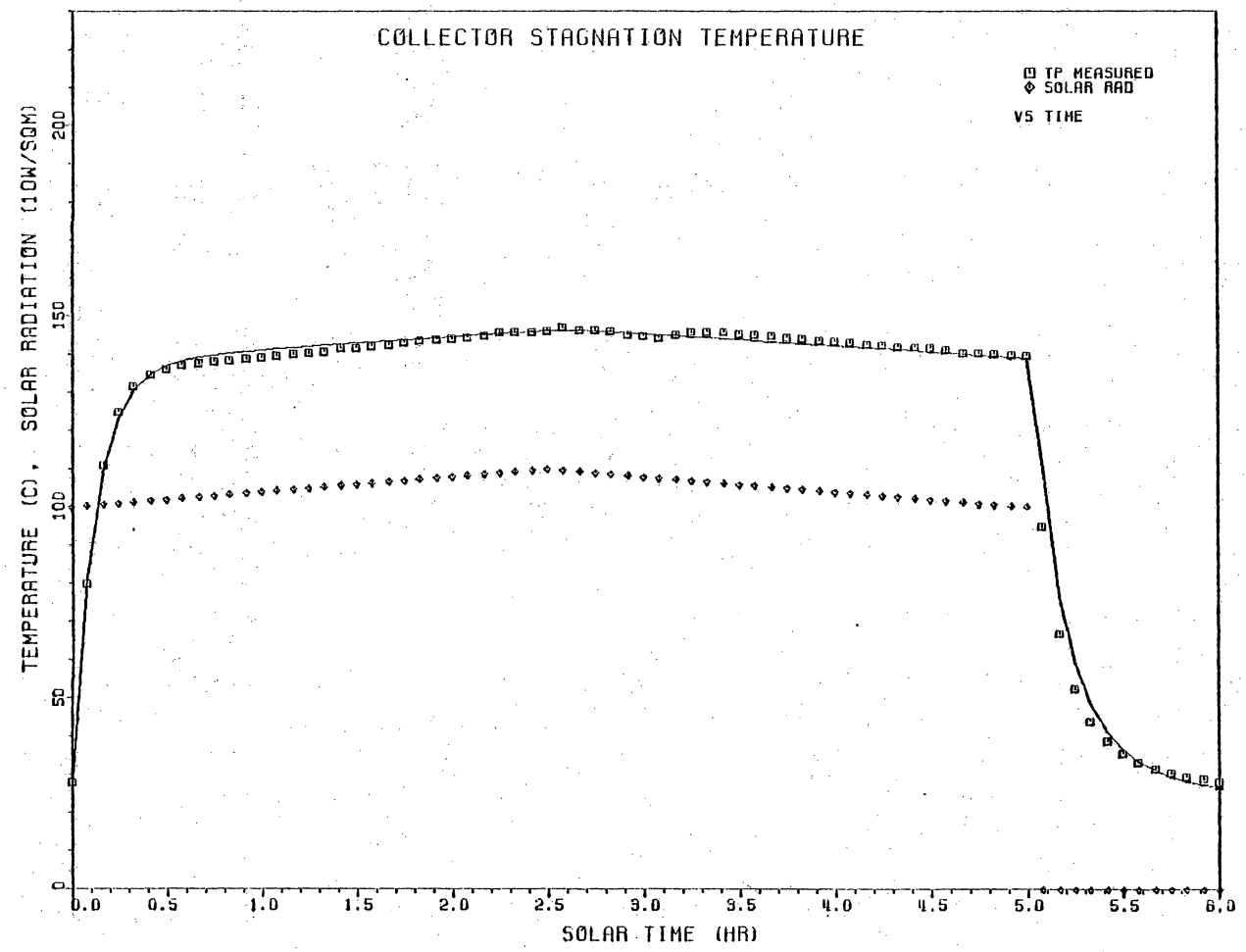

FIG. 4.14 COMPARISON OF MEASURED AND CALCULATED ABSORBER TEMPERATURES OF COLLECTOR E USING SOLAR SIMULATOR AT TEST SITE 5

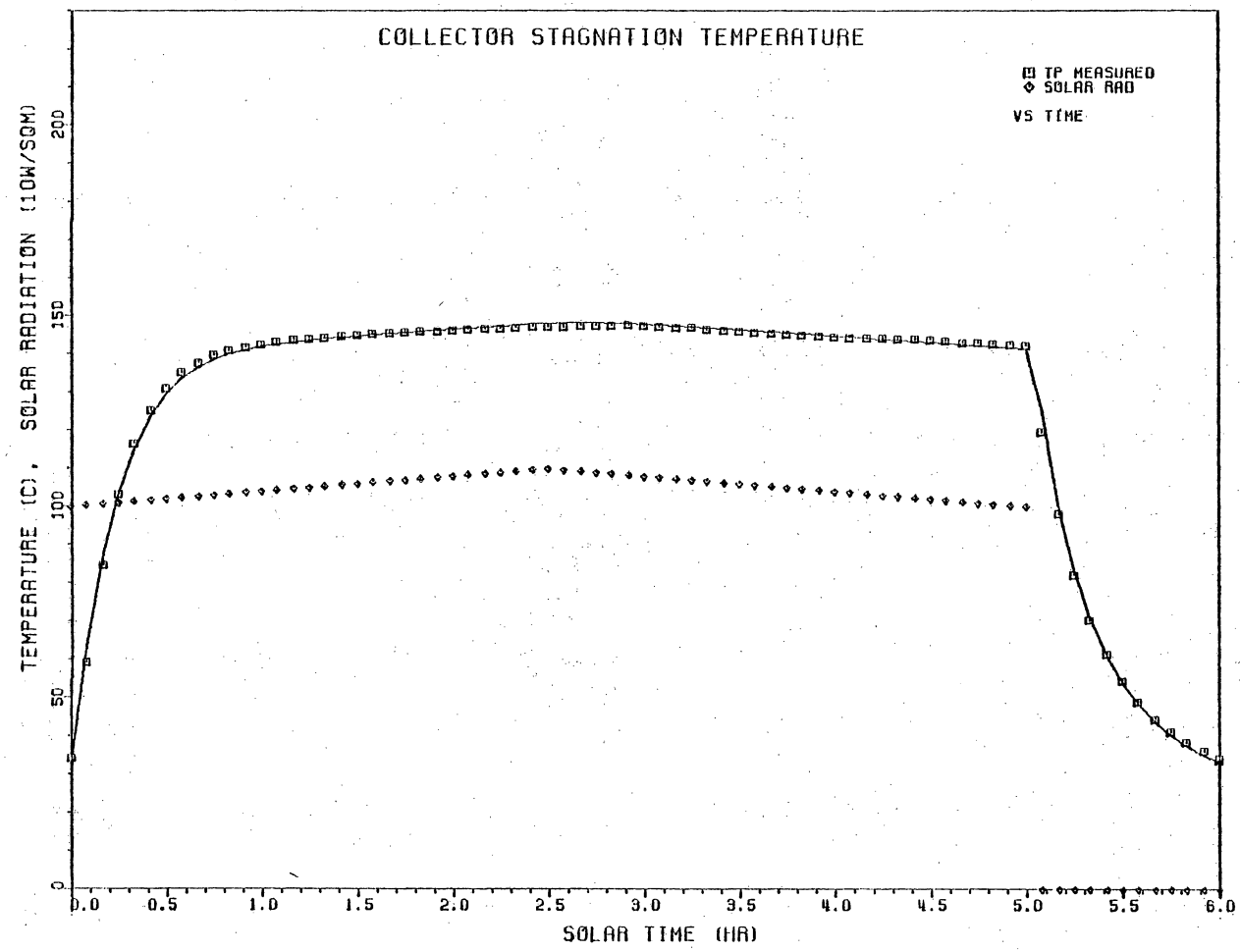

FIG. 4.15 COMPARISON OF MEASURED AND CALCULATED ABSORBER TEMPERATURES OF COLLECTOR H USING SOLAR SIMULATOR AT TEST SITE 5

and 4.15 were recorded at 5-minute intervals. Collectors E and H from Figs. 4.14 and 4.15 were horizontal during the tests. The derived parameters ($m_p C_p$) and k_{in} along with statistical data used to compare the measured and calculated results for Figs. 4.12-4.15 are in Table 4.2. Again, the agreement between measured and calculated results is good.

Figure 4.4, Figs. 4.7-4.15, and Tables 4.1 and 4.2 experimentally validate the steady-state, transient, and two-dimensional absorber plate temperature distribution models. The agreement in all cases is at least acceptable for using the models for sensitivity studies and test method evaluation. The transient model was experimentally verified with indoor and outdoor data at VPI&SU for collectors D and I, with outdoor data at test site 4 for collectors A and B, and with solar simulator data at test site 5 for collectors E and H. These transient data comparisons point out the versatility of the model with respect to different collector designs and with respect to indoor, outdoor, and solar simulator environments. The next section presents results from the steady-state model in determining the sensitivity of stagnation temperature with respect to collector property changes and environmental conditions.

4.2 Sensitivity Studies

Three important factors which affect the applicability of a test standard to determine collector property changes after environmental exposure are sensitivity to property changes, sensitivity to environmental conditions, and experimental uncertainty. In this section, each one of these factors is considered. The steady-state model is used for determining the sensitivity to property changes and environmental conditions. An analysis developed by Kline and McClintock [41] is used to determine the experimental uncertainty associated with stagnation temperature test methods.

Experimental Uncertainty

Before an uncertainty analysis can be performed, the stagnation temperature of the absorber plate must be normalized with respect to ambient temperature and solar radiation. Changes in ambient temperature or solar radiation between initial and post-exposure tests would cause the stagnation temperature to change independent of property changes. A satisfactory normalization of the stagnation temperature can be obtained by the following energy balance on the absorber plate.

$$(\hat{\tau\alpha})G - U_L(T_p - T_a) = 0 \tag{4.3}$$

Rearranging yields

$$(T_p - T_a)/G = (\hat{\tau\alpha})/U_L \tag{4.4}$$

Thus, the parameter, $(T_p - T_a)/G$, is only a function of the solar optical properties of the collector in the form of $(\hat{\tau\alpha})$ and the thermal properties in the form of the overall heat loss coefficient, U_L. Therefore, changes in optical or thermal properties of the collector result in a change of $(T_p - T_a)/G$. However, the parameter, $(T_p - T_a)/G$, is not totally independent of environmental conditions. Parameters such as η_d and θ can cause small variations in $(\hat{\tau\alpha})$ and parameters such as V_w, T_a, T_s, T_p, and β can cause significant variations in U_L. The effects caused by these parameters are discussed following the experimental uncertainty analysis.

The instruments used to measure $(T_p - T_a)/G$ are a differential thermocouple to measure the temperature difference, $(T_p - T_a)$, and a pyranometer to measure the solar radiation, G. The measurement uncertainty associated with measuring $(T_p - T_a)$ using a differential thermocouple is approximately $\pm$ 0.5 C. The measurement uncertainty associated with measuring G with a WMO class I pyranometer is composed of several separate uncertainties. The temperature compensation, linearity, and cosine response of the pyranometer each introduce a $\pm$ 1 per cent uncertainty in the measurement. These uncertainties statistically combine to give an overall uncertainty in the pyranometer of $(1^2 + 1^2 + 1^2)^{1/2} = \pm 1.7$ per cent. In addition, a $\pm$ 1 per cent error is assumed in the recording apparatus for both G and $(T_p - T_a)$. The uncertainties in G and $(T_p - T_a)$, including recording errors, are

$$\omega_G = [(0.017G)^2 + (0.01G)^2]^{1/2} = \pm 0.02G \tag{4.5}$$

$$\omega_{(T_p - T_a)} = [0.5^2 + [0.01\ (T_p - T_a)]^2]^{1/2} \tag{4.6}$$

The uncertainty in $(T_p - T_a)/G$, as a result of both G and $(T_p - T_a)$, is determined by a Kline and McClintock [41] analysis as follows. Let

$$\chi = (T_p - T_a)/G \tag{4.7}$$

Then

$$\omega_\chi = \pm [(\frac{\partial \chi}{\partial G}\ \omega_G)^2 + (\frac{\partial \chi}{\partial (T_p - T_a)}\ \omega_{(T_p - T_a)})^2]^{1/2} \tag{4.8}$$

Substitution of the partial derivatives of Eq. 4.7 into Eq. 4.8 yields

$$\omega_\chi = \pm \chi[(-\omega_G/G)^2 + (\omega_{(T_p - T_a)}/(T_p - T_a))^2]^{1/2} \tag{4.9}$$

Finally, with the substitution of Eq's. 4.5 and 4.6 into Eq. 4.9

$$\omega_\chi = \pm \chi[(0.02)^2 + (0.01)^2 + (0.5)^2/(T_p - T_a)^2]^{1/2} \tag{4.10}$$

Thus, ω_χ for a stagnation collector with $(T_p - T_a)$ = 150 C is

$$\omega_\chi = \pm 0.23\ \chi \tag{4.11}$$

The next sub-section is concerned with evaluating the influence of environmental conditions on the parameter χ.

Sensitivity to Environmental Conditions

Changes in η_d, θ, V_w, T_a, T_s, β, and G can cause a slight change in $(\hat{\tau\alpha})$ and U_L, which in turn, change χ. Although G does not effect U_L directly, a change in G would cause a change in T_p, which would effect

U_L. Figures 4.16 and 4.17 show the variation of χ as a function of environmental conditions for collectors D and E. Collectors D and E were chosen because these collectors are, respectively, the best and poorest performing collectors analyzed. The other collectors used in this analysis showed similar results. The environmental conditions V_w, T_a, and G have the largest effect on χ in Figs. 4.16 and 4.17. These parameters affect U_L and not $(\hat{\tau\alpha})$. The parameters η_d and θ which effect $(\hat{\tau\alpha})$, have an insignificant effect on χ. The inclination angle of the collector, B, has a noticeable effect on collector D but little effect on collector E. Collector D is influenced more by β than collector E because free convection is more dominant in collector D than collector E as a result of the selective surface absorber plate. In general, the environmental conditions affect the low performance collector E more on a percentage basis than the high performance collector D. It should be pointed out that the range of environmental conditions in Figs. 4.16 and 4.17 is quite large. The environmental conditions would probably not change by this amount between initial and post exposure tests. If T_a, G, β, and V_w do not change more than 20 C, 200 W/m^2, 60°, and 2 m/s, respectively, between initial and post exposure tests, then the effect of each environmental condition on χ is within $\pm$ 3 per cent. These limitations on the ranges for T_a, G, and β should be easily met in practice, but the range on V_w might be more difficult to achieve. In addition, worst case combinations of several of these environmental conditions could lead to larger changes in $(T_p - T_a)/G$, but the frequency of such occurrence would be low.

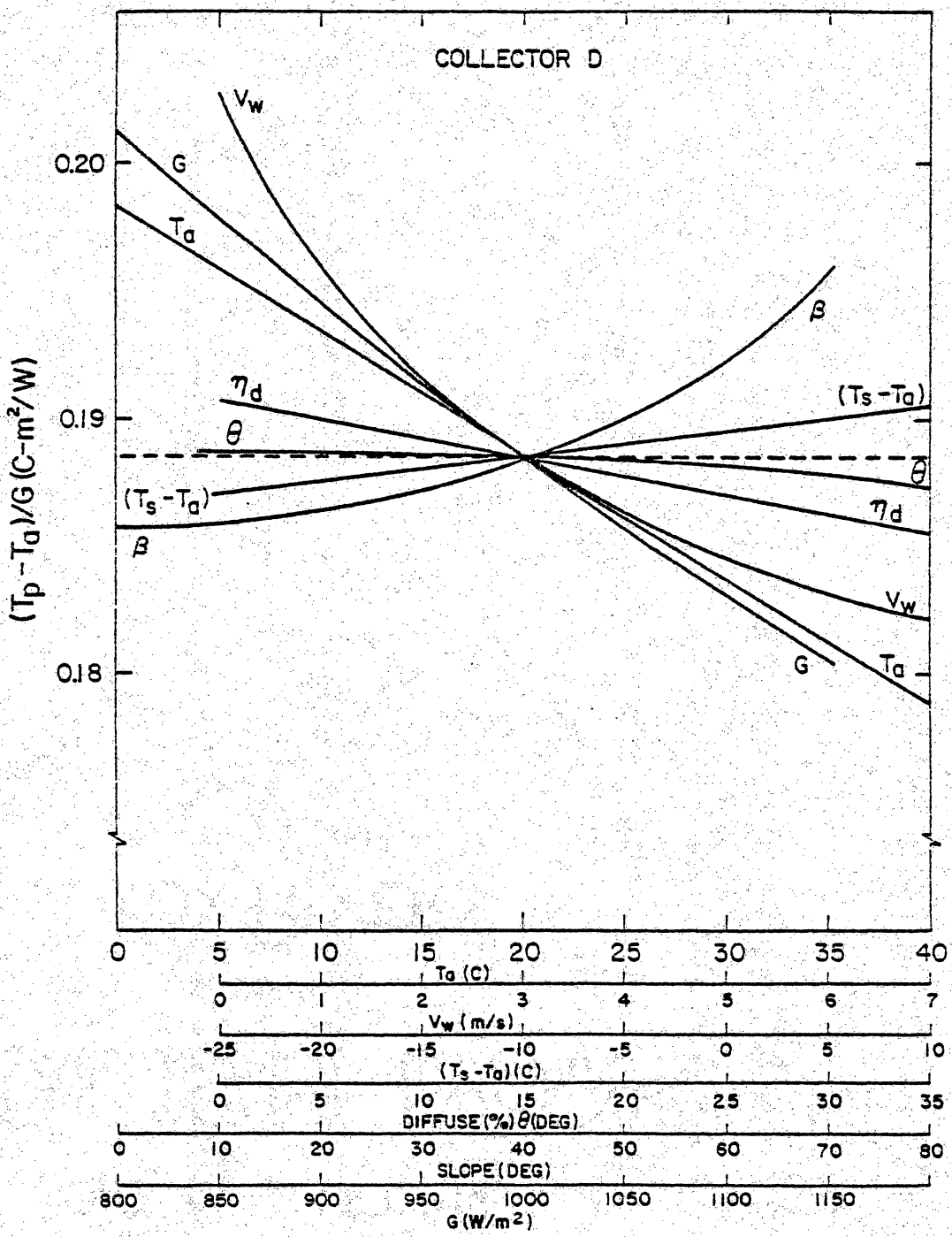

Fig. 4.16 Sensitivity of the Normalized Stagnation Temperature Parameter to Environmental Conditions for Collector D

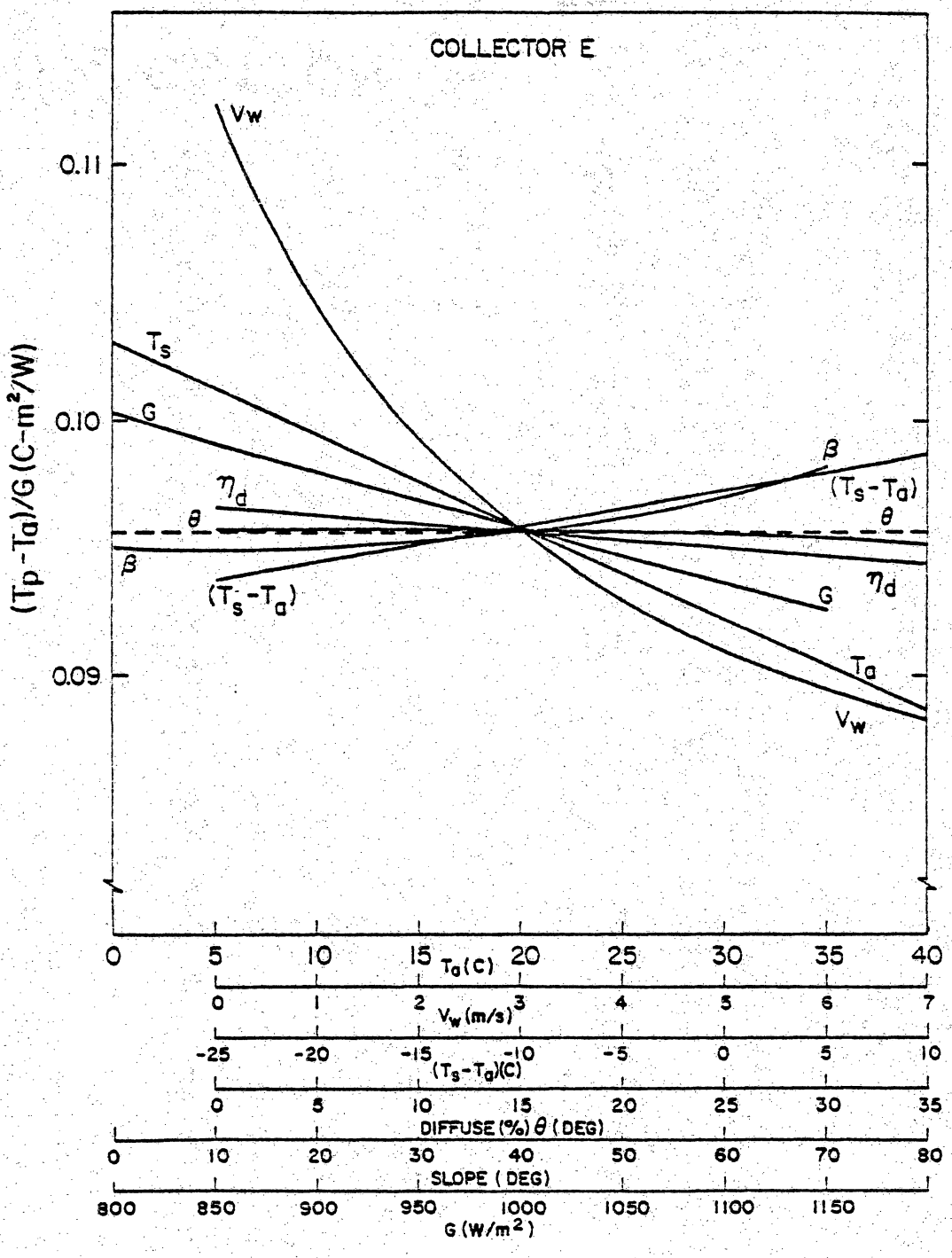

Fig. 4.17 Sensitivity of the Normalized Stagnation Temperature Parameter to Environmental Conditions for Collector E

Sensitivity to Collector Property Changes

The collector properties that are critical to collector thermal performance are $\hat{\tau}$, $\hat{\alpha}_p$, and ε_p. The sensitivity of the absorber plate temperature to a change in these properties for collectors D and E is shown in Fig. 4.18. A change in ε_p for collector E is not included in Fig. 4.18, because $\varepsilon_p = 0.87$ and increases in this value would cause small decreases in the absorber plate stagnation temperature. A decrease in $\hat{\tau}$ for collector D causes the largest amount of change in T_p. The reason for this is that collector D has two covers and $\Delta\hat{\tau}$ represents the change in each cover. The sensitivity to property changes is higher for collector D than collector E. This higher sensitivity results from collector D having a higher T_p than collector E and the change in T_p is a fraction of $(T_p - T_a)$. Values for G and T_a used to generate Fig. 4.18 are 1000 W/m^2 and 20 C, respectively. The corresponding absorber plate stagnation temperatures for collectors D and E are 227 C and 134 C, respectively. Thus, a property change of 0.1 in $\hat{\alpha}_p$ and $\hat{\tau}$ for collector E would cause a decrease in χ of 6.5 per cent and 4.4 per cent, respectively. A property change of 0.1 in $\hat{\alpha}_p$, $\hat{\tau}$, and ε_p for collector D would cause a decrease in χ of 6.0 per cent, 8.6 per cent, and 5.9 per cent, respectively. Using Eq. 4.10, the uncertainty in χ for collectors D and E is $\pm$ 2.3 per cent. (Note that the term $(0.5)^2/(T_p - T_a)^2$ in Eq. 4.10 adds very little to the overall uncertainty. The majority of the uncertainty is contributed by the pyranometer error.) Using an uncertainty of $\pm$ 2.3 per cent, the uncertainty bands of the initial and post tests would become completely separated with changes in χ of greater

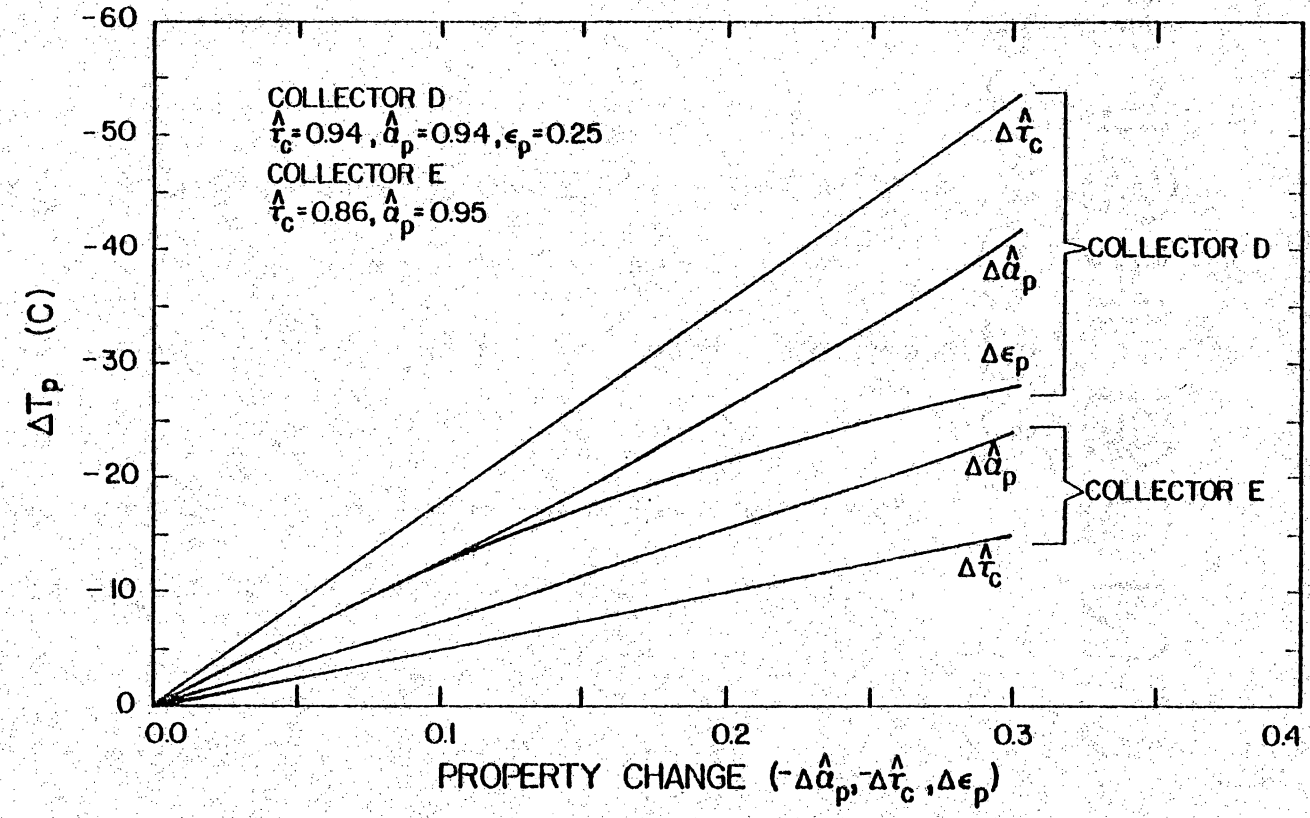

Fig. 4.18 Sensitivity of the Absorber Plate Temperature of Collectors D and E to Collector Property Changes

than 4.6 per cent. Thus, property changes on the order of 0.1 in $\hat{\alpha}_p$, $\hat{\tau}$, and ε_p would be detectable using this method, with the exception of $\hat{\tau}$ for collector E which would be only marginally detectable. This result, however, assumes that the environmental conditions were essentially constant. Large variances in environmental conditions may preclude determining property changes of the order of 0.1 in $\hat{\alpha}_p$, $\hat{\tau}$, and ε_p.

One additional source of error in these measurements is the effect of transients on the measurement of χ. This source of error is considered in the next section.

4.3 Instantaneous Method

The measurement uncertainty, sensitivity to property changes, and sensitivity to environmental conditions for the parameter χ were developed in the last section. In addition to these factors, a test method incorporating the instantaneous measurement of χ must take into account transients in T_p caused by changes in G. Even on clear days, the heat capacity of the collector can lead to errors in measurements of the steady-state T_p in the morning and afternoon hours. Figure 4.19 uses the data from Fig. 4.9 with the parameter χ plotted as a function of solar time. The sudden change around 9:30 solar time in Fig. 4.19 is a result of a momentary period of cloud cover. This jump indicates how sensitive the measurement of χ is to even short durations of cloud cover. The remaining part of the day was about as clear as is possible. During the quasi-steady portion of the day from one hour before to one hour after solar noon, the parameter χ varied by $\pm$ 1.5 per cent. During clear days, measurements taken during this two hour time period would probably be within $\pm$ 1.5 per cent for most collectors having heat capacities similar to collector I.

Since perfectly clear days are infrequent for many locations, a procedure is needed to determine the amount of time after a period of cloud cover before quasi-steady measurements can be made. The following discussion and analysis provides an estimate for the length of this waiting period.

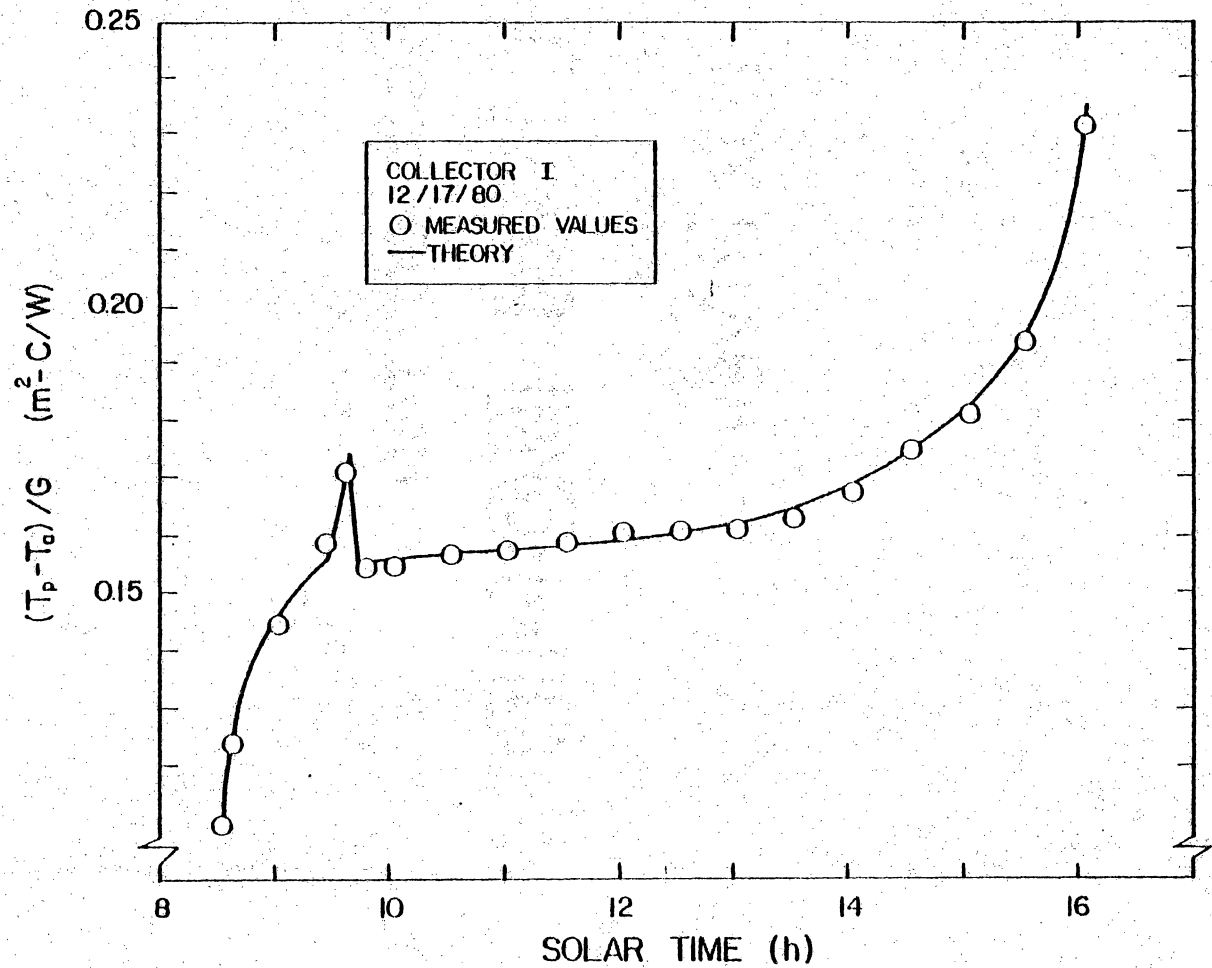

Fig. 4.19 Normalized Stagnation Temperature Parameter as a Function of Solar Time for Collector I on 12/17/80

Response to Transients

The basis for the following analysis is the assumption that the entire heat capacity of the collector can be represented by an effective heat capacity "lumped" in the absorber plate. In addition, the following assumptions are made:

1. A cloud is represented by a step change in solar radiation from the initial value to zero.
2. The heat losses are represented by a constant heat loss coefficient. The coefficient, however, is different for the heating and cooling cases.
3. All other properties are constant.

The solution to this first-order lumped system with time is represented by the following well known equation.

$$\theta = \theta_o \exp(- t/\tau_c) \tag{4.12}$$

where: $\theta = T_p - T_a$

θ_o = initial value of $(T_p - T_a)$

$\tau_c = (mC)_e/\overline{U}_{L,C}$

$\overline{U}_{L,C}$ = average loss coefficient during cooling

After a cloud cover duration of Δt, it is assumed that the solar radiation returns to its original level by a step change. The absorber plate temperature as a function of time after Δt is represented by

$$\theta = \theta_o + \theta_o [\exp (- \Delta t/\tau_c) - 1] \exp [- (t - \Delta t)/\tau_h]; \quad \text{for } t \geq \Delta t \tag{4.13}$$

where: Δt = cloud duration

$\tau_h = (mC)_e/\overline{U}_{L,h}$

$\overline{U}_{L,h}$ = average loss coefficient during heating

The initial condition used for Eq. 4.13 is

$$\theta = \theta_o \exp (- \Delta t/\tau_c) \text{ at } t = \Delta t \tag{4.14}$$

If the recovery time, R, is defined as the amount of time required after the period of cloud cover for θ/θ_o to be equal to ν, then solving Eq. 4.13 for $(t - \Delta t)$ when $\theta/\theta_o = \nu$ yields

$$R = \tau_h \ln \left[\frac{1 - \exp (- \Delta t/\tau_c)}{1 - \nu} \right] \tag{4.15}$$

To validate Eq. 4.15 and to illustrate the method, data obtained using the indoor instrumented collector are analyzed. Figure 4.20 shows the absorber plate stagnation temperature response to step changes in the input power. The cooling response represents θ/θ_o as a function of time after a step change in input power from 1200 to 0 W. The heating response represents θ/θ_o as a function of time after a step change in input power from 0 to 1200 W. The solid lines represent the simplified theory and the circles represent measured data. A least-squares fit to the experimental data was used to determine τ_c and τ_h. Values for τ_c and τ_h were determined to be 32 and 18 minutes, respectively. A more detailed analysis showed that the reason τ_c and τ_h are not equal is a result of the temperature dependence of U_L (refer to Eq. 4.2). The simplified theory matches the measured data very well in Fig. 4.20.

An additional test on the indoor instrumented collector was performed to determine the recovery time, R, after a momentary 10-minute shut-off of power. Figure 4.21 shows the results of this test. The solid line in Fig. 4.21 was determined by using Eqs. 4.12 and 4.13 with Δt = 10 minutes, τ_c = 32 minutes, and τ_h = 18 minutes. From Fig. 4.21

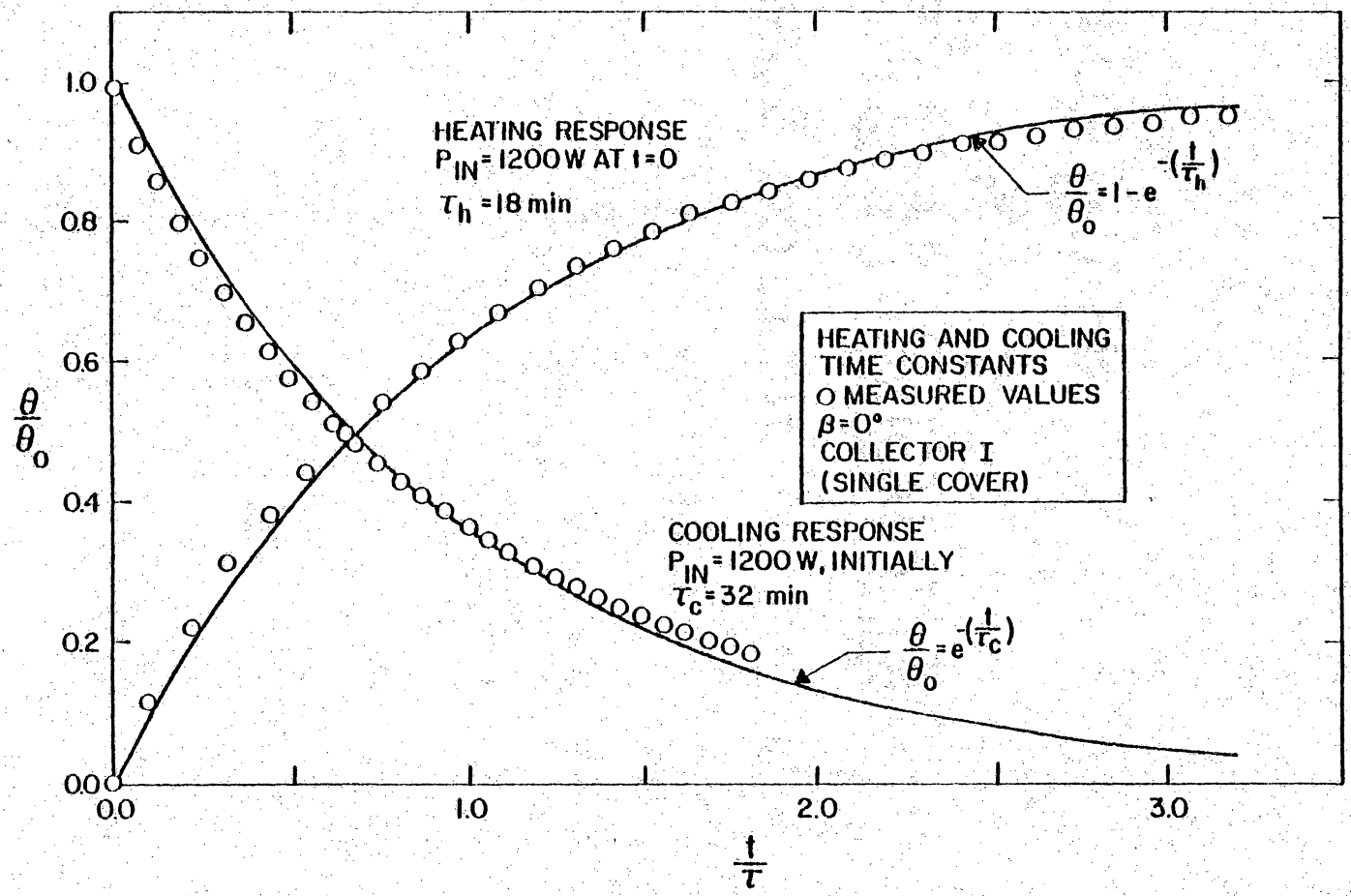

Fig. 4.20 Comparison of Measured and Calculated Heating and Cooling Absorber Plate Temperature Responses to Step Changes in Input Power for Collector I Indoors

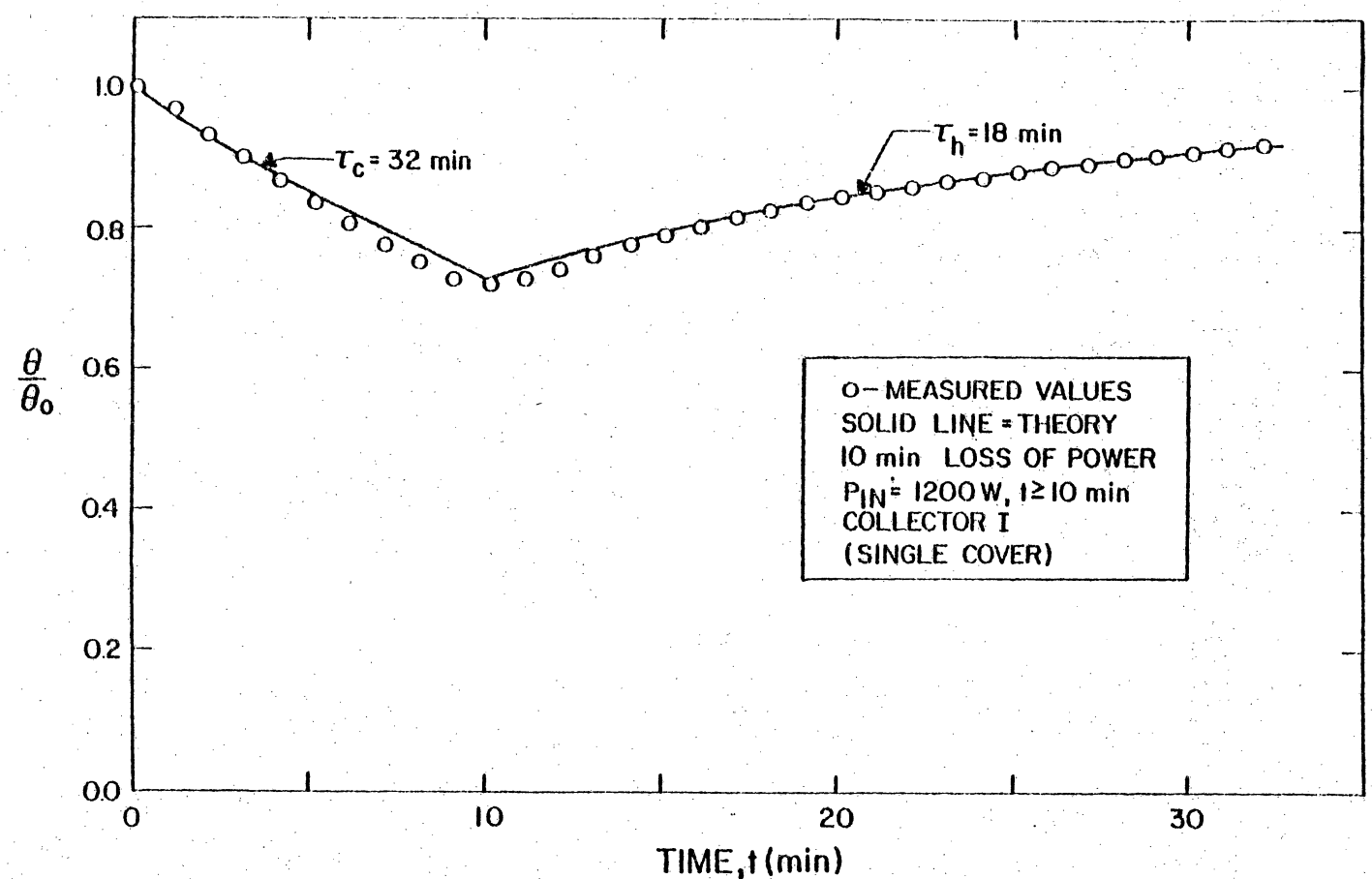

Fig. 4.21 Comparison of Measured and Calculated Absorber Plate Temperature Response to a Momentary 10 Minute Shut-Off of Power for Collector I Indoors

the recovery time, R, required for $\theta/\theta_o = \nu$ to become 0.90 is 18.1 minutes. The recovery time calculated by Eq. 4.15 for this test is 17.8 minutes.

Figure 4.21 validates the simplified theory used in Eq. 4.15 to calculate the recovery time. But, in order to use Eq. 4.15, τ_c and τ_h must be known. These time constants can be obtained outdoors near solar noon by suddenly shading and exposing a stagnating collector. Practical problems, however, may limit the usefulness of the previously mentioned instantaneous method. First, added testing time would be required to determine τ_c and τ_h. Secondly, θ/θ_o should be chosen as 0.98 to obtain accurate measurements after a period of cloud cover. This value of θ/θ_o would correspond to a recovery time of 47 minutes after a 10 minute cloud cover. Therefore, one 10-minute duration of cloud cover near solar noon practically precludes obtaining accurate results for that day. Although these results were obtained using only one collector, collector I is a representative collector with an average heat capacity and these results should be typical.

Outdoor Results

Outdoor measurements were made on collectors D and I to validate the instantaneous method previously described. Figure 4.22 shows the results of these measurements. The data used to construct Fig. 4.22 were all taken on very clear days between December, 1980 and February, 1981. Only clear days were chosen to minimize transients and to focus mainly on the effects of environmental conditions and experimental

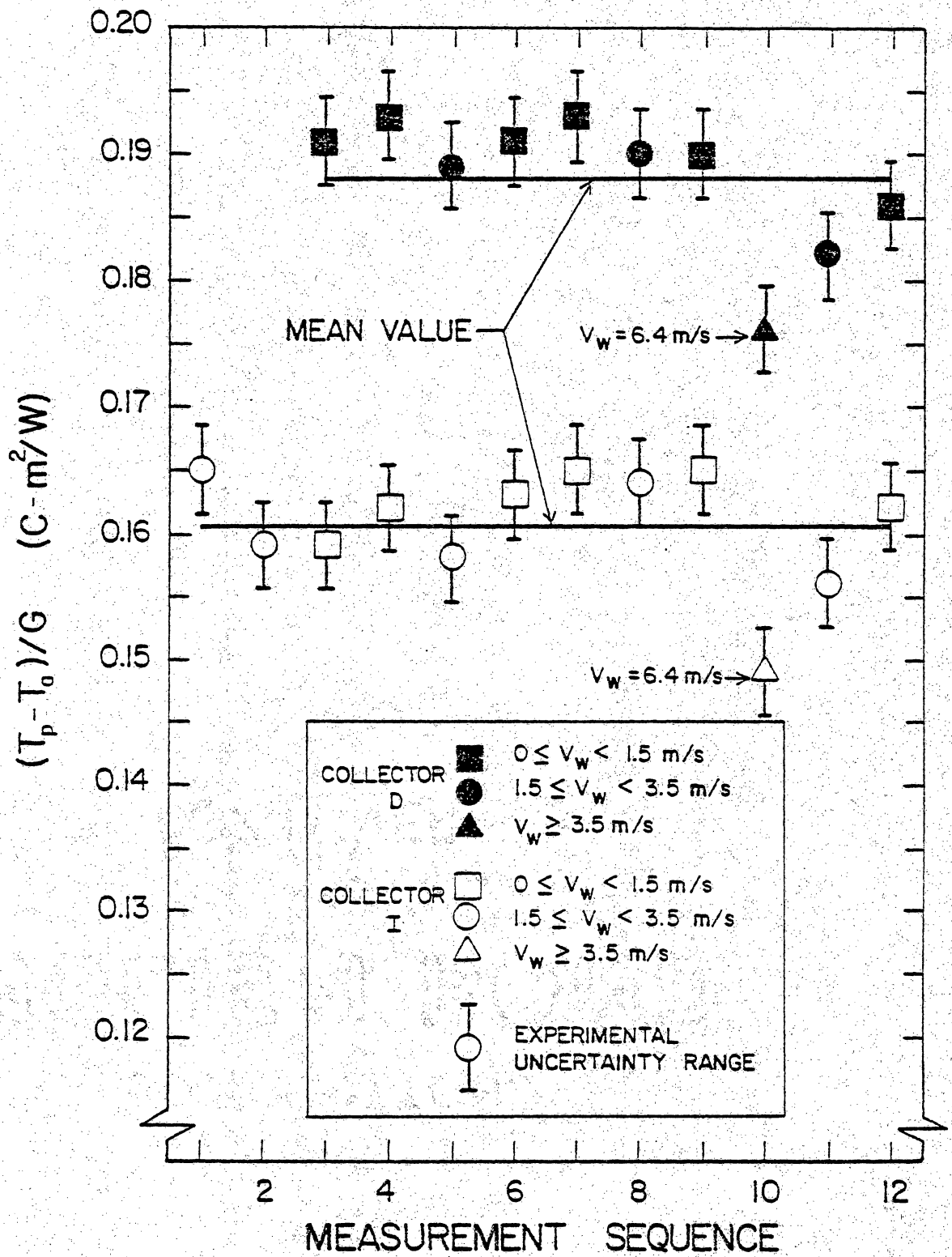

Fig. 4.22 Measured Values of the Normalized Stagnation Temperature Parameter at Solar Noon on Clear Days for Collectors D and I at VPI&SU

uncertainty. Both solid lines in Fig. 4.22 represent the mean values of $(T_p - T_a)/G$ for collectors D and I. The measurement sequence used for the abscissa represents the chronological sequence that the data were taken, but the number of days between each measurement varies. It is assumed that performance of collectors D and I did not change during this three month period. This assumption is reasonable because the NBS Durability and Reliability Program [2] and other previous tests have shown the performance of both collectors do not change after a three month period. With the assumption that the performance of both collectors remained constant, the scatter of data in Fig. 4.22 is a result of experimental uncertainty and environmental conditions. The only environmental condition which showed a predictable effect on the results was the wind speed. Most of the data taken with wind speeds less than 1.5 m/s fell above the mean value. The only data point taken with wind speeds above 3.5 m/s fell well below the mean value. There is a definite sequential correlation between the data taken on collectors D and I. The high and low values for collectors D and I tend to follow the same trends with time. This correlation of trends is most likely a result of environmental conditions.

The experimental uncertainty associated with the measurements is shown by error bands on the data points. The scatter in the measurements is equal to or better than the experimental uncertainty when the data point taken with $V_w = 6.4$ m/s is omitted. With limitations on wind speed and for very clear days, it appears that the instantaneous method can determine property changes in $\hat{\alpha}_p$, $\hat{\tau}$, and ε_p in the amount of 0.1 or less. Data taken on days other than very clear have transients that

make determining accurate quasi-steady measurements difficult. The next section investigates a method which integrates $(T_p - T_a)$ and G over the period of a day to eliminate the effects of short term transients.

4.4 All-Day Integration Method

The limitations associated with an instantaneous method used to measure $(T_p - T_a)/G$ were discussed in the last section. A method based on integrating the parameters $(T_p - T_a)$ and G over the period of one day is now considered. The main advantage of an integration method is the elimination of the problems associated with transients in the measured parameters. This section is divided into sub-sections dealing with the theory of the method, sensitivity to environmental conditions, sensitivity to property changes, and preliminary measured results.

Theory

The transient stagnation temperature of the absorber plate can be represented by the following equation which is obtained from an energy balance on the absorber plate.

$$(\hat{\tau\alpha})\ G - U_L\ (T_p - T_a) = (mC)_e\ dT_p/dt \tag{4.16}$$

where $(mC)_e$ is the effective heat capacity of the collector lumped at the absorber plate. Integrating Eq. 4.16 over the period of one day yields

$$\int_0^{24h} (\hat{\tau\alpha})\ G\ dt - \int_0^{24h} U_L\ (T_p - T_a)\ dt =$$

$$(mC)_e\ [T_p(24h) - T_p\ (0h)] \tag{4.17}$$

With the assumption that the absorber plate temperature at midnight is the same as 24 hours before, Eq. 4.17 can be reduced to

$$\int_{\dot{0}}^{24h} (\tau\hat{\alpha})\ G\ dt = \int_{0}^{24h} U_L\ (T_p - T_a)\ dt \tag{4.18}$$

Next, the definitions of the mean daily $(\tau\hat{\alpha})$ and the mean daily U_L are introduced.

$$(\overline{\tau\alpha}) = \int_{0}^{24h} (\tau\hat{\alpha})\ G\ dt \Big/ \int_{0}^{24h} G\ dt \tag{4.19}$$

$$\overline{U}_L = \int_{0}^{24h} U_L\ (T_p - T_a)\ dt \Big/ \int_{0}^{24h} (T_p - T_a)\ dt \tag{4.20}$$

Substitution of Eqs. 4.19 and 4.20 into Eq. 4.18 yields

$$\int_{0}^{24h} (T_p - T_a)\ dt = [(\overline{\tau\alpha})/\overline{U}_L] \int_{0}^{24h} G\ dt \tag{4.21}$$

Thus, if changes in $(\overline{\tau\alpha})$ or $\overline{U}_L$ occur during exposure, measurements of $\int (T_p - T_a)\ dt$* and $\int G\ dt$ could be used to detect the change. The ratio $[(\overline{\tau\alpha})/\overline{U}_L]$, however, is not only a function of collector properties. The value of $(\overline{\tau\alpha})$ would be a function of the average incident angle of beam radiation and the average diffuse fraction for the day. The value of $\overline{U}_L$ would be a function of the average V_w, T_a, T_s, and β for the day. Thus, the all-day integration method, like the instantaneous method, is a function of the environmental conditions.

Figure 4.23 shows three solar radiation profiles with very different characteristics but equal values for $\int G\ dt$. Profiles 1, 2, and 3

*In the following discussion, the symbol $\int$ denotes integration over a 24 hour period.

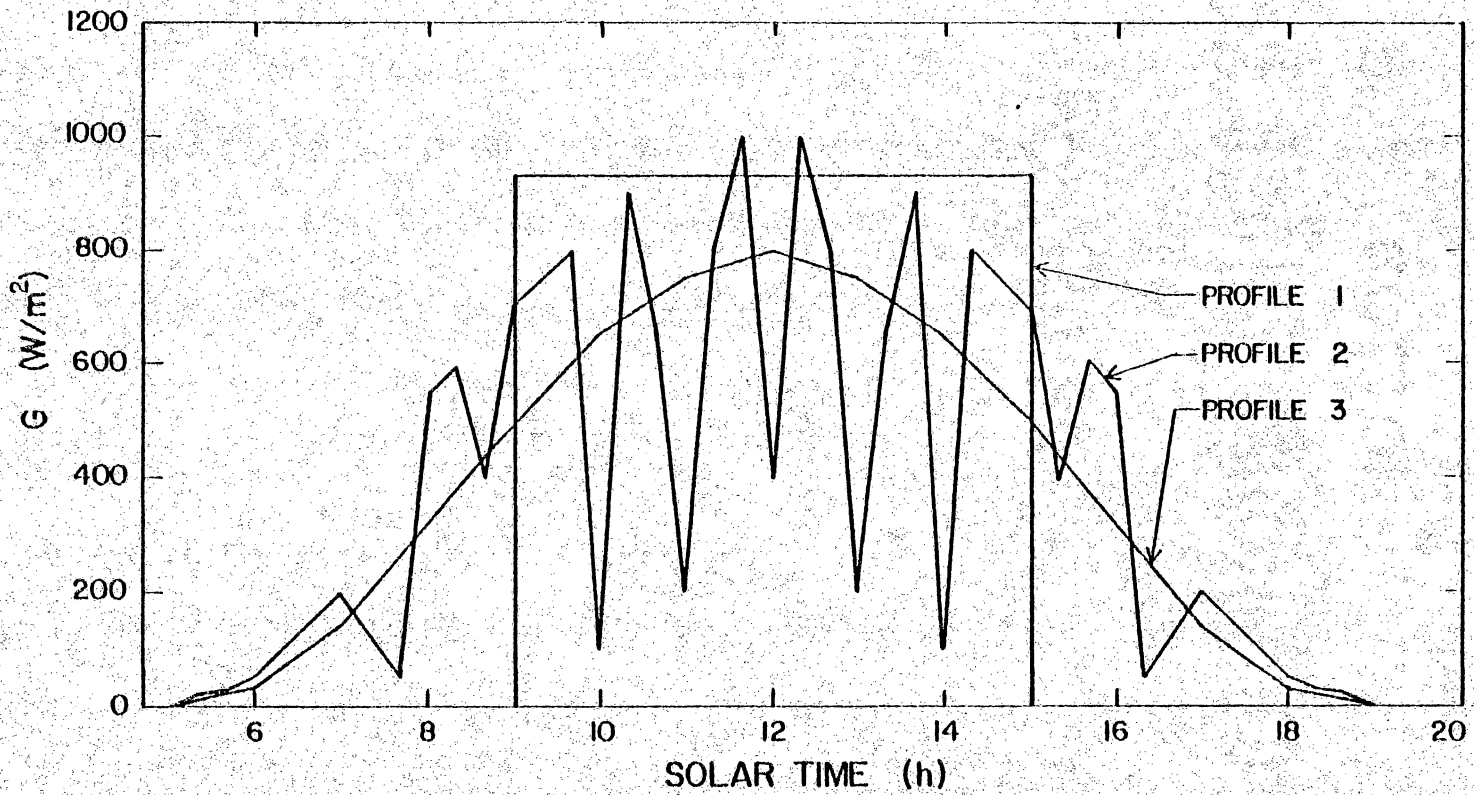

Fig. 4.23 Three Solar Radiation Profiles with Equal Values of Integrated Solar Radiation Used to Test the All-Day Integration Method

represent a square step change in solar radiation, a clear day with intermittent cloud cover, and a hazy day with solar radiation equal to 80 per cent of that on a clear day, respectively. These three profiles are used in combination with the transient model to determine the effect of the solar radiation profile on $\int(T_p - T_a)\,dt$ for collectors A, B, D, and E. The results of this study are shown in Table 4.3. The three different profiles resulted in little differences in the values of $\int(T_p - T_a)\,dt$. The largest differences are between profiles 1 and 3. The difference in $\int(T_p - T_a)\,dt$ between profiles 1 and 3 for collector D is 3.9 per cent. However, the difference between the more realistic profiles (profiles 2 and 3) is about 1 per cent or less. Thus, the integration method can be used for cloudy days as well as clear days.

The next area of concern is how to compare results for long days in the summer with short days in the winter. In addition, the amount of solar radiation during a summer or winter day can be a variable. Figure 4.24 shows calculated results for collector B obtained using 20, 40, 60, 80, and 100 per cent of clear day solar radiation for representative days in March, June, September, and December. The theoretical values, indicated by the open symbols, are the results from these 20 different days. The solid line is a best fit curve to these theoretical values. The effect of day length and shape of each solar radiation profile is included in Fig. 4.24. Note that the relation between $\int(T_p - T_a)\,dt$ and $\int G\,dt$ is not linear. This nonlinearity is a result of $\overline{U}_L$ being a function of T_p. A decrease in thermal performance of

Table 4.3 Effect of Solar Radiation Profile on the Results of the All-Day Integration Method

Environmental Conditions:

$n = 81$, $\phi = 40°$, $B = 40°$, $\eta_d = 0.15$

$T_a = 10$ C, $V_w = 2.0$ m/s, $\int_0^{24h} G\,dt = 20.1$ MJ/m^2

Collector	Integrated $(T_p - T_a)$			Maximum Difference (%)
	Profile 1 (C-h)	Profile 2 (C-h)	Profile 3 (C-h)	
A	894	901	905	1.2
B	769	785	790	2.6
D	1110	1149	1155	3.9
E	575	579	589	2.4

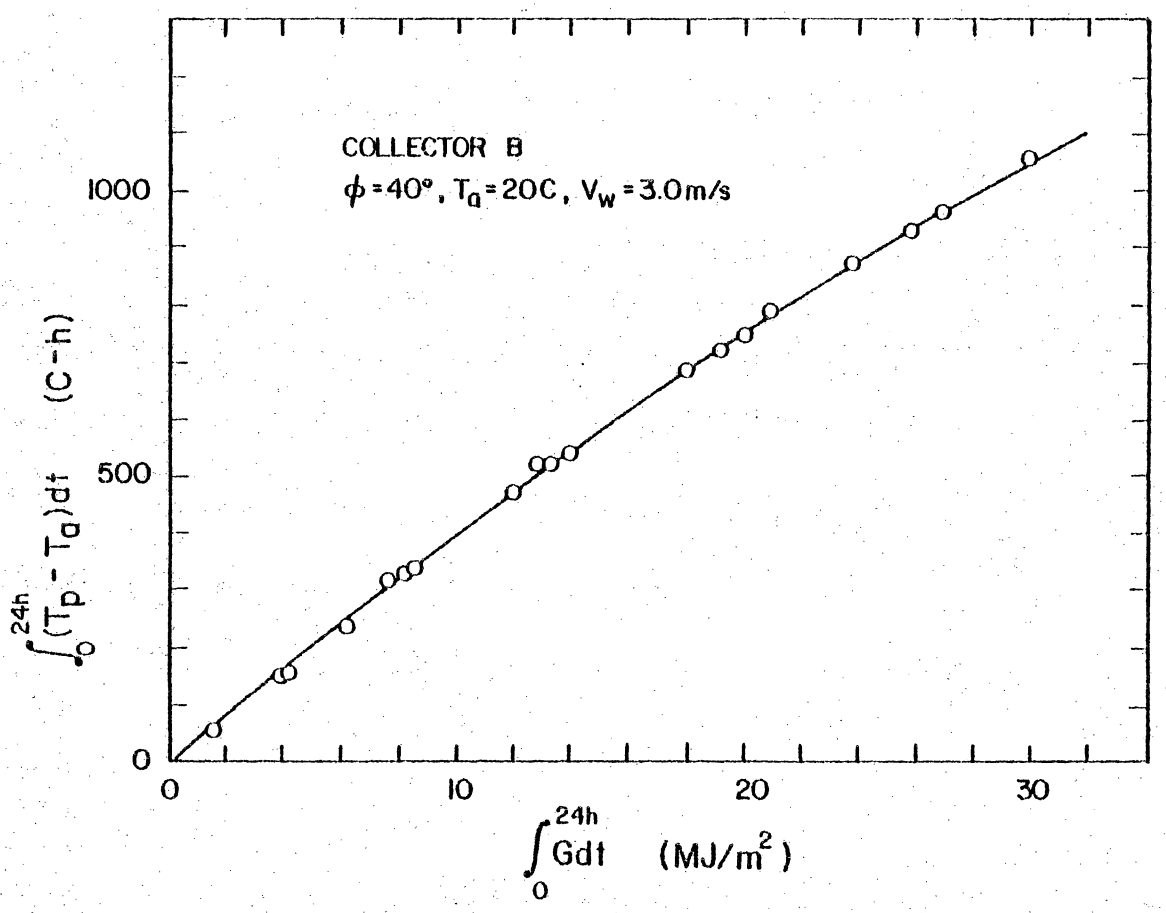

Fig. 4.24 Theoretical Results of the All-Day Integration Method for Collector B with Constant Environmental Conditions for a One-Year Period

collector B after environmental exposure would result in post exposure measurements falling below the solid line in Fig. 4.24.

An attempt to normalize the theoretical values in Fig. 4.24 by the day length, τ_d, is shown in Fig. 4.25. The reasons for this normalization would be to group winter and summer values together and use more familiar units such as (C) and (W/m^2). However, the normalization by τ_d introduced considerably more scatter in the results in Fig. 4.25 as compared to Fig. 4.24. The increased scatter is most likely caused by moving summer values down and to the left and moving winter values up and to the right as compared with Fig. 4.24. Therefore, the results throughout this discussion will be plotted unnormalized as in Fig. 4.24. The next sub-section discusses the effects of environmental conditions on the all-day integration method.

Sensitivity to Environmental Conditions

Environmental conditions affect the results of the all-day integration method in a manner similar to the effects on instantaneous measurements. The solar radiation profile was determined to have little effect on the results of the all-day integration method in the last sub-section. Figures 4.26 and 4.27 show the effect of V_w, T_a, T_s, β, θ, and η_d on $\int(T_p - T_a)\,dt$ for collectors D and E. The solar radiation profile used to generate these results was a clear day in March with $\int G\,dt = 26.9$ MJ/m^2. Similar studies were performed on the other collectors used in this investigation and the results from these studies are bounded by the curves in Figs. 4.26 and 4.27. The same trends discussed for the

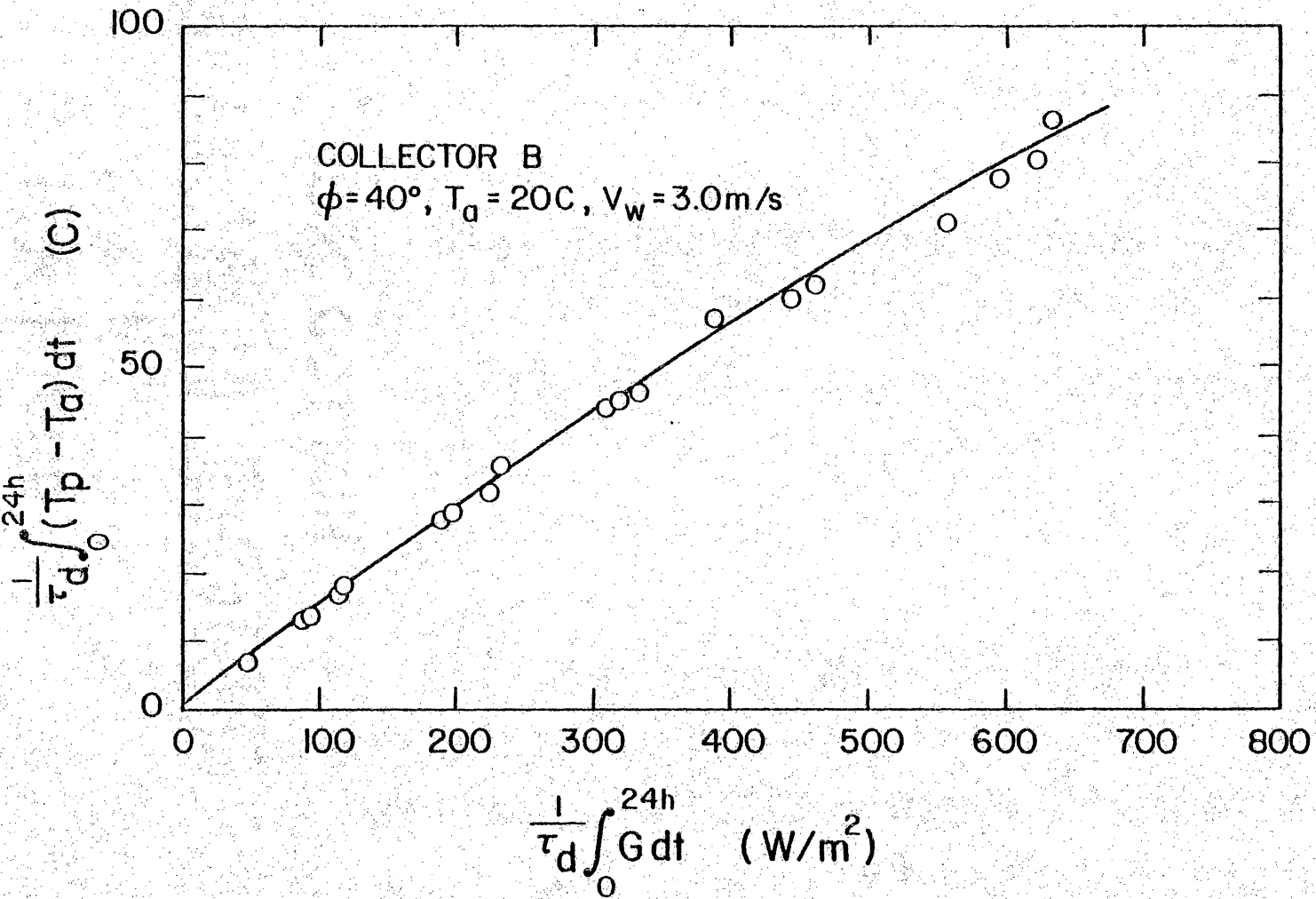

Fig. 4.25 Theoretical Results of the All-Day Integration Method Normalized by Day Length for Collector B with Constant Environmental Conditions for a One-Year Period

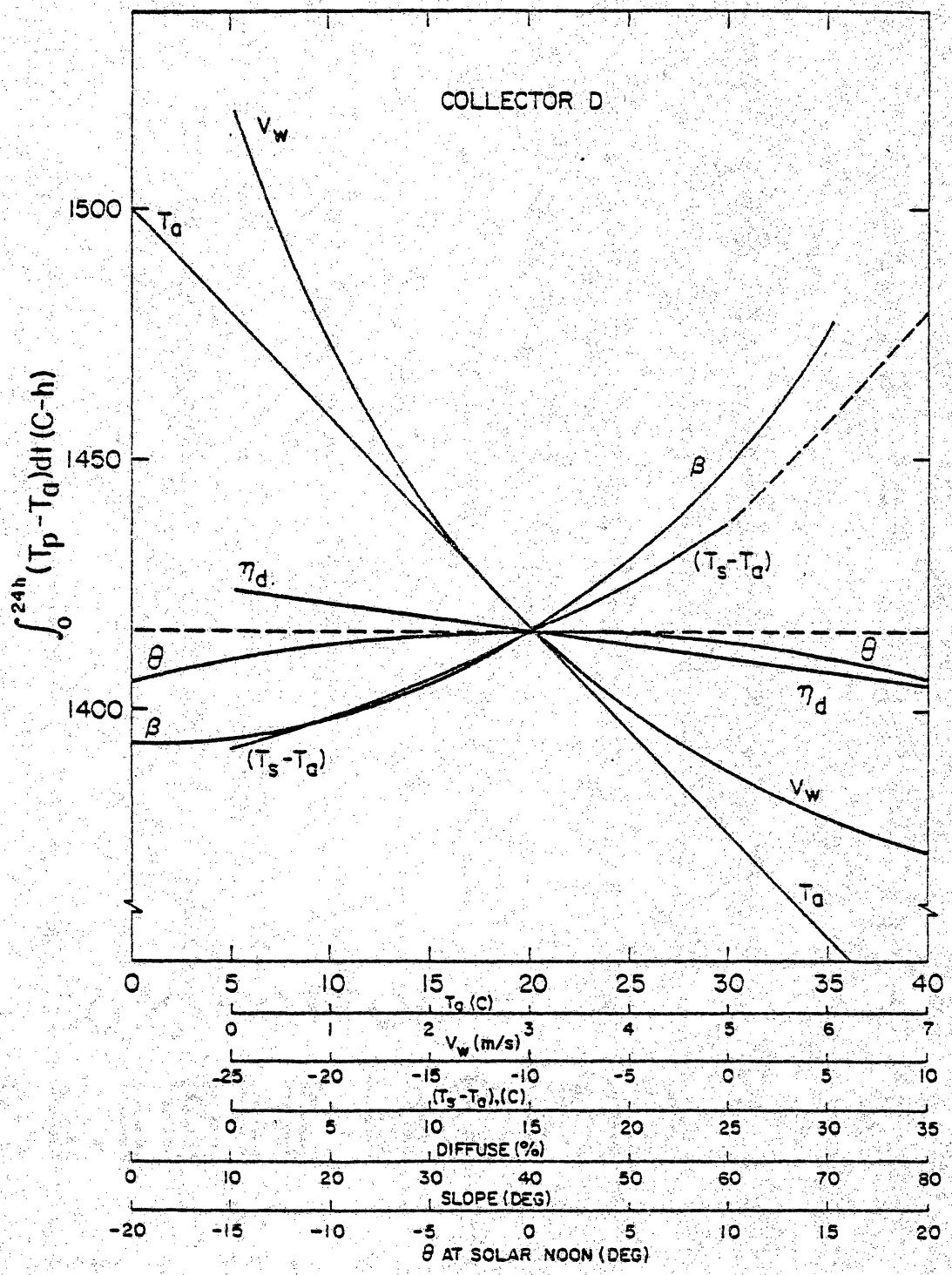

Fig. 4.26 Sensitivity of the All-Day Integration Method to Environmental Conditions for Collector D

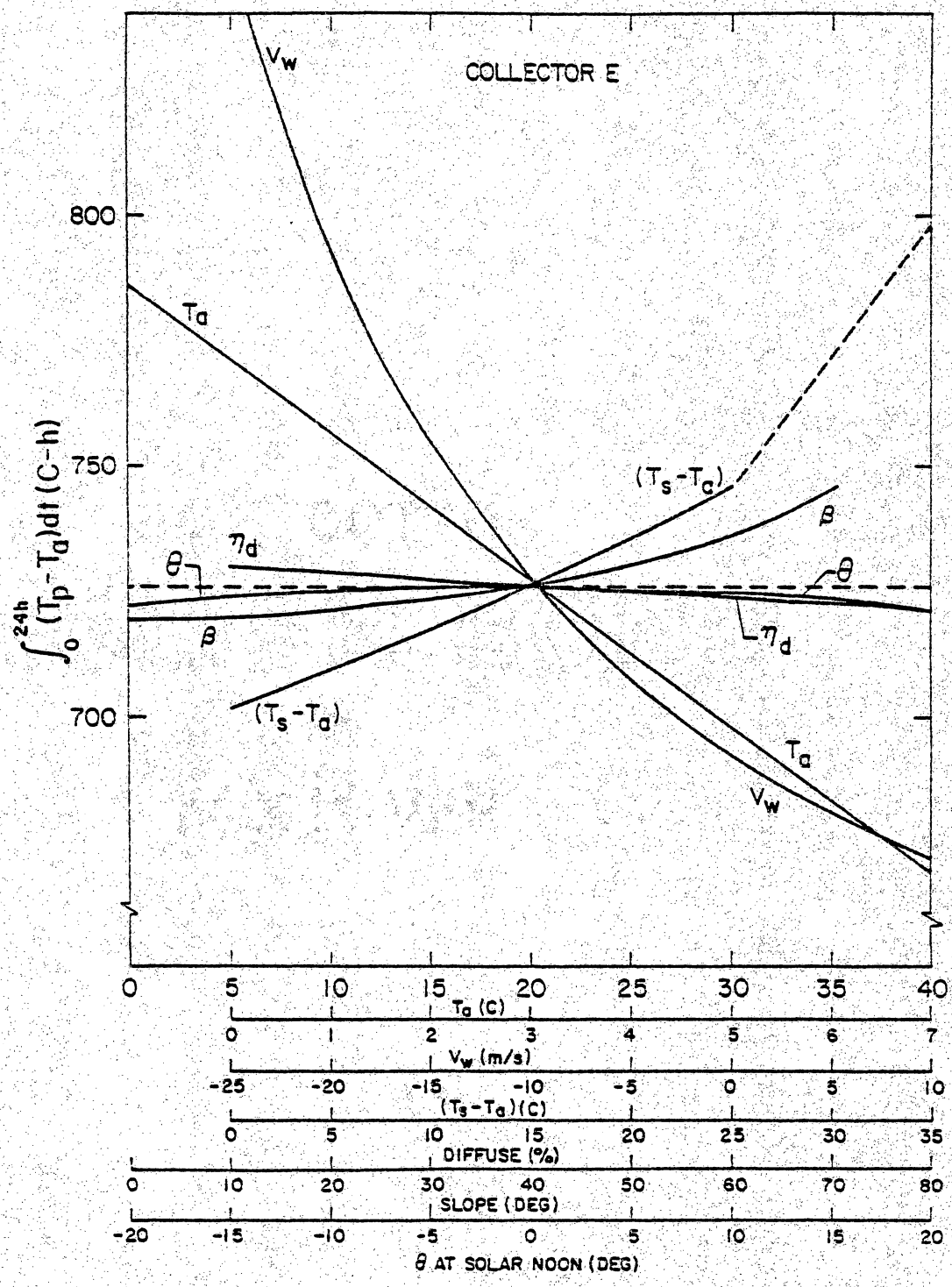

Fig. 4.27 Sensitivity of the All-Day Integration Method to Environmental Conditions for Collector E

instantaneous results are present for the integrated results. The results again show that the wind speed and ambient temperature are the dominant effects on both collectors D and E and that the inclination angle has a noticeable effect on collector D. The curve representing the effects of T_s on $\int(T_p - T_a)\,dt$ is dashed when $T_s > T_a$. This line is dashed because the only way that T_s could be greater than T_a would be during an indoor test using a solar simulator. Since a solar simulator would use an instantaneous method, the results for $T_s > T_a$ are unrealistic. As in Figs. 4.16 and 4.17, the environmental conditions affect collector E more on a percentage basis than collector D in Figs. 4.26 and 4.27. The effect of environmental conditions on $\int (T_p - T_a)\,dt$ can be held within $\pm$ 3 per cent if V_w, T_a, and β do not change more than 2 m/s, 15 C, and 60°, respectively, between initial and post-exposure tests. As with the instantaneous method, the integration method is influenced the most by wind speed.

Sensitivity to Collector Property Changes

The sensitivity to property changes of the all-day integration method is, in general, equivalent to the sensitivity to property changes of the instantaneous method. The results, however, are reported in a different format. Figure 4.28 shows how a change in $\hat{\alpha}_p$ from 0.96 to 0.86 affects the results of the all-day integration method. Similar results are obtained for equal changes in $\hat{\tau}$ and ε_p for other collectors. The environmental conditions were kept constant in the construction of Fig. 4.28 so that only the effects of changing $\hat{\alpha}_p$ would show up. The

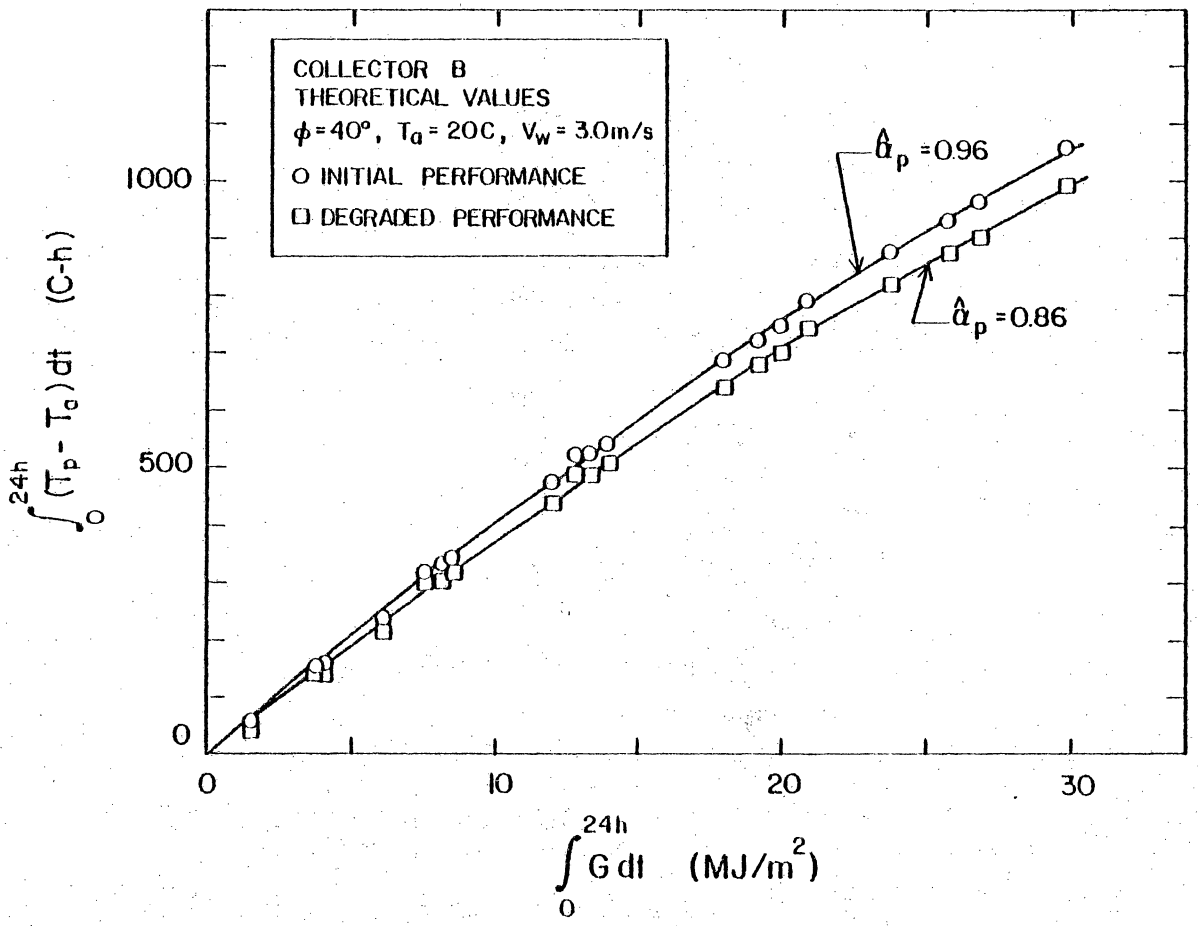

Fig. 4.28 Sensitivity of the All-Day Integration Method to a Change in $\hat{\alpha}_p$ from 0.96 to 0.86 for Collector B

initial or baseline theoretical values in Fig. 4.28 are the same values as in Fig. 4.24. The change resulting from $\hat{\alpha}_p$ decreasing from 0.96 to 0.86 becomes increasingly difficult to detect when $\int G\, dt$ becomes less than 20 MJ/m^2. Thus, in practice, only the clear and near-clear days contribute to determining property changes.

The experimental uncertainty in determining a datum point for this method is about $\pm$ 6 C-h in the direction of $\int(T_p - T_a)\, dt$ and about $\pm$ 2 per cent in the direction of $\int G\, dt$. The uncertainty in $\int(T_p - T_a)\, dt$ is essentially negligible and the uncertainty in $\int G\, dt$ would statistically permit determining property changes in $\hat{\alpha}_p$, $\hat{\tau}$, and ε_p of about 0.10 or less.

A comparison between the instantaneous and all-day integration methods reveal that both of these methods are similar with respect to experimental uncertainty, sensitivity to environmental conditions, and sensitivity to collector property changes. However, the all-day integration method is free from transients which limits the usefulness of the instantaneous method. In the author's judgment, the all-day integration method appears to have the most potential of the two methods.

Outdoor Measurements

Outdoor experimental data taken on collector I for the months of December, January, and February, 1981 are presented. The absorber plate stagnation temperature along with G, η_d, T_a, T_s, and V_w were measured continuously during these months. Some of the data from these three months were not used because of instrument problems and malfunctions.

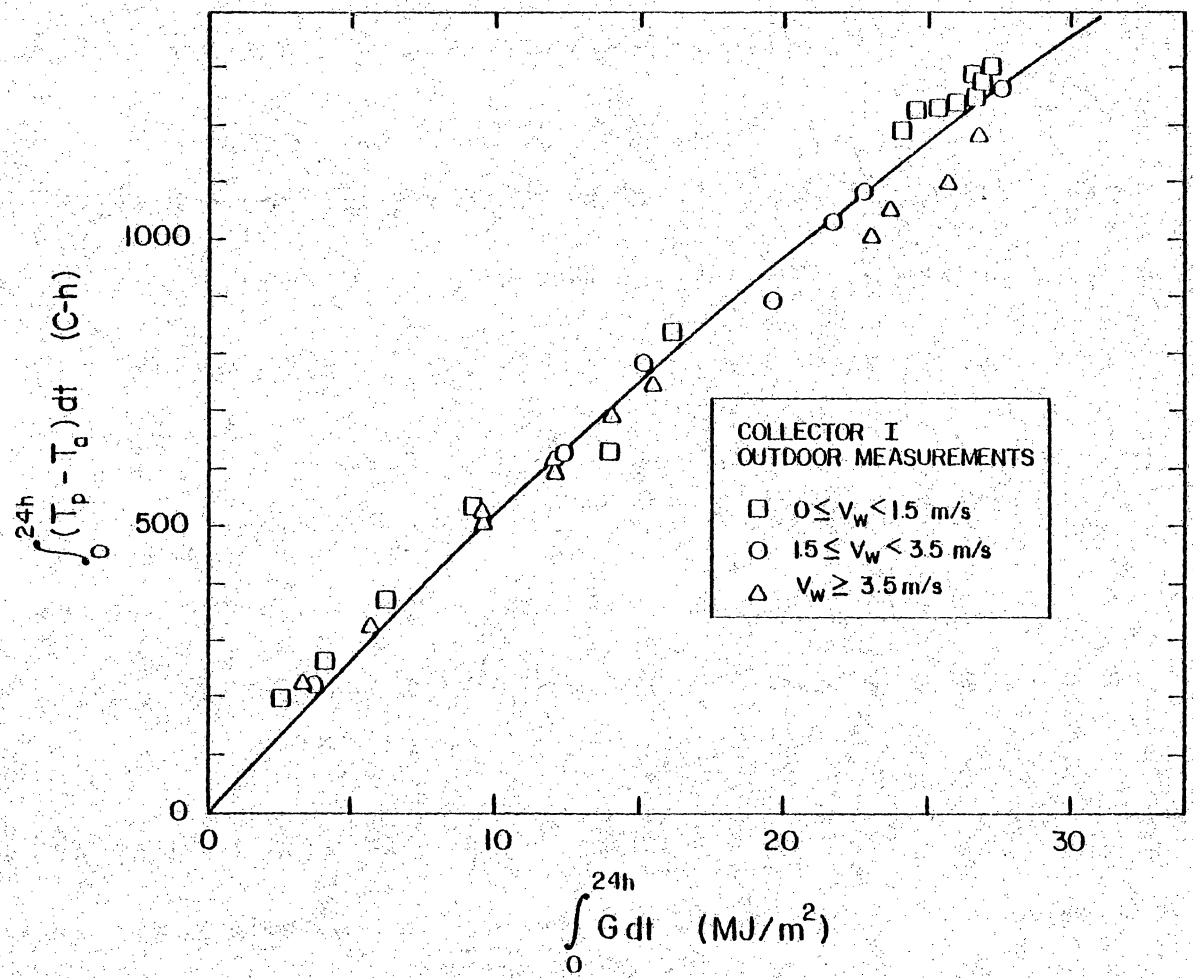

Fig. 4.29 Outdoor Measured Results Using the All-Day Integration Method for Collector I at VPI&SU

Figure 4.29 shows the results from these measurements presented in terms of the all-day integration method. The absorber plate stagnation temperature was measured at the center of the plate for the data in Fig. 4.29. The solid line in Fig. 4.29 was generated by a least-squares fit using a second-order polynomial forced through the origin. Data from the NBS Durability and Reliability program [2] and measurements from other tests have shown that the thermal performance of collector I is altered little, if any, after three months of stagnation exposure. With the reasonable assumption that the thermal performance of collector I did not change over this three month test period, all the scatter in Fig. 4.29 can be attributed to experimental error and environmental effects. The only strong trend in the data is the effect of wind speed on the results. Except for one set of points, all the data measured with daily average wind speeds less than 1.5 m/s are above the regression line, while all the data measured with daily average wind speeds greater than 3.5 m/s are below. This result tends to verify the earlier analytical result that the wind speed would influence the data more than the other environmental conditions. It is evident from Fig. 4.29 that if small property changes are going to be determined using this method, limits on wind speed variation or corrections for wind speed effects must be made.

A practical difficulty in generating Fig. 4.29 was the large number of man-hours needed to reduce the data. Data for collector D were not reduced primarily for this reason. Reducing the data to evaluate $\int(T_p - T_a)\,dt$ required most of the time. Since the relation

between temperature and thermocouple voltage is not linear, a direct integration of thermocouple voltage and then a conversion to temperature would lead to inaccuracies in the integrated temperature. The problem was resolved, however, by piecewise integrating the thermocouple voltage versus time in one millivolt increments. The integrated values in mV-h for each millivolt section (i.e., 0-1, 1-2, . . . 9-10 mV) was then converted to C-h by the average sensitivity, in C/mV, for each one millivolt section. The integrated segments were then added to obtain the total integrated value for the day. A detailed study of the error introduced by segmenting the integration into one millivolt segments showed a maximum error of 2 C-h. This amount of error is acceptable since it is undetectable in a graph such as Fig. 4.29. The voltage output from the pyranometer is linear with respect to solar irradiance. Thus, the time required to reduce $\int G\, dt$ was minimal as compared to the temperature integration.

The next section discusses the important results obtained thus far in Chapter 4 dealing with stagnation temperature test methods.

4.5 Summary of Results

Stagnation temperature test methods for determining collector property changes have been investigated and analyzed. The potential advantages of using stagnation temperature over the current energy output method are less measurement uncertainty, increased sensitivity to property changes, and less complicated test procedures and apparatus. The investigation, however, uncovered several limitations associated with using stagnation temperature to determine collector property changes. These limitations are primarily the strong effect of environmental conditions, particularly wind speed, on test results; a highly nonisothermal absorber plate resulting from edge heat losses and internal air stratification; and the slow time response of the absorber temperature to changes in solar radiation.

The potential advantages of a stagnation temperature test method were shown to be only marginally better than the current energy output method. The experimental uncertainty associated with the stagnation temperature method is only slightly less than that associated with the current method. The main reason for the small difference in experimental uncertainty between the two methods is that both methods depend strongly on measurements of solar radiation; these measurements dominate the experimental uncertainty. It is the author's opinion that the most significant limitation in either method is the relatively large experimental uncertainty associated with measuring solar radiation. Furthermore, the higher sensitivity to property changes of the stagnation temperature method over the energy output method may be overshadowed by

the effects of transients, changes in environmental conditions, and variations in absorber plate temperature. Cloud cover on the order of 10-minutes duration was shown to affect temperature measurements as long as 45 minutes after the cloud cover disappeared. Wind speed was shown both experimentally and analytically to have strong effects on measured results. Differences in wind speed greater than 2 m/s between initial and post-exposure tests could preclude determining significant property changes. The criterion for defining a mean absorber plate temperature from measurements could also influence results. Indoor tests on collector I showed that edge heat losses produced absorber plate temperature variations as much as 20 C. Also, outdoor tests showed that internal air stratification could result in temperature differences between the lower and upper third-sections of collectors D and I of 32 C and 24 C, respectively. These temperature variations on the absorber could adversely influence the interpretation of results if temperature measurement locations or the inclination angle of the collector changed between initial and post exposure tests.

Four measurement techniques for determining an appropriate stagnation temperature to reveal property changes were tried and analyzed. Techniques based on measuring the external cover temperature, the air temperature inside the flow tube header, and the temperature of air flowing through the absorber plate flow tubes were considered to be unsatisfactory. Measuring the absorber plate temperature from the backside with a spring loaded thermocouple probe was the recommended measurement technique.

The analytical models developed in Chapter 3 were experimentally verified and found to be acceptable for sensitivity studies and test method evaluation. The standard deviation of residual errors between measured and calculated temperatures was in all cases less than $\pm$ 5 C when parameter estimation theory was used to determine the absorber energy storage capacity and insulation thermal conductivity. Results from the analytical model verifications indicate that better agreement between measured and calculated temperatures may be possible if temperature dependent heat transfer properties are taken into account. However, the lack of measured property data as a function of temperature may pose practical problems in incorporating this refinement.

An instantaneous method and an all-day integration method of using absorber plate stagnation temperature to determine collector property changes were analytically and experimentally investigated. Analytical results showed that both methods have approximately the same measurement uncertainty and sensitivity to property changes and environmental conditions. The instantaneous method was determined to be highly sensitive to transients caused by changes in solar radiation. An equation for determining the temperature recovery time after a period of cloud cover was developed; however, the additional tests required for determining the heating and cooling time constants may limit the usefulness of this equation. The instantaneous method, in the author's opinion, is limited to testing on very clear days or with solar simulators. A solar simulator would resolve problems dealing with transients and variations in test conditions but the high cost and differences in energy spectrums

between natural and artifical solar radiation must be considered. The all-day integration method eliminates the problems resulting from outdoor transients. In addition, it was determined that the results obtained using this method were independent of solar radiation profile. The all-day integration method, in the author's opinion, is the better method for outdoor testing. To increase the accuracy of either method, it is recommended that the absorber plate temperature be measured in the center of the absorber and that variations in wind speed, ambient temperature, and inclination angle be kept to a minimum between initial and post exposure tests.

The results of this investigation can be extended into an area similar to determining property changes in actual full-size collectors. This area could be experimental parameter studies of different collector materials. Several standard exposure boxes could house different collector absorber, cover, or insulation materials. These boxes would then be exposed to stagnating conditions and the absorber plate temperatures monitored. The test boxes should have a large enough area to perimeter ratio to relatively minimize edge heat losses. Relative differences in initial thermal performance could be detected by differences in absorber stagnation temperature during the first day of exposure. Long-term differences in thermal performance could be monitored by comparison of stagnation temperature as a function of time. The effects of environmental conditions, transients, and experimental uncertainty would be minimized in a relative test of this type. Since temperature comparisons are relative to other collector materials and designs, measurements of solar radiation or ambient temperature would not directly affect

results. The only experimental uncertainties in the comparisons would be that associated with the temperature measurement, which would be relatively small. This type of testing could be beneficial to manufacturers evaluating several different variations of a material product.

5. CONCLUSIONS AND RECOMMENDATIONS

The following conclusions result from investigating stagnation temperature test methods for determining collector property changes:

1. Comparison of measured and calculated stagnation temperatures revealed that the analytical models developed in Chapter 3 predict measured temperatures to within a standard deviation of $\pm$ 5 C for the six typical collectors considered.

2. Stagnation temperature test methods are highly sensitive to changes in environmental conditions between initial and post exposure tests. Wind speed was shown to have the most influence on test results.

3. Transients as a result of even momentary periods of cloud cover can cause large errors in test results using methods based on instantaneous measurements. The all-day integration method, however, eliminated the problems associated with transients as a result of intermittent cloud cover.

4. The temperature distribution of an absorber plate during stagnation is highly nonisothermal. Edge heat losses and thermal stratification of the air between absorbers and covers can cause the absorber temperature to vary by as much as 40 C over the surface of the absorber.

5. The experimental uncertainty associated with stagnation temperature test methods is only marginally less than the current energy output test method. The experimental uncertainty associated with the pyranometer represents the majority of uncertainty in both methods.

6. Measuring the absorber plate temperature with a spring-loaded thermocouple probe proved to be the best method for measuring the stagnation temperature of a solar collector.

7. Even with limitations placed on the variation of environmental conditions, proposed stagnation temperature test methods are, at best, marginally superior to current energy output methods.

Further investigations dealing with stagnation temperature test methods should include the following studies:

1. Long-term (greater than one year) investigations of the all-day integration method. A solar collector with well-established material aging characteristics should be used in this study.

2. Evaluation of the instantaneous stagnation temperature method in combination with a solar simulator. Studies evaluating the cost and the ability of solar simulators to reproduce natural outdoor results should be included.

REFERENCES

1. Streed, E. R., and D. Waksman, "NBS Solar Collector Durability/ Reliability Program," ASTM Special Technical Publication No. 691, American Society for Testing and Materials, 1916 Race St., Philadelphia, Pa. 19103, 1980.

2. Waksman, D., E. R. Streed, and T. Seiler, "NBS Solar Collector Durability/Reliability Test Program," NBS Technical Note No. 1136, Jan. 1981.

3. Streed, E. R., and D. Waksman, "Uncertainty in Determining Thermal Performance of Liquid-Heating Flat-Plate Solar Collectors," NBS Technical Note #1140, Feb. 1981.

4. "ASHRAE Standard 93-77, Methods of Testing Solar Collectors Based on Thermal Performance," American Society for Heating, Refrigeration, and Air Conditioning Engineers, Inc., 345 E. 47th Street, N. Y. 10017, April 1977.

5. Streed, E. R., W. C. Thomas, A. G. Dawson, B. D. Wood, and J. E. Hill, "Results and Analysis of a Round-Robin Test Program for Liquid-Heating Flat-Plate Solar Collectors," Solar Energy, Vol. 22, 1979, pp. 235-249.

6. Thomas, W. C., "Effects of Test Fluid Composition and Flow Rates on the Thermal Efficiency of Solar Collectors," VPI&SU Report No. 80-03, Mechanical Engineering Department, VPI&SU, Blacksburg, Va., Appendix C, 1980.

7. Duffie, J. A. and W. A. Beckman, Solar Energy Thermal Process, Wiley, New York, 1974.

8. Thomas, W. C., "Solar Collector Test Procedures: Development of a Method to Refer Measured Efficiencies to Standardized Test Conditions," VPI&SU Report No. VPI-E-80.23, Mechanical Engineering Department, VPI&SU, Blacksburg, Va., 1980.

9. Padillo, R., "Solar Collection Systems - The Rationale," ASHRAE Journal, Vol. 19, June 1977, pp. 42-46.

10. Zerlaut, G. A., W. T. Dokos, and R. F. Heiskell, "Stagnation Testing of Flat-Plate Solar Collectors: Use of the Governing Equation in Diagnostics," Proceedings of the 1977 Flat-Plate Solar Collector Conference, Feb. 28 - March 2, 1977, Orlando, Florida.

11. Henderson, B., W. E. Schultz, and R. Barber, "Results of Long Term Natural Weathering Effects on Solar Collectors Under Stagnation Conditions," Sun II, Proceedings of the International Solar Energy Society, Silver Jubilee Congress, Atlanta, Georgia, May 1979, Vol. 1, pp. 405-407.

12. Yen, H., "Solar Collector Accelerated Stagnation/Exposure Test Report," Wyle Laboratories, Solar Energy Systems Division, Wyle #TR-531-22, April 20, 1978.

13. Waksman, D., E. Streed, and A. Dawson, "The Influence of Environmental Exposure on Solar Collectors and Their Materials," Proceedings of the 1980 Annual Meeting of the American Section, International Solar Energy Society, Phoenix, Az., June 1980, pp. 415-419.

14. "Intermediate Minimum Property Standards for Solar Heating and Domestic Hot Water Systems," NBSIR 77-1226, National Bureau of Standards, Washington, D. C., March 1977.

15. "Interim Performance Criteria for Solar Heating and Cooling Systems in Commercial Buildings, "NBSIR 76-1187, National Bureau of Standards, Washington, D. C., Nov. 1976.

16. Waksman, D., E. Streed, T. Reichard, and L. Cattaneo, "Provisional Flat-Plate Solar Collector Testing Procedures, First Revision," NBSIR 78-1305A, National Bureau of Standards, Washington, D. C., June 1978.

17. Morehouse, J. H., and R. I. Vachon, "A No-Flow Method for Measuring Solar Collector Performance," ASME Paper #77-WA/SOL-5, Winter Annual Meeting, Atlanta, Georgia, Nov. 1977.

18. Goodman, R. D., and A. G. Menke, "Effect of Cover Plate Treatment on Efficiency of Solar Collectors," Solar Energy, Vol. 17, 1975, pp. 207-211.

19. Gordon, J. M., D. Govaer, and Y. Zarmi, "Temperature-Dependent Collector Properties from Stagnation Measurements," Technical Note, Solar Energy, Vol. 25, 1980, pp. 465-466.

20. Birnbreier, H., "Durability Tests by Stagnation Temperature Measurements," International Energy Agency's Solar Heating and Cooling Program, Task III, Heidelberg, West Germany, Dec. 1978.

21. Eckert, E. R. G. and W. C. Carlson, "Natural Convection in an Air Layer Enclosed Between Two Vertical Plates with Different Temperatures," International Journal of Heat and Mass Transfer, Vol. 2, 1961, pp. 106-120.

22. Dropkin, D. and E. Somerscales, "Heat Transfer by Natural Convection in Liquids Confined by Two Parallel Plates Which are Inclined at Various Angles with Respect to the Horizontal," Journal of Heat Transfer, Vol. 87, 1965, pp. 77-84.

23. Catton, I., P. Ayyaswamy and R. M. Clever, "Natural Convection Flow in Finite, Rectangular Slot Arbitrarily Oriented with Respect to the Gravity Vector," International Journal of Heat and Mass Transfer, Vol. 17, 1974, pp. 173-184.

24. Ozoe, H. and H. Sayama, "Natural Convection in an Inclined Square Channel," International Journal of Heat and Mass Transfer, Vol. 17, 1974, pp. 401-406.

25. Arnold, J. N., I. Catton and D. K. Edwards, "Experimental Investigation of Natural Convection in Inclined Rectangular Regions of Differing Aspect Ratios," Journal of Heat Transfer, Vol. 98, 1976, pp. 67-71.

26. Buchberg, H., I. Catton and D. K. Edwards, "Natural Convection in Enclosed Spaces - A Review of Applications to Solar Energy Collection," Journal of Heat Transfer, Vol. 98, 1976, pp. 182-188.

27. Hollands, K. G. T. and L. Konicek, "Experimental Study of the Stability of Differentially Heated Inclined Air Layers," International Journal of Heat and Mass Transfer, Vol. 16, 1973, pp. 1467-1476.

28. Hollands, K. G. T., G. D. Raithby, and L. Konicek, "Correlation Equations for Free Convection Heat Transfer in Horizontal Layers of Air and Water," International Journal of Heat and Mass Transfer, Vol. 18, 1975, pp. 879-884.

29. Hollands, K. G. T., T. E. Unny, G. D. Raithby, and L. Konicek, "Free Convection Heat Transfer Across Inclined Air Layers," Journal of Heat Transfer, Vol. 98, 1976, pp. 189-193.

30. Randall, K. R., J. W. Mitchell, and M. M. El-Wakil, "Natural Convection Characteristics of Flat-Plate Collectors," Heat Transfer in Solar Energy Systems, J. R. Howel and T. Min, Editors, ASME, New York, 1977, pp. 9-16.

31. Hollands, K. G. T. , "Dimensional Relations for Free Convective Heat Transfer in Flat-Plate Collectors," Renewable Alternatives: Procedings of the Annual Conference of the Solar Energy Society of Canada, Aug. 20-24, 1978, Published by Solar Energy Society of Canada, Winnipeg, Manit, Vol. 1, paper 1.1.5.

32. McAdams, W. H., Heat Transmission, McGraw-Hill Book Co., Inc., New York, 1954, 3rd ed., pp. 249-250.

33. Ramsey, J. W. and M. Charmchi, "Variances in Solar Collector Performance Predictions Due to Different Methods of Evaluating Wind Heat Transfer Coefficients," Technical Note, Journal of Heat Transfer, Vol. 102, 1980, pp. 766-768.

34. Sparrow, E. M., J. W. Ramsey, and E. Mass, "Effect of Finite Width on Heat Transfer and Fluid Flow About an Inclined Rectangular Plate," Journal of Heat Transfer, Vol. 101, 1979, pp. 199-205.

35. Ramsey, J. W., J. T. Borzoni, and T. H. Holland, "Development of Flat-Plate Solar Collectors for the Heating and Cooling of Buildings," NTIS #N75-264951, June 1975, pp. 123-144.

36. Junkins, J. L., An Introduction to Optimal Estimation of Dynamical Systems, Sijthoff S. Noordhoff International Publishers B.V., Alphen aan den Rijn, The Netherlands, 1978, pp. 1-42.

37. Beck, J. V. and K. J. Arnold, Parameter Estimation in Engineering and Science, John Wiley and Sons, New York, 1977, pp. 334-413.

38. Gauss, K. F., Theory of the Motion of the Heavenly Bodies Moving About the Sun in Conic Sections, 1809, reprinted by Dover Publications, Inc., New York, 1963.

39. Johnson, L. W., and R. D. Riess, Numerical Analysis, Addison-Wesley Co., Reading, Mass., 1977, pp. 299-302.

40. Lunde, A. R., "National Bureau of Standards - Solar Collector Reliability Test Program - Baseline Performance Tests," Boeing Contract Report No. NB79SBCA0047, Feb., 1980.

41. Kline, S. J., and F. A. McClintock, "Describing Uncertainties in Single - Sample Experiments," Mechanical Engineering, January, 1953, pp. 3-8.

APPENDIX A

Listing of Instrument Manufacturers

Instrument or Recording Device	Manufacturer	Model	Serial Number
Paranometer	Eppley Laboratory, Inc.	PSP	13493F3
Pyrheliometer	Eppley Laboratory, Inc.	NIP	16453E6
Pyrgeometer	Eppley Laboratory, Inc.	PIR	19639F3
Anemometer	Weather Measure Corp.	W103-B	1182
Thermocouples	Custom Built	Type T	
Electronic Integrators	AGM Electronics, Inc.	EA 4013 with ten each of EA 4028 and EA 4011	
24-Channel Multi-Point Recorder	Honeywell	Y15305836-24-01-0-000-(607)-10	U8260992002
2-Channel Mechanical Integrating Strip Chart Recorder	Tractor Westronics, Inc.	LD11D	1683
2-Channel Strip Chart Recorder	Varian Aerograph	G-2500	2581
Digital Multimeter	Hewlett-Packard	3466A	1716A-07539
Digital Multimeter	Hewlett-Packard	3465A	1546A-04511
AC Watt Meter	Weston Electric Instrument Corp.	905	457
AC Current Meter	Weston Electric Instrument Corp.	904	7100
24-Position Thermocouple Switch	Minneapolis-Honeywell	Type T	
20-Position Thermocouple Switch	Omega Engineering, Inc.	Type T	
Current Transformer	Weston Electrical Instrument Corp.	461	16142
Variable Voltage	Standard Electrical Products Corp.	1500B	
Foil Thermocouples	Omega Engineering, Inc.	C02-T	
Electric Strip Heaters	Electrofilm, Inc.	112000-231, 261, and 291	

APPENDIX B

One-Cover Steady-State and Transient Equations

This appendix lists the steady-state and transient energy balance equations for a one-cover solar collector in a stagnating mode. The assumptions used are those listed in Sections 3.1 and 3.2. The development and solution technique for the following equations is similar to those found in Sections 3.1 and 3.2.

Steady-State Equations

Energy balances on the absorber plate and cover yield

$$(h_{p1} + U_B)\, T_p - h_{p1} T_{c1} = (\hat{\tau\alpha})G + J_2 - J_1 + U_B\, T_a \tag{B.1}$$

$$-h_{p1} T_p + (h_{p1} + h_w)\, T_{c1} = (\hat{\alpha}_1)G + J_1 + J_4 - J_2 - J_3 + h_w T_a \tag{B.2}$$

The solar wavelength radiosities are

$$\hat{J}_{b1} = 0 \tag{B.3}$$

$$\hat{J}_{b2} = \hat{\tau}_1(1 - \eta_d) + \hat{\rho}_1 \hat{J}_{b1} \tag{B.4}$$

$$\hat{J}_{b3} = \hat{\tau}_1 \hat{J}_{b1} + \hat{\rho}_1(1 - \eta_d) \tag{B.5}$$

$$\hat{J}_{d1} = (1 - \hat{\alpha}_p)\, \hat{J}_{d2} + (1 - \hat{\alpha}_p)\, \hat{J}_{b2} \tag{B.6}$$

$$\hat{J}_{d2} = \hat{\tau}_{d1}\, \eta_d + \hat{\rho}_{d1}\, \hat{J}_{d1} \tag{B.7}$$

$$\hat{J}_{d3} = \hat{\tau}_{d1}\, \hat{J}_{d1} + \hat{\rho}_{d1}\, \eta_d \tag{B.8}$$

The above equations are solved simultaneously for $\hat{J}_{b1} - \hat{J}_{b3}$ and $\hat{J}_{d1} - \hat{J}_{d3}$. The values for $(\hat{\tau\alpha})$ and $(\hat{\alpha}_1)$ are

$$(\hat{\tau\alpha}) = \hat{J}_{b2} + \hat{J}_{d2} - \hat{J}_{d1} \tag{B.9}$$

$$(\hat{\alpha}_1) = 1 - \hat{J}_{b2} - \hat{J}_{b3} + \hat{J}_{d1} - \hat{J}_{d2} - \hat{J}_{d3} \tag{B.10}$$

The following equations relate the infrared radiosities $J_1 - J_4$

$$J_1 = \varepsilon_p \sigma T_p^4 + (1 - \varepsilon_p) J_2 \tag{B.11}$$

$$J_2 = \varepsilon_{c1} \sigma T_{c1}^4 + \rho_{c1} J_1 + \tau_{c1} J_4 \tag{B.12}$$

$$J_3 = \varepsilon_{c1} \sigma T_{c1}^4 + \rho_{c1} J_4 + \tau_{c1} J_1 \tag{B.13}$$

$$J_4 = \sigma T_s^4 \tag{B.14}$$

Radiosities $J_1 - J_4$ are obtained by solving Eqs. A.11 - A.14 simultaneously. Values for h_{p1}, h_w, and U_B are calculated as in Section 3.1.

Transient Equations

Energy balances on each component of the one-cover collector, including the energy stored in each component, yield

$$(\hat{\tau\alpha})G + J_2 - J_1 - h_{p1}(T_p - T_{c1}) - 2k_{in}(T_p - T_{in})/\delta_{in} = m_p C_p dT_p/dt \tag{A.15}$$

$$(\hat{\alpha}_1)G + J_1 + J_4 + h_{p1}(T_p - T_{c1}) - J_2 - J_3 - h_w(T_{c1} - T_a) = m_{c1} C_{c1} dT_{c1}/dt \tag{A.16}$$

$$2k_{in}(T_p - T_{in})/\delta_{in} - 2k_{in}(T_{in} - T_{BC})/\delta_{in} = m_{in} C_{in} dT_{in}/dt \tag{A.17}$$

$$2k_{in}(T_{in} - T_{BC})/\delta_{in} - (h_w + h_r)(T_{BC} - T_a) = m_{BC} C_{BC} dT_{BC}/dt \tag{A.18}$$

Values for $(\hat{\tau\alpha})$, $(\hat{\alpha}_1)$, h_{p1}, h_w, and J_1 - J_4 are the same as those used in the steady-state analysis of a one cover collector. Equations A.15 - A.18 are solved for T_p, T_{c1}, T_{in}, and T_{BC} by the numerical integration technique in Section 3.2.

The vita has been removed from the scanned document

STAGNATION TEMPERATURE TEST METHODS FOR DETERMINING SOLAR COLLECTOR THERMAL PERFORMANCE DEGRADATION

by

Aaron Grayson Dawson, III

(ABSTRACT)

An analytical and experimental investigation was undertaken to evaluate a proposed method for determining the thermal degradation of materials used in flat-plate solar collectors. The proposed method is based on measuring stagnation (no-flow) temperatures of the absorber plate. A comparison of the advantages and limitations of the proposed method is made with the conventionally used existing method which is based on measuring the energy output from the collector. Previous investigations have shown that the existing test method may not be sufficiently sensitive to detect expected changes in material properties, is influenced by the test environment, and is relatively expensive to perform. The material properties of interest are primarily the cover transmittance, the solar absorptance of the absorber, the infrared emittance of the absorber, and the thermal conductivity of insulation.

Experimental results were obtained from both on and off-campus test sites. The data includes those from solar simulator tests and indoor tests using a highly instrumented solar collector. This indoor collector was equipped with electrical strip heaters mounted on the back-

side of the absorber plate to simulate absorbed solar radiation in a controlled environment. The experiments included an investigation of four techniques for measuring the absorber stagnation temperature.

Steady-state and transient analytical models are developed to evaluate stagnation temperature test methods. These models are validated using extensive experimental data.

The proposed method is based on measuring stagnation temperatures before and after prolonged exposure to prevailing environmental conditions. While these measurements are simpler than those required in the energy output method, other factors, such as transient effects, are important for outdoor tests. Test methods using instantaneous and all-day integrated stagnation temperatures are considered. Both of these test methods were shown to be highly sensitive to environmental conditions. Wind speed was shown to potentially have the most serious influence on results. The measured temperature distribution of the absorber plate was shown to be highly nonisothermal as a result of collector edge heat losses and thermal stratification of the air underneath collector covers. Instantaneous measurements were observed to be very sensitive to transients as a result of intermittent cloud cover. All-day integrated measurements were not affected by such transients.

The investigation revealed that proposed stagnation temperature test methods have potential in determining collector property changes after environmental exposure. Results indicate that the proposed method is more sensitive to small property changes than the current energy output method. However, variations in environmental conditions should be

limited or taken into account when using stagnation temperature test methods.